UCRL 3094

UNIVERSITY OF CALIFORNIA

Radiation Laboratory

AN ELECTROSTATIC BETA-RAY SPECTROMETER WITH A DOUBLE RETARDING FIELD

TWO-WEEK LOAN COPY

This is a Library Circulating Copy which may be borrowed for two weeks. For a personal retention copy, call Tech. Info. Division, Ext. 5545

DISCLAIMER

This document was prepared as an account of work sponsored by the United States Government. While this document is believed to contain correct information, neither the United States Government nor any agency thereof, nor the Regents of the University of California, nor any of their employees, makes any warranty, express or implied, or assumes any legal responsibility for the accuracy, completeness, or usefulness of any information, apparatus, product, or process disclosed, or represents that its use would not infringe privately owned rights. Reference herein to any specific commercial product, process, or service by its trade name, trademark, manufacturer, or otherwise, does not necessarily constitute or imply its endorsement, recommendation, or favoring by the United States Government or any agency thereof, or the Regents of the University of California. The views and opinions of authors expressed herein do not necessarily state or reflect those of the United States Government or any agency thereof or the Regents of the University of California.

UCRL-3094
Instrumentation Distribution

UNIVERSITY OF CALIFORNIA
Radiation Laboratory
Berkeley, California

Contract No. W-7405-eng-48

AN ELECTROSTATIC BETA-RAY SPECTROMETER WITH A DOUBLE RETARDING FIELD

Herbert Raymond Johnston
(Thesis)

October 26, 1955

Printed for the U. S. Atomic Energy Commission

Contents

		Page
	Abstract	5
I.	Introduction	6
II.	Electrostatic Beta-Ray Spectrometers	8
III.	Double-Retarding-Field Electrostatic Beta-Ray Spectrometer	12
	A. Introductory Discussion	12
	B. Mathematical Theory	14
	a. First Retarding Field	14
	b. Second Retarding Field	16
	c. Effect of Apparatus Dimensions	16
	d. Effect of Finite Dimensions of Sample Holder	19
	C. Electron-Focusing System	19
	a. General Discussion	20
	b. Determination of Electron Trajectories in the Reflector	24
	1. General	24
	2. Use of Rubber-Membrane Potential Model for Two-Dimensional Fields	25
	3. Application of the Rubber-Membrane Model to Three-Dimensional Axially Symmetric Fields	27
	D. Electron-Detection System	36
	a. General Discussion	36
	b. Secondary Electron Multiplier	39
	E. Noise Sources	45
	a. Gamma and Alpha Radiations	46
	b. Other Sources of Noise	48

Contents (Continued)

F. Theoretical Transmission and Resolution 49

IV. Apparatus 55

A. Spectrometer 55

a. General Description. 55

b. Sample Holder. 60

B. Auxiliary Equipment 64

a. Power Supplies 64

b. Preamplifier, Scaler, and Count-Rate Meter 65

c. Vacuum System 66

V. Experimental. 68

A. Monokinetic Source 68

a. Introduction 68

b. Procedure 75

c. Results and Conclusions 76

B. Radioactive Source 80

a. Introduction 80

b. Sample Selection and Preparation 83

c. Procedure 84

d. Results and Conclusions 85

Appendices

A. Motion of Electrons in Uniform Electrostatic Fields 88

B. Characteristics of Electrons Emerging from a Uniform Retarding Field 92

C. Graphical Method for Plotting Electron Trajectories in Electrostatic Fields 95

Contents (Continued)

D. Equations of Motion of a Sliding Mass Point . . . 98

E. Potential Field Calculations 100

Acknowledgments 109

Table of Symbols 110

References 111

AN ELECTROSTATIC BETA-RAY SPECTROMETER WITH A DOUBLE RETARDING FIELD

Herbert Raymond Johnston

Radiation Laboratory and Department of Electrical Engineering
University of California, Berkeley, California

October 26, 1955

ABSTRACT

A novel type of beta-ray spectrometer is described. It uses two retarding electrostatic fields of slightly different magnitudes to distinguish between beta particles of different energies, and a secondary electron multiplier as a detector. The nominal beta energy range of the machine as constructed is from 1 to 50 kev.

The mathematical theory of the spectrometer is given. Calculated solid-angle transmission is of the order of 0.14% of 4π and the resolution can be varied from 0.5 to 2.0% (on an energy basis) by varying the potentials of the electrodes. It is about equal in transmission and somewhat superior in resolution to the flat magnetic spectrometer. It is especially useful in the lower energy ranges that cannot be measured with magnetic spectrometers, which usually employ thin-window G-M counters as detectors, since their magnetic field would interfere with the operation of an electron multiplier.

The results of testing the spectrometer with a monokinetic source of electrons are given. These tests confirm the predictions made from theoretical considerations within the approximations involved. The radioactive sample used to test the machine was an organic compound of tritium. The results were consistent with the known characteristics of the tritium spectrum.

I. INTRODUCTION

For many years, arrangements of electric and magnetic fields have been used for the determination of velocities and of the ratio of charge to mass of fundamental particles and ions. Proof of the existence of the electron and a measurement of its ratio of charge to mass was accomplished by J. J. Thompson[1] in 1897. He employed crossed electric and magnetic fields for this purpose. Also in 1907 J. J. Thompson[2] used a similar arrangement of electric and magnetic fields to construct the first mass spectroscope, which is a device for the determination of the ratio of the charge to the mass of ions.

In 1918, A. H. Dempster[3] published information on his mass spectrograph, which accomplished the separation of ions with different values of ratio of charge to mass by deflection through an angle of 180° by means of a uniform magnetic field. This device required that the ion beam be homogeneous with respect to velocity.

Aston in 1919[4] reported on a mass spectrometer employing a combination of electric and magnetic fields. Since the initial work of Aston, a great number of modifications in mass spectrometers have been introduced. Nearly all these modifications employ a combination of electric and magnetic fields.[5, 6, 7]

The problems encountered and the techniques used in mass spectroscopy are similar to those of beta-ray spectroscopy. However, the basic problem is a little less difficult in beta-ray spectroscopy, since the ratio of charge to mass of the beta particle is constant when the velocity is constant.

The term "beta" radiation or particle goes back to 1899 when Giesel[8] showed that the radiation from a radium source contained at least two components, one that was (apparently) not deflected by a magnetic field and another which was deflected by the magnetic field. The first or undeflected portion was termed "alpha" radiation and the deflected portion the "beta" component. In 1903 Rutherford[9] showed that if the magnetic field was sufficiently strong, the so-called alpha portion of the radiation was also resolved into two components--the alpha rays, which were deflected in a direction opposite to the beta rays, and a "gamma" component, which was undeflected in the strongest electric or magnetic fields.

The beta radiation from radioactive substances was subsequently identified as high-speed electrons ejected from the nuclei of radioactive atoms. Also the alpha rays were shown to be the nuclei of helium atoms stripped of their outer electrons and hence positively charged. The gamma rays were shown to be high-frequency electromagnetic radiations similar to x-rays.

It was realized for some time that the beta rays from the radioactive substances were a mixture of electrons of different energies. It was also realized that these electrons would be deflected in a magnetic field according to their mass-velocity product (mv) or momentum.

The first practical and useful beta-ray spectrograph was described by Danysz[10] in 1912, and it consisted of the deflection of beta particles through 180° in a uniform magnetic field. Electrons of constant momenta (mv) came to a focus in a line on a photographic plate. This type of beta-ray spectrograph was improved and used by Rutherford and Robinson[11] in 1913.

The so-called flat magnetic beta-ray spectrographs as used by Danysz and described above are to be contrasted with a second type of magnetic beta-ray spectrometer known as the helical type. The latter type utilizes the focusing properties of an axially symmetric magnetic field. A source of beta particles is located on the axis of the magnetic field, and electrons of equal momenta are brought to a focus again on the axis after traversing the field in a helical spiral path. The above device was proposed by Kapitza[12] in 1924 and incorporated into a working instrument by Tricker[13] in 1925.

An excellent summary of the theory and practice of magnetic beta-ray spectrometers was published in 1950 by Persico and Geoffrion.[14]

II. ELECTROSTATIC-FIELD BETA-RAY SPECTROMETERS

In certain types of experiments it may be desirable to use electrostatic instead of magnetic fields for beta-ray spectroscopy. The use of electrostatic fields may be desirable when a secondary electron multiplier is to be used as a particle detector, since the proximity of a strong magnetic field may prevent the proper operation of the electron multiplier. It is to be noted that the use of the electrostatic-field spectrometers is ordinarily confined to the low-energy portion of the beta spectrum, because extremely high voltages would be required for high-energy particles.

Electrostatic beta-ray spectrometers may be divided into two general classifications: the radial-field focusing type and the retarding-field type. The first classification may be further subdivided into the two-dimensional field and the three-dimensional field focusing types.

The two-dimensional focusing type makes use of an inverse first-power electrostatic field between portions of two concentric circular conducting cylinders. This device was investigated theoretically in 1929 by Hughes and Rojansky.[15] They found that a two-dimensional inverse first-power radial electrostatic field had a refocusing property for electron orbits, provided these orbits satisfied certain conditions. The orbits of electrons of the same initial velocity tend to refocus at a point 127° from the starting point. This is to be contrasted with the case of the uniform magnetic field, where good refocusing occurs at 180°.

Hughes and McMillen[16] in 1929 described equipment for checking the conclusions reached by Hughes and Rojansky. The general theory of the focusing properties of a cylindrical condenser has also been investigated by Herzog[17] and Rogers.[18] A mass spectrometer described by Bainbridge and Jordan[19] employs an electrostatic 127° analyzer of the above-described type.

The three-dimensional, focusing type of electrostatic beta-ray spectrometer was first suggested by Aston[4] in 1919. The theory of the focusing of charged particles by means of a spherical condenser was worked out and demonstrated by Purcell[20] in 1938. This device has some advantages over the cylindrical-condenser type of spectrograph,

since it has a much larger aperture (better geometry), but the device is far more difficult to construct.

The retarding-field type of electrostatic beta-ray spectrometer may be also divided into two categories: one with a single retarding field and a second with two slightly different retarding electrostatic fields. Hamilton and Gross in 1950 published a description of a beta-ray spectrometer with a single retarding electric field.[21]

The basic arrangement of the Hamilton and Gross spectrometer is shown in Fig. 1. This figure shows a cross section of the device, which is essentially of a hemispherical shape. S is the source of beta activity, which is placed in a field-free region inside the grid G_1. Between G_1 and G_2 there is a retarding potential of E_0 volts. Between G_2 and the collector plate P there is a small accelerating field, mainly for the purpose of suppressing secondary electron emission from the collector plate P.

In Fig. 1 we have three electron trajectories indicated. Trajectory a represents the path of an electron that had more than enough initial velocity to overcome the retarding field and reach the collector plate P. Trajectory b is one of an electron with not quite enough initial energy, and c represents the trajectory of an electron with only about half enough energy to surmount the field.

For a given retarding field of E_0 volts between G_1 and G_2, only beta particles with energies greater than E_0 volts can overcome the retarding field and reach the collector plate. For a sufficiently large retarding field, no electrons can surmount the field and no current is registered by the electrometer. As the retarding field is reduced, more and more electrons are allowed to reach the collector plate, and consequently more and more current is indicated by the electrometer.

The relation between the retarding potential E_0 and the current as measured by the electrometer may now be plotted graphically. Since the current is a measure of the relative number of electrons able to surmount the retarding field, the spectrum measured is an integral spectrum from which the ordinary spectrum must be obtained by differentiation.

This device has the advantage of having a large solid angle (2π) of collection, but it has all the disadvantages of any equipment that must

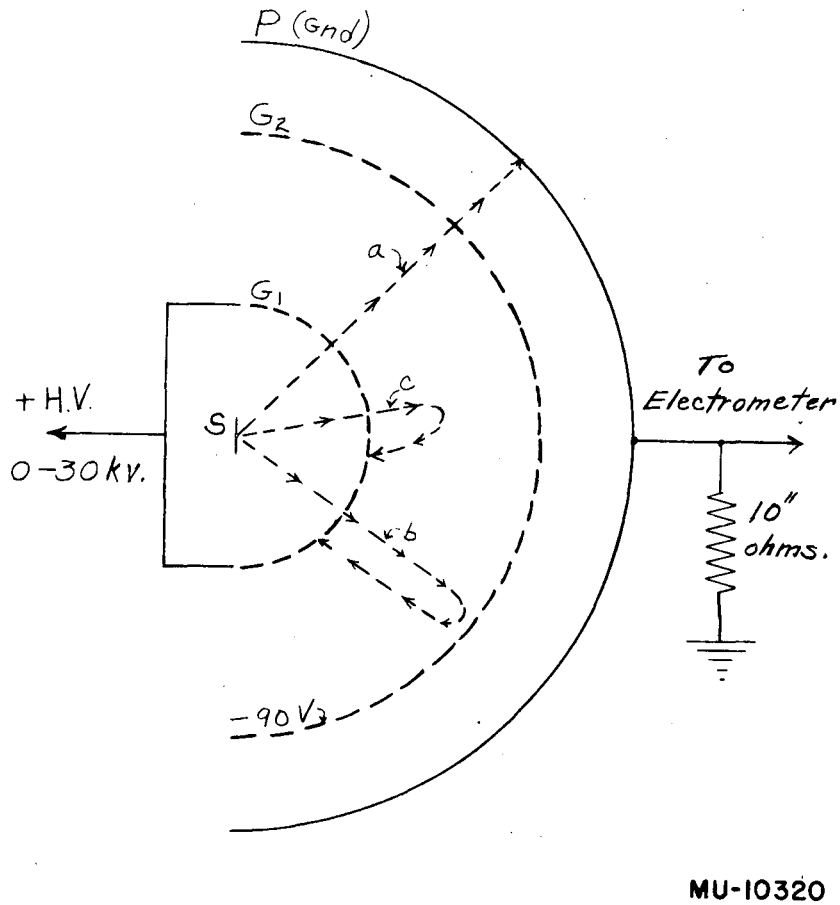

Fig. 1. Single-retarding-field electrostatic spectrometer.

measure very small currents by means of an electrometer. It has the further disadvantage that the measured spectrum must be differentiated to obtain the customary spectrum.

The two-retarding-field electrostatic beta-ray spectrometer is the subject of this dissertation and is treated in the next chapter.

III. DOUBLE-RETARDING-FIELD ELECTROSTATIC BETA-RAY SPECTROMETER

A. Introductory Discussion

In a two-retarding-field electrostatic spectrometer, the operation is considerably different from one using only a single retarding field. In the single-retarding-field device, all electrons above a certain energy, as determined by the single retarding-field potential, are collected and measured as above. In the double-retarding-field apparatus, the first potential field, of V_1 volts, rejects all electrons of energy greater than V_1 volts. The second retarding field, of $(V_1 - \Delta V_1)$ volts, rejects all electrons of energies less than this potential. Thus, in general, only beta particles of energy spread ΔV_1 volts are allowed to actuate the recording or measuring system.

The basic operation of the two-retarding-field spectrometer is illustrated in Fig. 2. The beta-active sample S is mounted in the center of circular grid G_1. Trap T prevents beta particles from coming down into the counting system directly from the sample. G_3 is a ground plane, and trajectory a represents the path of a beta particle whose energy exceeds that of the potential of G_1 (V_1). These electrons strike the collector plate P, which is maintained at a positive potential to suppress low-energy secondary electron emission when the primary electron a strikes the plate.

Trajectory b represents the path of an electron with not quite enough energy to overcome the first retarding field, and it therefore comes to a stop before it reaches G_3 and then is accelerated back toward G_1. It passes through G_1 with exactly the same velocity as that with which it left the sample S. Now it undergoes retardation in the second field between G_1 and G_2. This electron b, however, has sufficient energy to overcome this field, and passes through G_2, where it strikes the first dynode of the secondary multiplier and is recorded in the counting system.

The third trajectory c represents the path of an electron that does not have sufficient energy to surmount the second retarding field, and it is again reflected from G_2 and is not counted. Thus only those electrons of a certain limited energy range are permitted to enter into

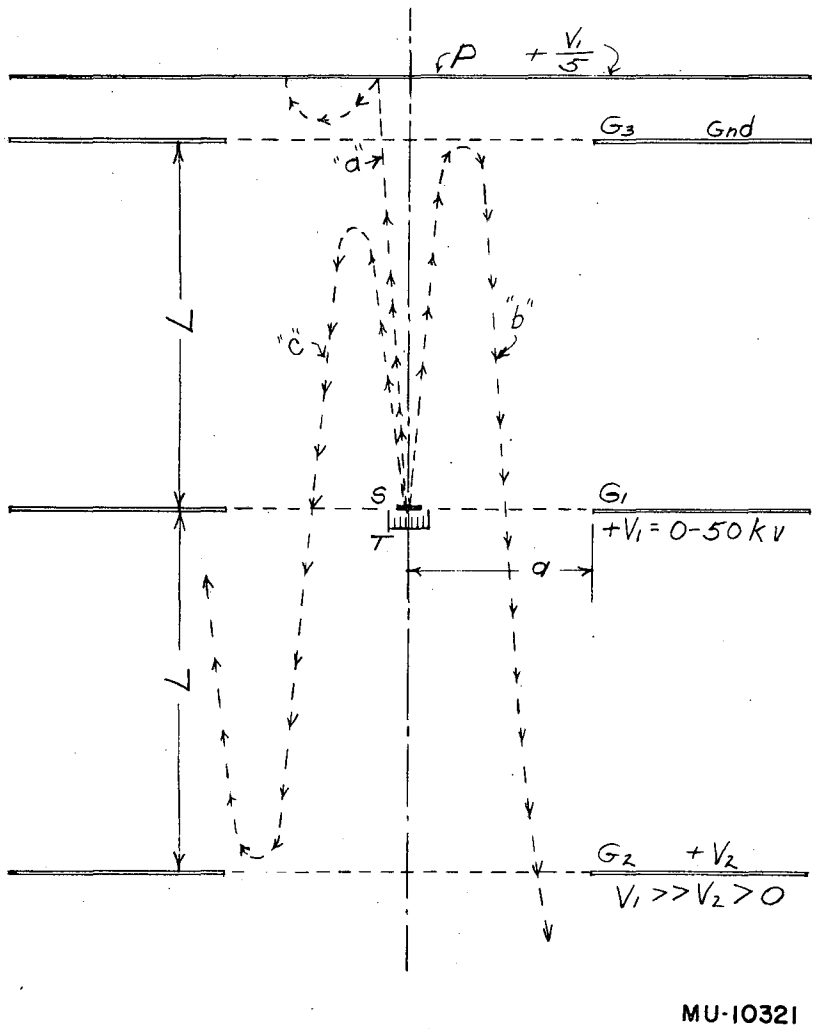

Fig. 2. Diagram showing principle of operation of double-retarding-field beta-ray spectrometer.

the measuring system. It is shown later how this resolution can be adjusted at will by varying the relative potentials in the system.

B. Mathematical Theory

One of the first problems in connection with the double-retarding-field spectrometer was to determine exactly what had to be the characteristics (energy and direction) of the electrons emitted from the sample S in Fig. 2 in order that they could pass through grid No. 2 (G_2). In the calculations that follow, the assumptions are made that the emitting sample has a flat beta spectrum from zero to large velocities, and that it emits uniformly in all directions in the upper hemisphere. Relativistic changes of mass are not considered.

a. First Retarding Field

In the upper space, between G_1 and G_2, electrons of energies somewhat greater than V_1 are lost by passing through G_3 and striking the collector plate P. See Fig. 2.

The basic formula to be used in Eq. (11A) from Appendix A, rewritten and renumbered as follows (mks units used):

$$y_{max} = n\, L \cos^2 \theta \,, \qquad (1)$$

where y_{max} = maximum height to which the electron rises in the first retarding field,

$n = \frac{V_e}{V_1} = \frac{\text{energy of electron in volts}}{\text{first retarding field in volts}}$,

L = perpendicular distance between G_1 and G_3 (meters),

θ = angle between axis of symmetry and initial path of electron (angle of emission).

If y_{max} is equal to or larger than L then the electrons are not returned to G_1 but are rejected by the first retarding field, since they pass through G_3 and are collected by plate P. Thus

$y_{max} = L = n\, L \cos^2 \theta$, and, solving for θ, we have

$$\theta = \cos^{-1}(1/n)^{1/2} \,. \qquad (2)$$

Equation (2) is plotted in Fig. 3 as Curve "A." All electrons that have characteristics of velocity and direction to the right of this curve (in the shaded area) do not pass through the system but are lost on plate P.

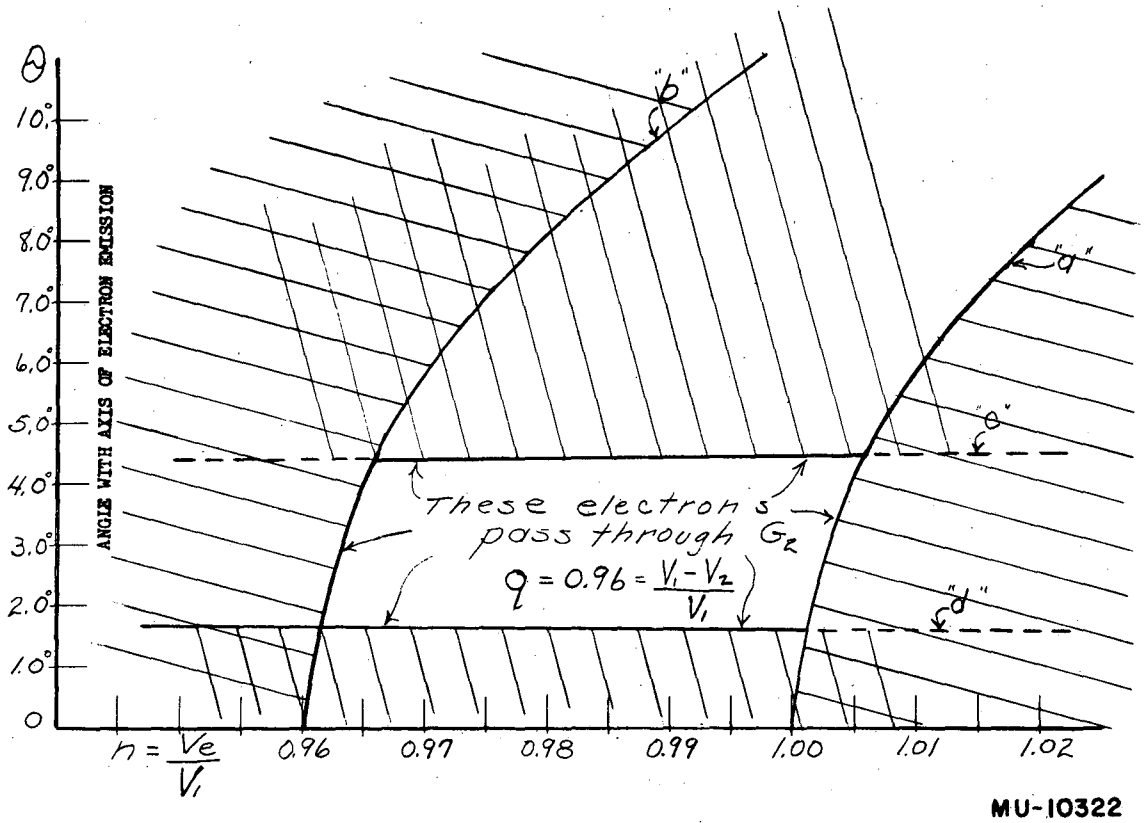

Fig. 3. Results of mathematical analysis.

b. Second Retarding Field

If the opening of G_1 is not limited, we can solve the problem of finding the relation between the parameters that will show what electrons are rejected by the second retarding field. This means finding what electrons are reflected by G_2 after they have passed through G_1 (see Fig. 2). The basic formula from Appendix A is Eq. (13A), which is rewritten and renumbered as follows:

$$y'_{max} = \frac{n\,L}{q} \cos^2\theta \,, \tag{3}$$

where $q = \frac{V_1 - V_2}{V_1}$; V_2 = potential of second retarding field (in volts). If y'_{max} is equal to or less than L (L is also the perpendicular distance between G_1 and G_2) then the electrons do not pass through G_2 but are reflected back to G_1. Thus

$$y'_{max} = L = \frac{n\,L}{q} \cos^2\theta; \text{ solving for } \theta, \text{ we have}$$

$$\theta = \cos^{-1} (q/n)^{1/2} \,. \tag{4}$$

In order to make a plot of this equation, we must assign a value to q, since it is not possible to plot three variables on a two-dimensional chart. In Fig. 3, a value of q = 0.96 has been chosen for this parameter. Equation (4) is plotted in Fig. 3 as Curve "B." All electrons that have characteristics of velocity and direction to the left of this curve (in the shaded area) do not pass through G_2 but are rejected by the second retarding field by reflection back to the plane of G_1.

c. Effect of Apparatus Dimensions

So far we have not limited the dimensions of the grids G_1 and G_2. It may be easily seen that the limiting dimension in this case is the radius of G_2, since in the actual instrument as constructed, the radii of G_1 and G_2 are identical. See Fig. 2.

Referring to Fig. 4 and to Eq. (12A) of Appendix A, we rewrite and renumber Eq. (12A) as follows:

$$x_{max} = 2\,n\,L \sin 2\theta \,. \tag{5}$$

In order to find x' of Fig. 4, we must use Eq. (15A) from Appendix A as follows:

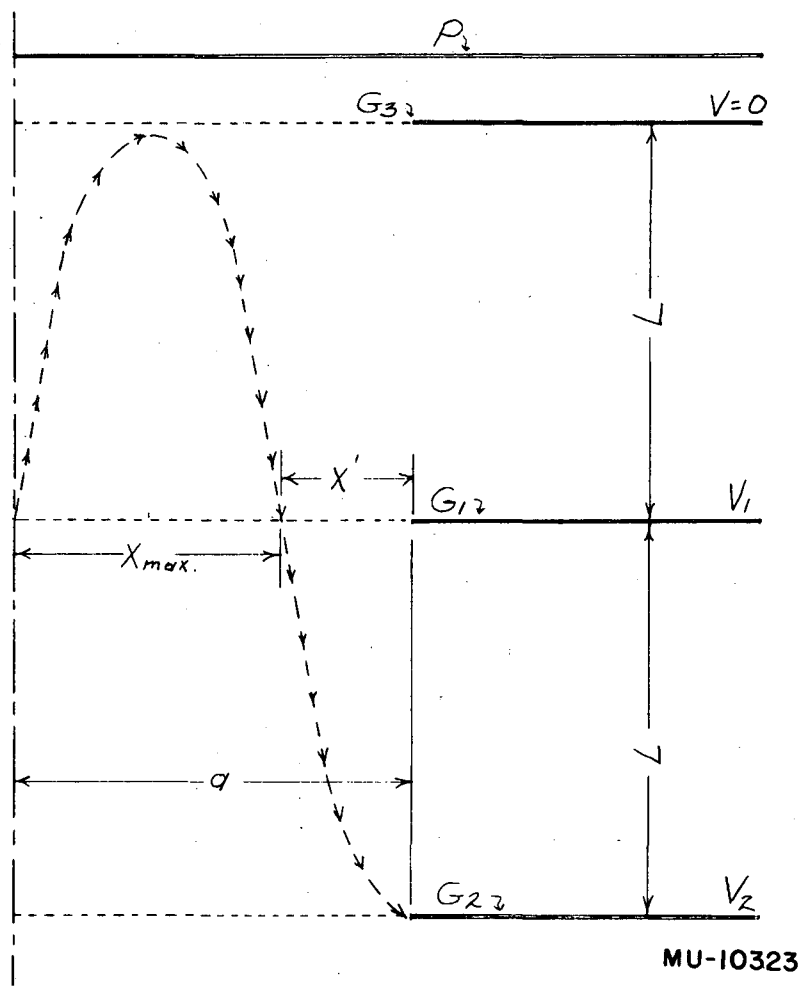

Fig. 4. Method of finding cutoff due to finite radius of G_2.

$$y' = -\frac{q\,(x')^2}{4\,n\,L\,\sin^2\theta} + \frac{x'}{\tan\theta}\,. \tag{6}$$

Let $y' = L$ in the above equation and then solve the quadratic for x'. There will be two values of x', and we want the smaller one, since this gives us the first intersecting value of x' with the plane of G_2. The required solution is

$$x' = \frac{n\,L}{q}\sin 2\theta\left[1 - \left(1 - \frac{q}{n\cos^2\theta}\right)^{1/2}\right]. \tag{7}$$

Now the limiting equation is

$$x_{max} + x' = a\,,$$

where a = radius of G_2 in meters.
Substituting in the above equation and simplifying, we have

$$\sin 2\theta\left[2 + 1/q\left\{1 - \left(1 - \frac{q}{n\cos^2\theta}\right)^{1/2}\right\}\right] = r/n\,, \tag{8}$$

where $r = a/L = 0.438$ in this equipment, since $L = 4$ inches and $a = 1.75$ inches.

It is practically impossible to solve Eq. (8) explicitly for θ in terms of the different parameters. In attempting to solve this equation, I realized that the values of θ would certainly be small, say less than 10°. Thus the $\cos^2\theta$ term would certainly not be much different from 1.00. The procedure is to assume a value of the independent variable n around unity (1.00) and calculate the value of θ with the assumption that $\cos^2\theta$ equals 1.

We next insert the first result in the $\cos^2\theta$ term and redetermine the value of θ. If we do this often enough, we converge on the value of θ for the particular assumed value of n. This must be done for each value of n in the required range of values.

It happens that this procedure gives good results after only two of the above steps. It is interesting to note that Eq. (8) is such that the value of θ is practically constant with respect to practical variations of q and n, and depends primarily on the value of the parameter r.

In the equipment under discussion, the value of θ came out approximately 4.5°, and is practically independent of n and q in the useful range of these parameters. Equation (8) is plotted in Fig. 3 as Curve "C." All electrons above this curve, in the shaded area, strike outside the radius G_2 and are lost.

d. Effect of Finite Dimensions of Sample Holder

So far we have assumed that the No. 1 grid opening (G_1) was not obstructed in any way. However, the sample holder is placed in the center of this grid structure, and some of the electrons that are reflected from G_3 strike the area of the sample holder and are lost.

The basic equation to be used to calculate this effect is Eq. (12A) from Appendix A, which we rewrite and renumber as follows:

$$x_{max} = 2\ n\ L \sin 2\theta\ . \tag{9}$$

Let x_{max} be equal to the radius of the sample holder, b. Thus

$$b = 2\ n\ L \sin 2\theta.$$

Solving for θ, we have

$$\theta = 1/2 \sin^{-1} (b/2nL)\ . \tag{10}$$

In the equipment as constructed, b = 0.4375 inches; L = 4.0 inches.

Equation (10) with the above constants inserted is plotted in Fig. 3 as Curve d. All electrons below this curve strike the sample holder and are lost.

C. Electron-Focusing System

It was proposed that a secondary electron multiplier be used as a device to detect electrons passing through the system of the spectrometer. It seemed undesirable, however, to try to arrange a secondary multiplier system with a first dynode of a size sufficient to be placed immediately beneath the grid G_2. This grid is 3.5 inches in diameter in the equipment as constructed. The use of a smaller first dynode then required that the electrons passing through G_2 be somehow redirected onto a smaller first-dynode structure.

a. General Discussion

The stream of electrons passing through G_2 is a highly divergent beam. The angle between the path of the entering electrons and the axis of the machine may have any value from 0° to 90°. The energy of the electrons may vary from zero to a value slightly larger than that of the potential of grid G_2. See Appendix B and Figs. 5 and 6.

The problem here was not quite the same as for other electron lenses, since it was not required to bring the electrons to a focus at a point but only to redirect the electrons onto a relatively small first dynode of the secondary multiplier. In the actual equipment, it was required to reduce the beam from 3.5 inches in diameter to 2.0 inches in diameter.

It was realized that the required focusing action could be accomplished by either magnetic or electrostatic field lenses. However, since the presence of a magnetic field would have been detrimental to the proper operation of a secondary electron multiplier and also detrimental to the operation of the spectrometer as a whole, an electrostatic lens system was used.

Preliminary work with rough sketches of electrostatic field plots and estimates of possible paths for electrons seemed to indicate that a pear-shaped structure similar to that shown in Fig. 7 would be necessary.

After considerable consideration had been given to the arrangement shown in Fig. 7, it was realized that only a certain fraction of the electrons emerging from grid G_2 can be made to pass through grid G_4 and to strike the first dynode of the electron multiplier. The presence of a certain amount of potential barrier or retarding field within the reflector makes it impossible for electrons to overcome this additional retarding field unless they have sufficient energy when they come through grid G_2. Thus the total energy of the electron, upon emergence from grid G_2, must be at least equal to the potential barrier or "saddle" point potential if it is to emerge from grid G_4 and strike the first dynode of the multiplier.

The focusing arrangement was then more than just a device for redirecting the electrons emerging from grid G_2. It was also an energy selector whose characteristics had to be combined with the selectivity

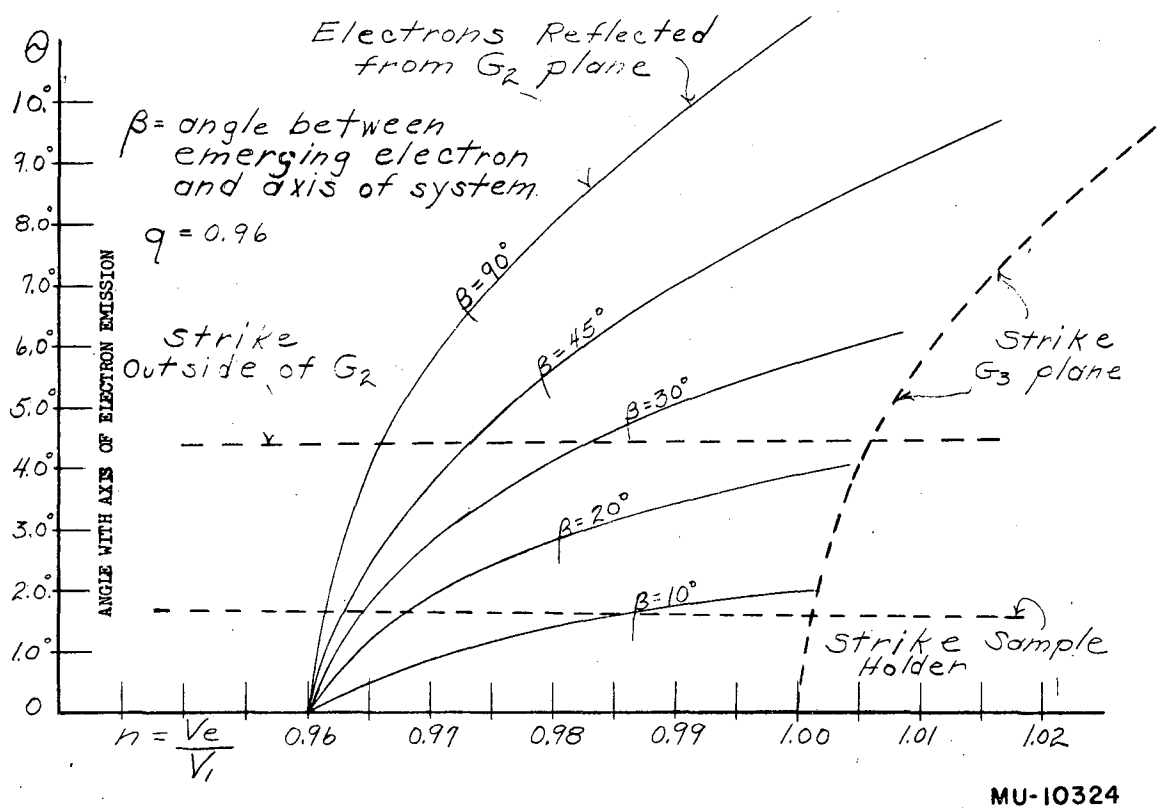

Fig. 5. Angle at which electron emerges from the second retarding field.

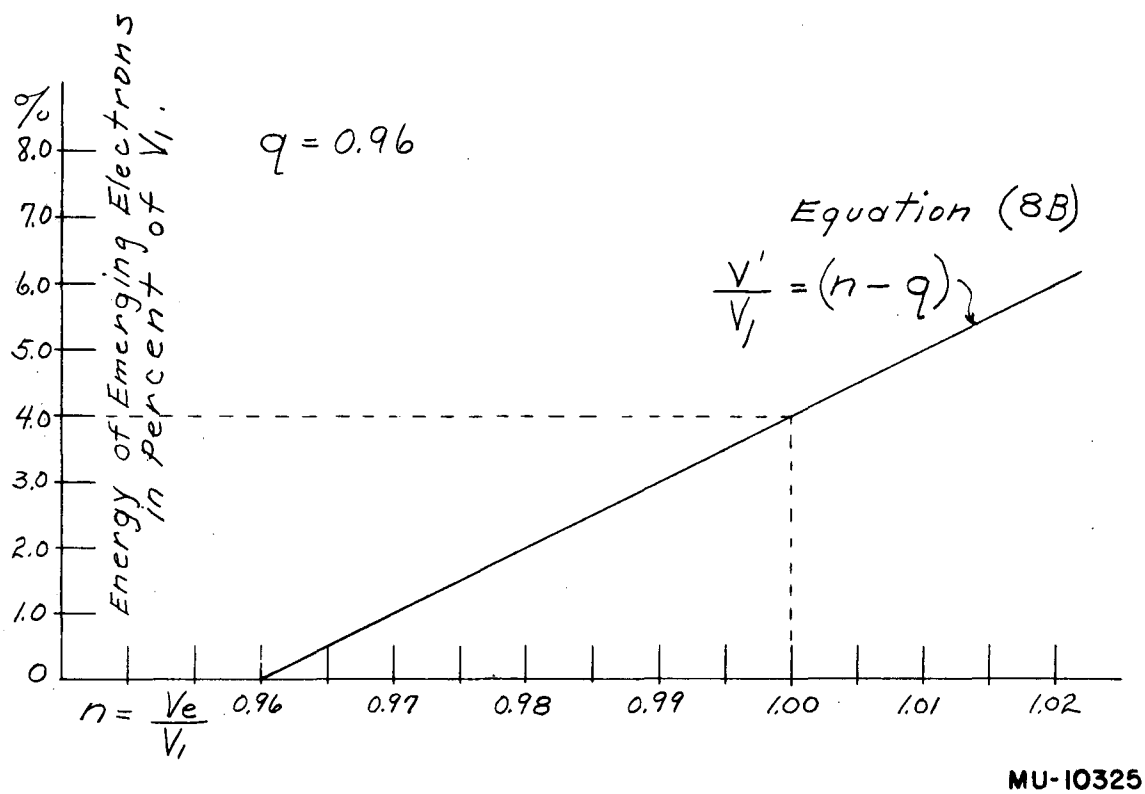

Fig. 6. Energy of electron emerging from second retarding field.

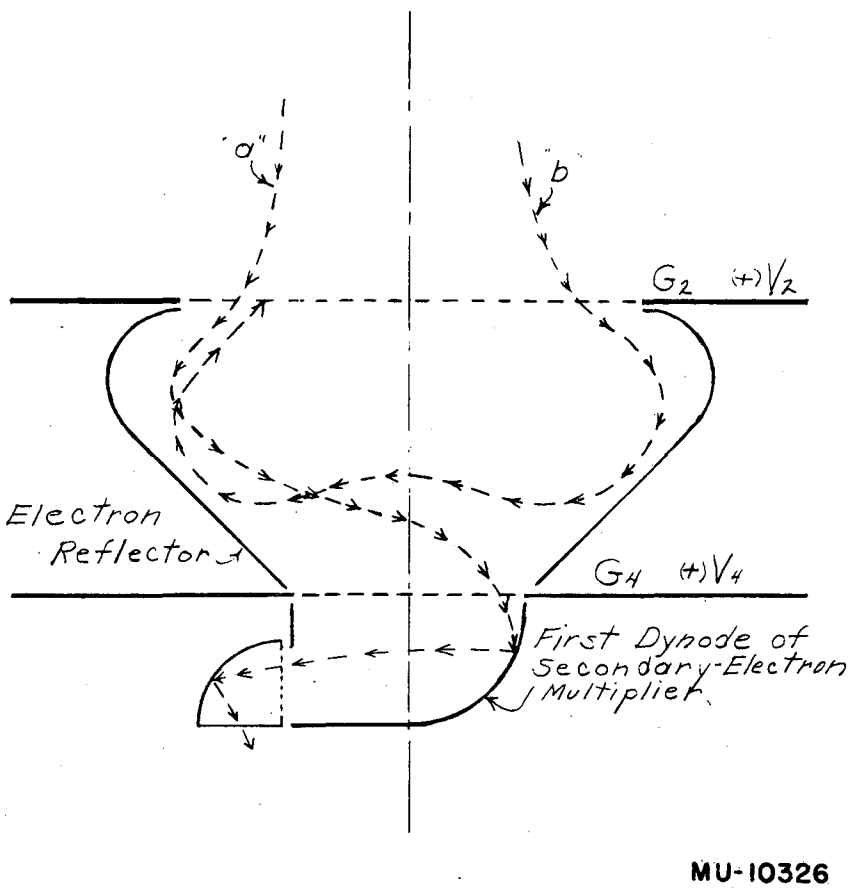

Fig. 7. Electrostatic lens system.

characteristics of the double-retarding-field spectrometer proper in order for one to be able to calculate and predict the over-all performance of the equipment.

b. Determination of Electron Trajectories in Reflector

Estimates or guesses concerning the paths of the electrons in a complicated electrostatic field such as is found within the reflector are of use only to obtain rough approximations that may indicate the direction in which to proceed to obtain the desired result.

1. General

Theoretically, it is possible to calculate the path of an electron from Eqs. (2A), (3A), and (4A) of Appendix A, provided that the potential V is given as a function of the coordinates. Practically, only the simplest cases are amenable to calculation, because the solution of the differential equations becomes extremely difficult or impossible. In general, the potential field cannot be obtained mathematically by a solution of Laplace's equation except for the simplest electrode configurations. This, in itself, prevents us from attempting to calculate electron paths in the reflector shown in Fig. 7.

There are a number of graphical methods for obtaining the path of an electron moving in an electrostatic potential field (Appendix C). However, all graphical procedures require an accurate (and large-size) potential field plot of the region in which the electron path is to be determined. It is to be noted that graphical methods fail to give good results in the neighborhood of a "singular point" or a "saddle" point of the field. The presence of a singular point in the electrostatic field of the reflector of Fig. 7 makes graphical methods unreliable and unsatisfactory when the electron passes close to this saddle point.

It is possible to obtain a relatively accurate field plot of complicated electrode structures by the use of a current-flow model as discussed by Spangenberg.[23] See also Pierce,[30] page 66. The electrode structure, in this case, is axially symmetrical and requires a wedge-shaped electrolyte as a part of the current-flow model as discussed on page 80 of Spangenberg.[23]

2. Use of the Rubber-Membrane Potential Model for Two-Dimensional Fields

The determination of electron trajectories in two-dimensional electrostatic field problems may be done by means of an analogue consisting of a stretched rubber membrane and small steel ball bearings.[23, 26, 27, 28]

A rubber membrane is stretched horizontally so that the surface tension is constant. A membrane in which only surface tension acts adjusts itself upon deformation in such a way that the area of the sheet is a minimum. The area of the surface may be written as an integral,

$$S = \int \left[1 + \left(\frac{\partial h}{\partial x} \right)^2 + \left(\frac{\partial h}{\partial y} \right)^2 \right]^{1/2} dx\, dy \,. \tag{11}$$

$$= \text{minimum}$$

This is a problem in the calculus of variations, which may be converted to the following differential equation:[26]

$$\left[1 + \left(\frac{\partial h}{\partial y} \right)^2 \right] \frac{\partial^2 h}{\partial x^2} - 2 \frac{\partial h}{\partial x} \frac{\partial h}{\partial y} \frac{\partial^2 h}{\partial x \partial y} + \left[1 + \left(\frac{\partial h}{\partial x} \right)^2 \right] \frac{\partial^2 h}{\partial y^2} = 0 \,. \tag{12}$$

If the squares of the first derivative are neglected, we have

$$\frac{\partial^2 h}{\partial x^2} + \frac{\partial^2 h}{\partial y^2} = 0 \,. \tag{13}$$

Equation (13) is Laplace's equation in rectangular coordinates in two dimensions.

Now we apply to the membrane and to the potential field the same limiting or boundary conditions. In other words, we give the rubber membrane a height proportional to the potential of the electrodes at corresponding points. Then at every point of the membrane the height is proportional to the potential at the corresponding point of the electrostatic field. At any point on the membrane, the maximum slope is proportional to the field strength E of the electrostatic field.

The assumption was made in the development of Eq. (13) that the first derivatives $\frac{\partial h}{\partial x}$, $\frac{\partial h}{\partial y}$ were negligible when squared. It is found that an accuracy of about one percent may be maintained in this

analogy if the angles of all lines on the surface of the membrane are kept at 6° or less with the horizontal. In an actual rubber-membrane model, it is not always practical to keep the slopes below this small angle. Consequently the accuracy of the potential field representation is somewhat impaired as the angles are made larger than 6°.

Now it can be shown that the equations of motion of a mass point, acting under the influence of gravity and sliding without friction on the surface of the stretched membrane, are of exactly the same form as the equations of motion of an electron moving in an electrostatic field. (See Appendix D and Reference 26.) The similarity of the form of the equations of motion for the sliding mass point and for the electron also depend on the assumption that the first derivatives or the slope of the membrane are very small compared to 1.

When the rubber-membrane analogy to the electric field is set up, the next problem is to have a mass point slide over the surface without friction. The sliding friction of any rubber membrane is very large and thus one is forced to substitute a rolling ball of some sort for the sliding mass point.

An exact mathematical formulation of the path of the rolling ball and the errors involved in its use is difficult to obtain.[23] However, it can be shown that the total kinetic energy that is picked up by the ball rolling without friction on the surface of the membrane is exactly equal to the loss of potential energy due to its change in elevation on the surface. The electron experiences the same energy relations in the potential field. The kinetic energy of the ball, however, is divided between translational and rotational energy, and as long as the ball rolls with a fixed circle of contact, the ratio between the two components of energy is constant and the path is a good approximation to that of the electron.[23]

In practical applications, several departures from idealized conditions may exist. The ball encounters a certain amount of friction when rolling over the surface of the rubber membrane and the membrane may be deformed by the weight of the ball. There may be irregularities in the thickness of the rubber and of the roughness of the surface. Also, very small slopes are not possible in most practical applications. The analogy cannot be modified to account for space-charge effects.

Owing to the uncertainties involved, the method must be checked by one of several means such as comparing the path of the ball with an electron path known mathematically.[26] It has been found that, if reasonable precautions are taken, the path of the ball on the membrane does, in fact, agree remarkably well with the corresponding electron path.

3. Application of the Rubber-Membrane Model to Three-Dimensional Axially Symmetric Fields

Frequently it is necessary to investigate the trajectories of electrons in an axially symmetric electrode structure. One possible approach is to determine the potential field plot from the appropriate current-flow model.[23] Then using this potential field plot, we may apply one of the several graphical methods for the determination of the paths of the electrons. (See Reference 30 and Appendix C.) It should be noted that this method is good only when the electrons' path lies in a plane that contains the axis of symmetry of the electrode structure. This requirement is satisfied if the source of electrons is located somewhere on the axis of symmetry of the field (in the absence of magnetic fields).

The above approach is sound in principle but tedious of application, especially if many paths are to be plotted. The use of machine plotting methods[24, 25] requires elaborate and expensive equipment, which was not available in this investigation. It was, therefore, decided to investigate the possibilities of using the rubber-membrane, steel-ball-bearing analogue to determine the approximate electron trajectories in the axially symmetric structures under study.

The theoretical justification for the use of the rubber-membrane potential model, in the two-dimensional case, rests on the fact that the differential equation involving the height distortion of the membrane can be reduced to Laplace's equation in two dimensions for small angles of slope. This is Eq. (13), as follows:

$$\frac{\partial^2 h}{\partial x^2} + \frac{\partial^2 h}{\partial y^2} = 0 \, . \qquad (13)$$

(See Appendix D and previous discussion for the theoretical basis for the use of rolling balls as analogues of electrons for the determination of trajectories on the membrane potential model.)

Let us now write Laplace's equation in cylindrical coordinates as follows:[29]

$$\frac{\partial^2 V}{\partial r^2} + \frac{1}{r}\frac{\partial V}{\partial r} + \frac{1}{r^2}\frac{\partial^2 V}{\partial \theta^2} + \frac{\partial^2 V}{\partial z^2} = 0 . \tag{14}$$

The equation must be modified for an axially symmetric field, which is a field that is independent of the angle θ. Rewriting, we have

$$\frac{\partial^2 V}{\partial r^2} + \frac{1}{r}\frac{\partial V}{\partial r} + \frac{\partial^2 V}{\partial z^2} = 0 . \tag{15}$$

In order to compare the two-dimensional Laplace Eq. (13) to the three-dimensional axially symmetric case, let us rewrite Eq. (15) and replace r by x and z by y, and also write V for h in Eq. (11), as follows:

$$\frac{\partial^2 V}{\partial x^2} + \frac{\partial^2 V}{\partial y^2} = 0 , \tag{13a}$$

$$\frac{\partial^2 V}{\partial x^2} + \frac{1}{x}\frac{\partial V}{\partial x} + \frac{\partial^2 V}{\partial y^2} = 0 . \tag{15a}$$

We note that Eqs. (13a) and (15a) are similar except that Eq. (15a) contains an added term $\frac{1}{x}\frac{\partial V}{\partial x}$. Given a similar configuration in cross section, of the electrode structures or boundary conditions for the above two equations, we see that Eq. (15a) approaches Eq. (13a) as x (or r) becomes increasingly larger. Of course, at the boundary, where there is a fixed potential at x (or r) equaling--say a, the two fields are identical.

The above paragraph may be rephrased as follows: Given similar boundary conditions, then if we assume a two-dimensional field distribution in a cross section of an axially symmetric field that includes the axis of symmetry, the errors involved become smaller as we approach the boundaries or electrodes.

In the electron reflector of the beta spectrometer under discussion, the field is axially symmetric. It is, however, of such a nature as to render the solution of Laplace's equation impossible either in the two-dimensional or the axially symmetric form in cylindrical coordinates.

In order to be able to estimate the errors involved in the assumption that we may use the two-dimensional rubber-membrane model as an analogue for a three-dimensional axially symmetric potential field, we can take as an example two easily calculated boundary-value problems. We select these problems so that the dimensions, voltages, and sections are identical in the two-dimensional and cylindrical cases.

We have chosen to calculate the potential distribution in a square, two-dimensional figure with sides at zero potential and opposite ends at unity potential (see Fig. 8). Also we have taken a right circular cylindrical box whose diameter is equal to its height. This box has its cylindrical sides at zero potential and its two circular ends at unity potential (see Fig. 9). (Also see Appendix E for an outline of the methods used to calculate these potential fields.)

Examining the two field plots, we notice that there is a considerable difference between the two. It may be noted, for example, in the axially symmetric case that the cylindrical sides do a better job of shielding the interior of the box from the effects of the potentials on the two circular ends. In other words, the potential at the center of the cylindrical box is lower by a considerable amount. In this case the saddle point or center potential is about 28% of the end voltages as against 50% for the two-dimensional case.

In order to compare the paths of electrons that traverse the two different potential fields, we have plotted, by graphical means, the trajectory of two electrons in each case. In Fig. 10 we see the path of an electron entering at an angle of 20° from the axis of symmetry, in the two-dimensional case. In Fig. 11 we have plotted the path of the same electron in the axially symmetric field of the cylindrical box. If we examine these two paths by superposition, we find that they are practically identical in shape.

In Figs. 12 and 13, we have plotted the paths of an electron that enters the two fields off center and at an angle of 20° with the axis of symmetry. We note that the two paths are not exactly identical but are very similar in shape. It is important to state that the energy of the entering electron is assumed to be 1.00 in terms of voltage or the same as the potential of the two end electrodes in all cases plotted.

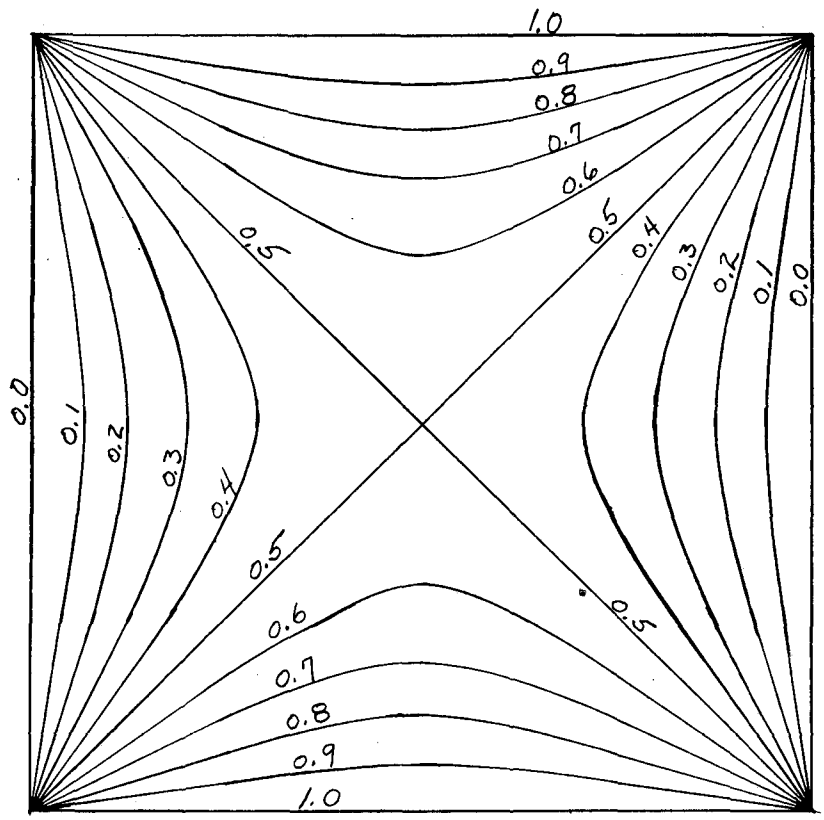

MU-10327

Fig. 8. Field plot of two-dimensional square box.

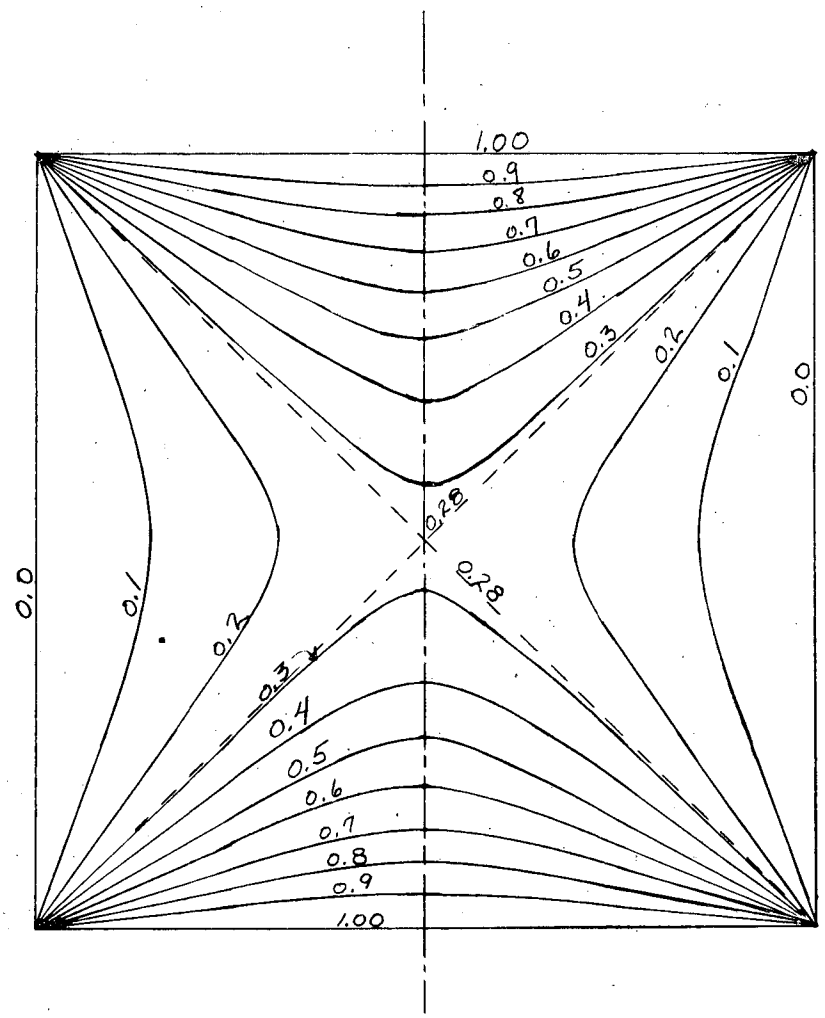

MU-10328

Fig. 9. Field plot of axial cross section of cylindrical box.

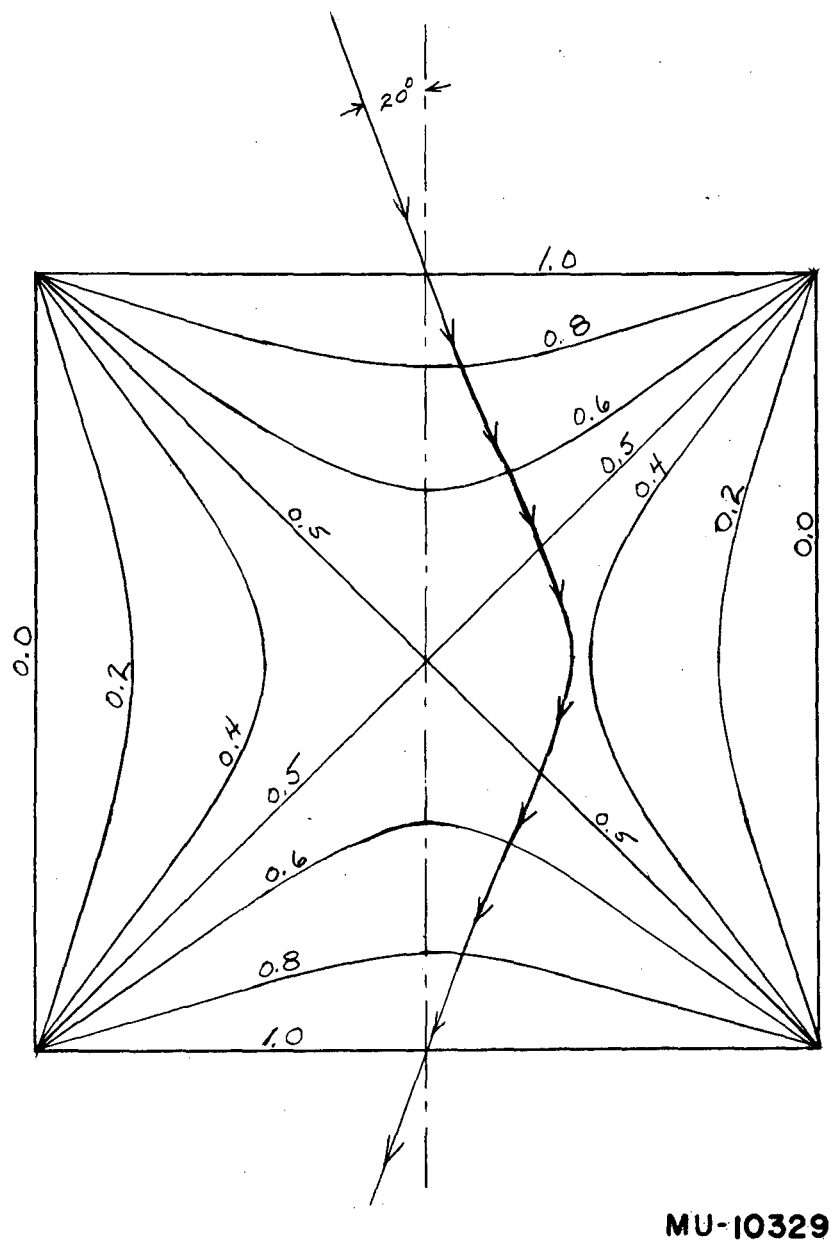

Fig. 10. Trajectory of 20° axial electron in two-dimensional box.

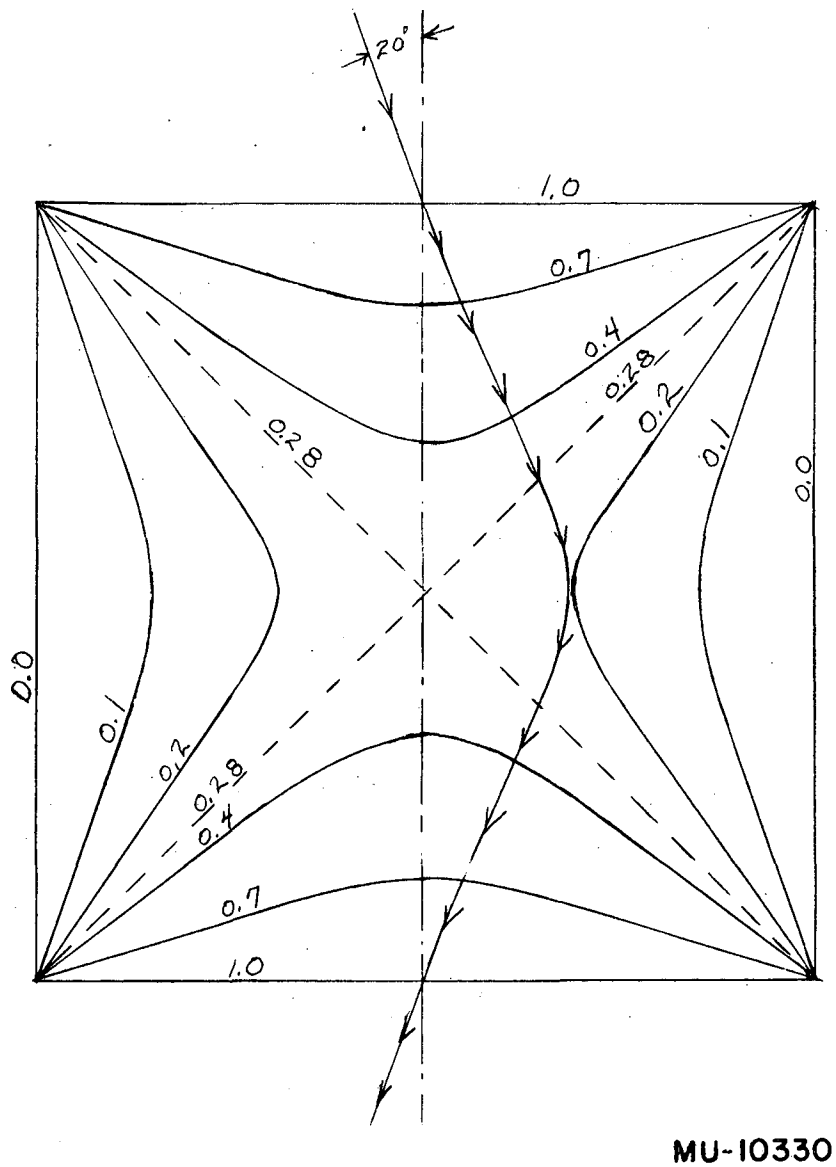

Fig. 11. Trajectory of 20° axial electron in cylindrical box.

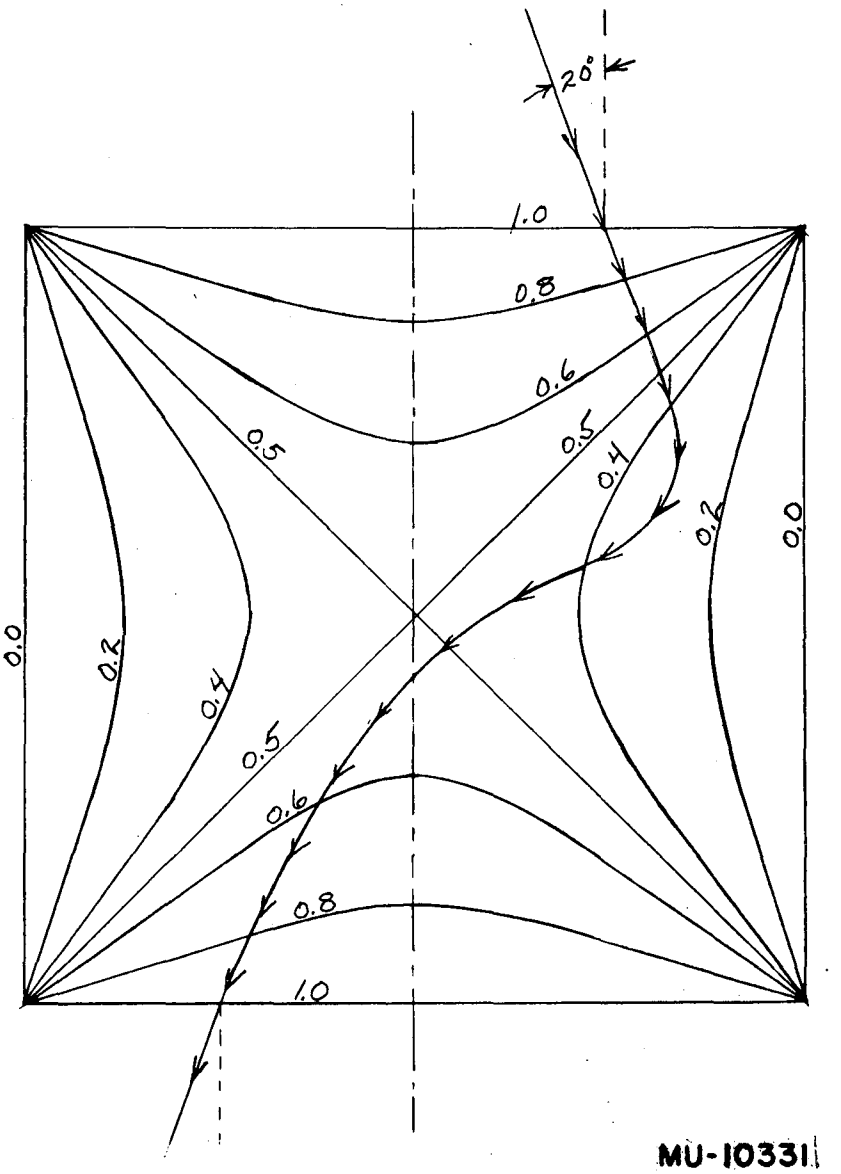

Fig. 12. Off-center electron trajectory in two-dimensional square box.

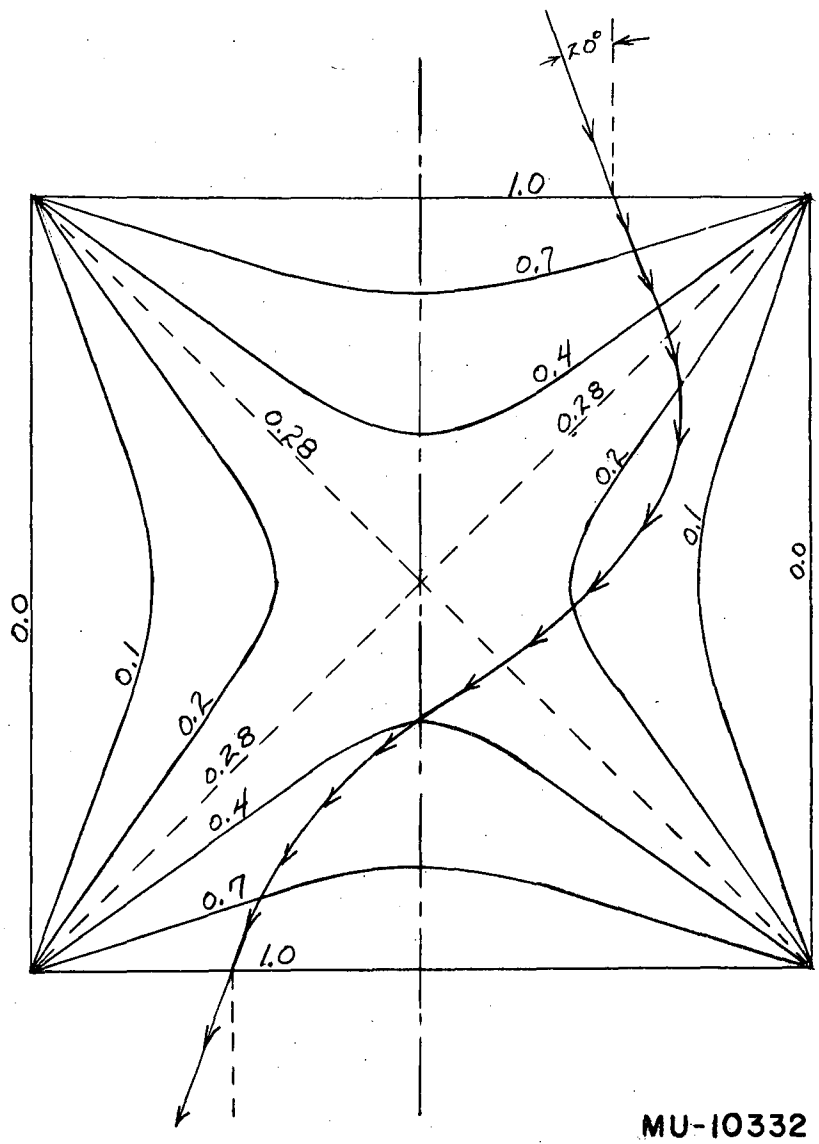

Fig. 13. Off-center electron trajectory in cylindrical box.

The conclusions that we may draw from the foregoing discussion may be stated as follows. Although the rubber-membrane model does not give a precise analogue of the potential distribution in a three-dimensional axially symmetric electrode structure, it is of use to obtain a semiquantitative picture of electron trajectory behavior that may be expected in this type of system. In the particular device under consideration, the rubber-membrane model was used principally as a method of choosing between several possible shapes for the reflector.

In Figs. 14 and 15 we see the four different shapes that were tried. Of all the shapes, reflector D in Fig. 15 seemed to be the most satisfactory. This was based on the determination of the largest angle of emergence of the electrons from G_2 that were consistently passed through the grid G_4 and into the first dynode of the electron multiplier. In all cases, the electron energy was made equal to the potential of G_2 and G_4, which were the same in the membrane analogue.

From the experiments on the reflector D and from the calculations that have been detailed, it is possible to find the approximate effect of the reflector on the selectivity of the system and to arrive at a predicted value of the geometry and of the selectivity of the complete apparatus.

D. Electron-Detection System

a. General Discussion

There are several means of recording or detecting beta particles in beta spectrometers. In the flat magnetic spectrograph, the spectrum is registered on a photographic plate and the relative blackening of the plate is translated into an electron-intensity distribution by means of a microphotometer. Investigations have shown that the relative blackening of the photographic plate is a linear function of electron intensity.

Almost all magnetic beta-ray spectrometers use a thin-window Geiger-Müller counter as the detecting device. When studies of low-energy spectra are made, it is necessary that the window be close to 100% transparent to the lowest energy electrons to be detected. The window must let in the electrons, but it must also keep the gas filling of the G-M tube out of the spectrometer as much as possible. (See

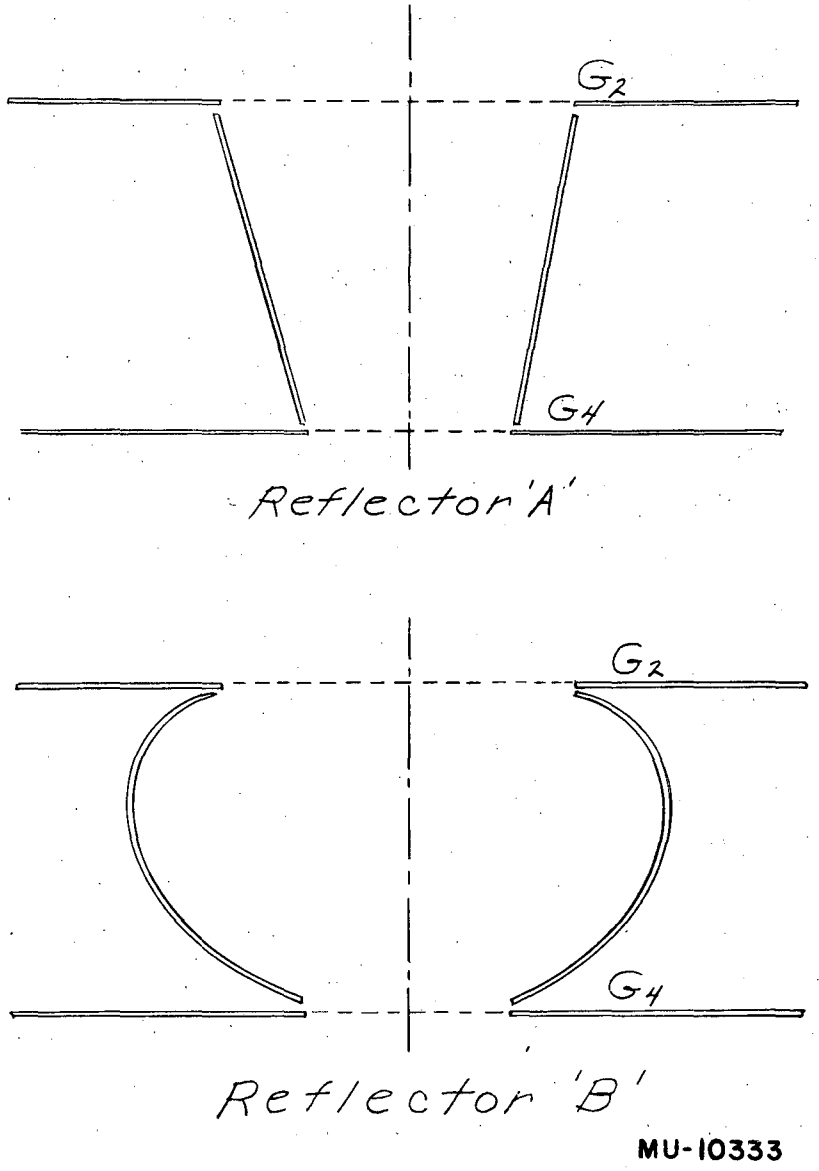

Fig. 14. Two possible reflector shapes, A and B.

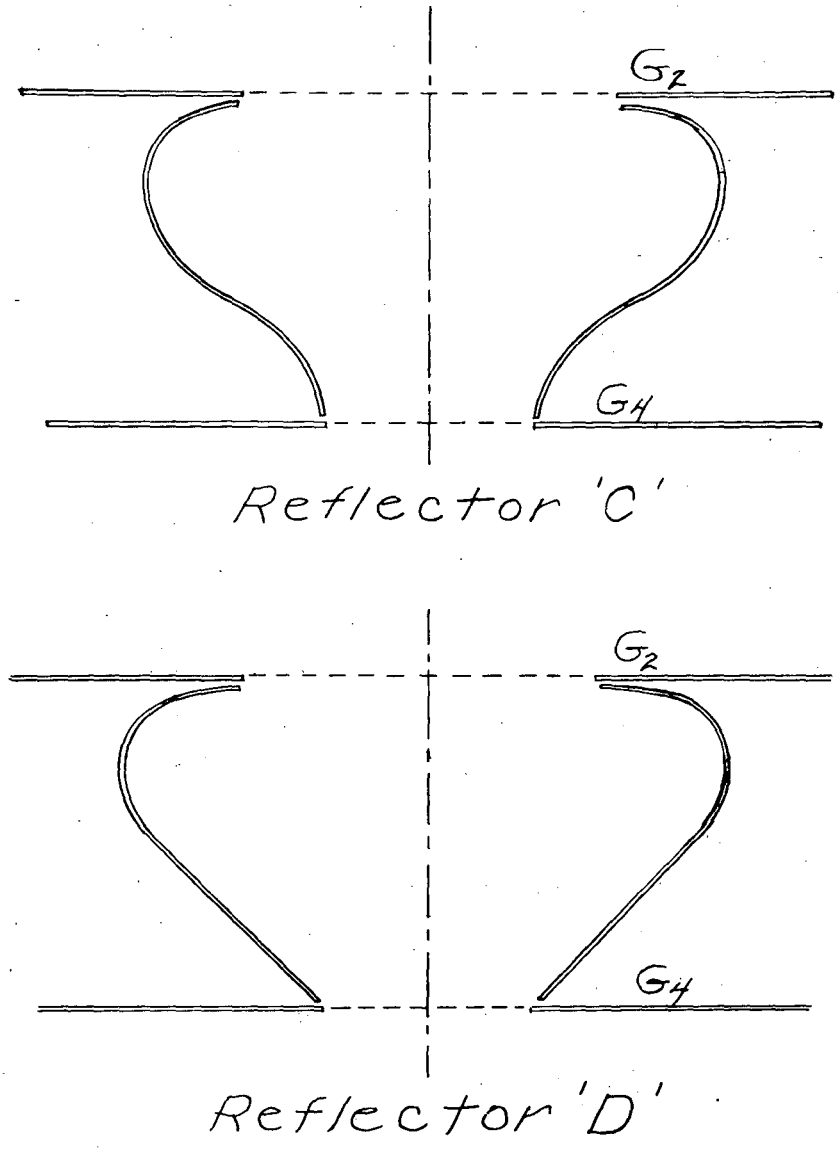

MU-10334

Fig. 15. Two possible reflector shapes, C and D.

Cook,[31] page 16.) Since very special window techniques must be applied if G-M tubes are to be used for low-energy beta particles (less than 10 to 15 kev), it would seem desirable to use some other kind of detector in this energy range.

Scintillation counters, which consist of an anthracene or a stilbene crystal and a photomultiplier tube, can be used as beta-particle detectors. In magnetic spectrometers, the photomultiplier tube must be used with a lucite light tube so that the multiplier tube can be removed from the immediate vicinity of the magnetic field of the spectrometer. In addition, it must be carefully shielded in the best possible manner from stray fields by the use of a mu-metal magnetic shield.

The use of a scintillation detector for low-energy electron detection requires the use of postacceleration. That is to say, an accelerating voltage is applied to the electrons after they have been selected by the magnetic field. The scintillation crystals require an energy of 50 to 100 kev if they are to be used efficiently as a light source in connection with the photomultiplier tube.

The secondary electron multiplier may be used for the detection of low-energy beta particles.[32,37] It offers the advantage over a G-M tube of not requiring gas for its operation, and we can thus dispense with the necessity of constructing thin windows.

b. Secondary Electron Multiplier

The phenomenon of secondary electron emission (see Spangenberg,[23] pages 48-57, and Wooldridge[34]) provides an ideal method for the detection of low-energy beta particles. The secondary-electron multiplier[27,33] is especially adapted to beta spectrometers using electrostatic fields instead of magnetic fields, since the presence of a magnetic field interferes with the proper operation of the multiplier.

The characteristics required of a secondary multiplier to be used in a beta spectrometer are somewhat different from those required of a multiplier to be used in a photomultiplier tube. The principal characteristic of the multiplier that is necessary in the double-retarding-field spectrometer under discussion is a relative insensitivity to deterioration of the dynode surfaces when exposed to the atmosphere for a few hours. This exposure unavoidably takes place when the radioactive sample is changed or inserted into the sample holder. Also it

is necessary that no further activation of the multiplier surfaces be required after the initial processing of the dynodes.

The best-known secondary-electron emitters are those that consist of an oxide film on a metal electrode base. Many combinations have been used.[23, 32, 35] By far the best secondary emission surface is cesium oxide on a silver base. The maximum emission ratio is of the order of 10 secondaries for each primary electron when the primary electron energy is about 400 to 500 electron volts. This sensitive surface, however, cannot be exposed to the atmosphere after its formation without a complete deterioration of its sensitivity due to oxygen contamination.

Beryllium-copper alloy has been used for this purpose, and satisfactory characteristics have been reported.[32] The latest alloy to be used for secondary-emission work, and the one used here, consists of 98.3% silver and 1.7% magnesium. When given the proper heat treatment, this alloy forms a magnesium oxide film on the surface of the metal, which has good secondary-emission characteristics.[36]

Another desirable characteristic for the secondary emitter used to detect beta particles is a relatively large thermal work function. This characteristic is necessary to insure that the background count due to the emission of thermal electrons from the first dynode of the multiplier be low. The silver-magnesium alloy seems to have a sufficiently high work function to satisfy this requirement.

Before assembly, the 18 dynodes of the multiplier were processed in a manner similar to that described by Rapaport.[36] The carefully cleaned dynodes were enclosed in an evacuated glass tube of sufficient size to contain the large first dynode, and the tube was placed in a small electric resistance furnace. The dynodes were subjected to a temperature of about 550° C for a few hours under a vacuum of better than 10^{-6} mm Hg. Water vapor was then introduced at a pressure of approximately 10^{-4} mm Hg by means of a dry-ice-and-acetone cold trap. The tube was then sealed off under the high vacuum, and the dynodes remained in this tube until assembled.

The electrodes showed a shiny yellow film over their entire surface. This is the magnesium oxide film, which is formed on the

surface of the alloy by means of the water vapor that was introduced into the system during the processing period.

Figure 16 gives a general picture of the secondary-electron multiplier that was used in this equipment. Figure 17 shows the multiplier installed in the spectrometer. It is to be noted that the first two dynodes are of the unfocused box type of dynode, such as is used in the DuMont photomultiplier tubes, and the remaining dynode arrangement is of the focused type described by Zworikin and Rajchman[27] and used by RCA in their photomultiplier tubes.

Rappaport[36] reports a secondary emission ratio of about 3.5 secondaries for each primary electron for the silver-magnesium alloy when processed as we have described. Although not stated, it is to be presumed that this figure was determined at the optimum primary electron energy, which is about 400 electron volts for practically all secondary-emission surfaces. The circuit components in this equipment were designed for a value of 400 volts between dynodes. This then requires a total of 18 multiplied by 400 or 7,200 volts, which may be supplied to the multiplier for maximum gain.

The over-all gain of the multiplier with the value of electron multiplication given above is, for 18 stages, 3.5^{18} or approximately 6.2×10^9. This is 6,200,000,000, a fantastically large and unnecessarily high gain. Of course, the gain can be reduced as necessary by reducing the voltage applied to the multiplier. The large theoretical gain allows us to maintain the desired gain by voltage adjustment even in the face of appreciable deterioration of the sensitive surfaces of the dynodes, which takes place every time we expose them to the atmosphere.

Figure 18 shows the circuit diagram of the secondary-electron multiplier and associated circuits. Note the double string of resistors used as a divider for tapping off the various dynode voltages. This was done primarily to simplify the circuit layout and avoid cross-over wiring between stages, which might have distorted the electric fields existing between the dynodes. This arrangement can also be observed in the photograph of the multiplier in Fig. 17.

The output of the multiplier is connected directly to the grid of a cathode follower stage, which is mounted close to the multiplier inside the vacuum tank. The output of the cathode follower feeds a

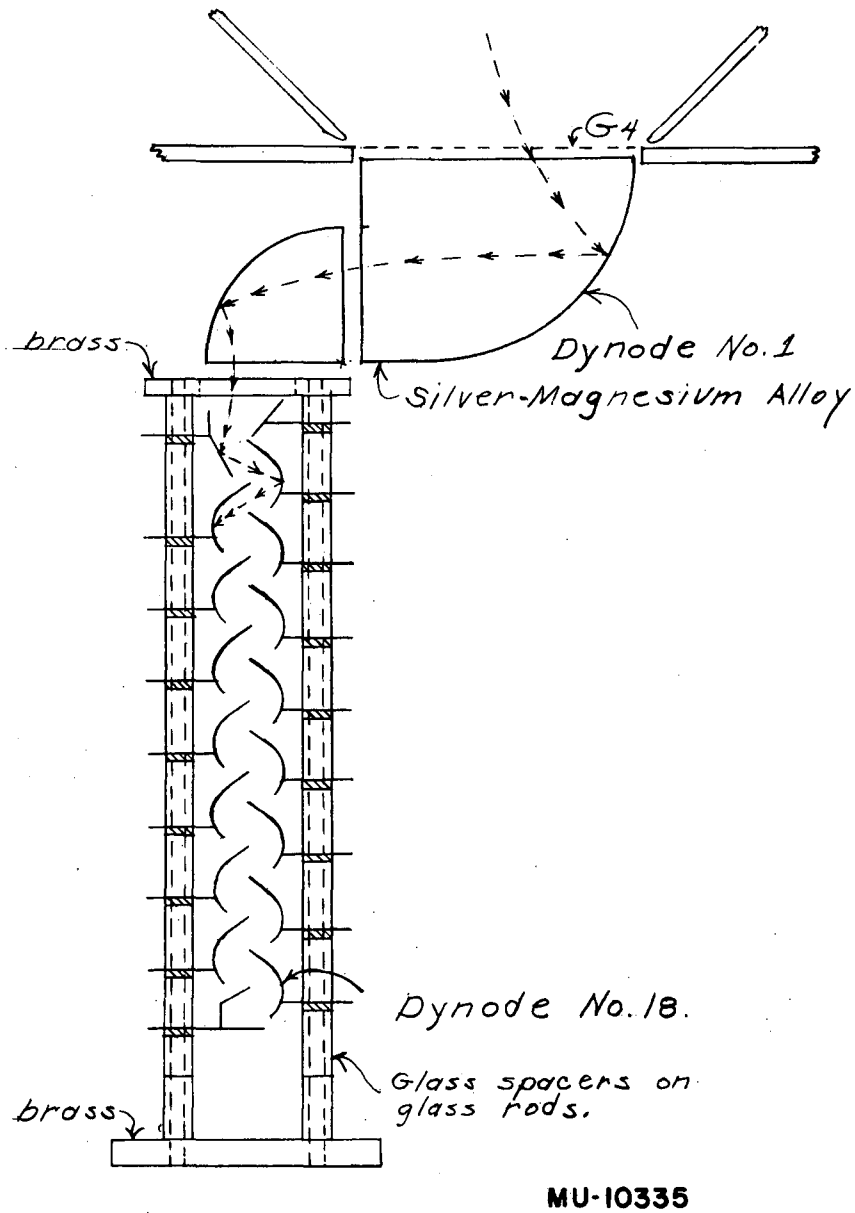

Fig. 16. Secondary-electron multiplier.

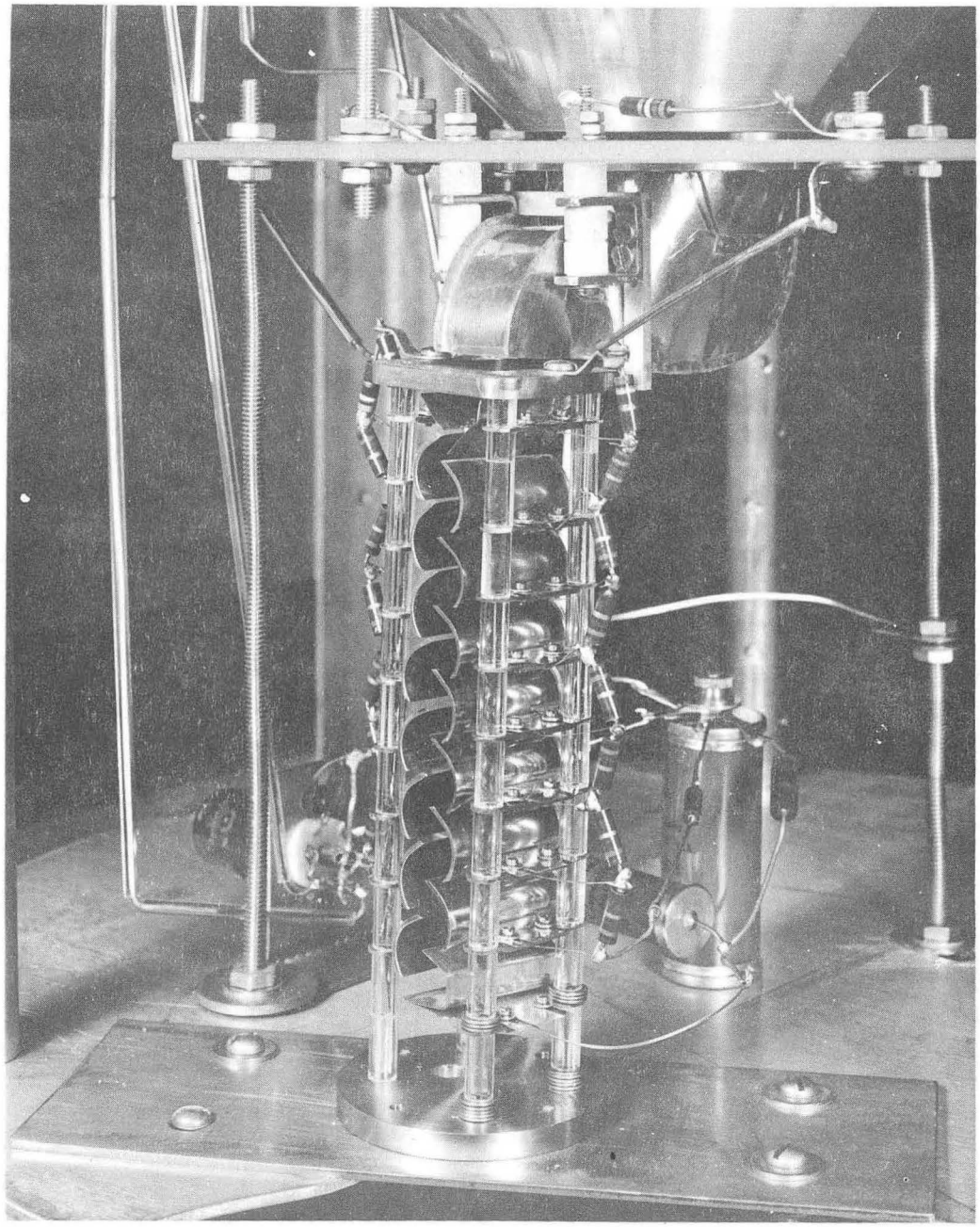

ZN-1399

Fig. 17. Electron multiplier.

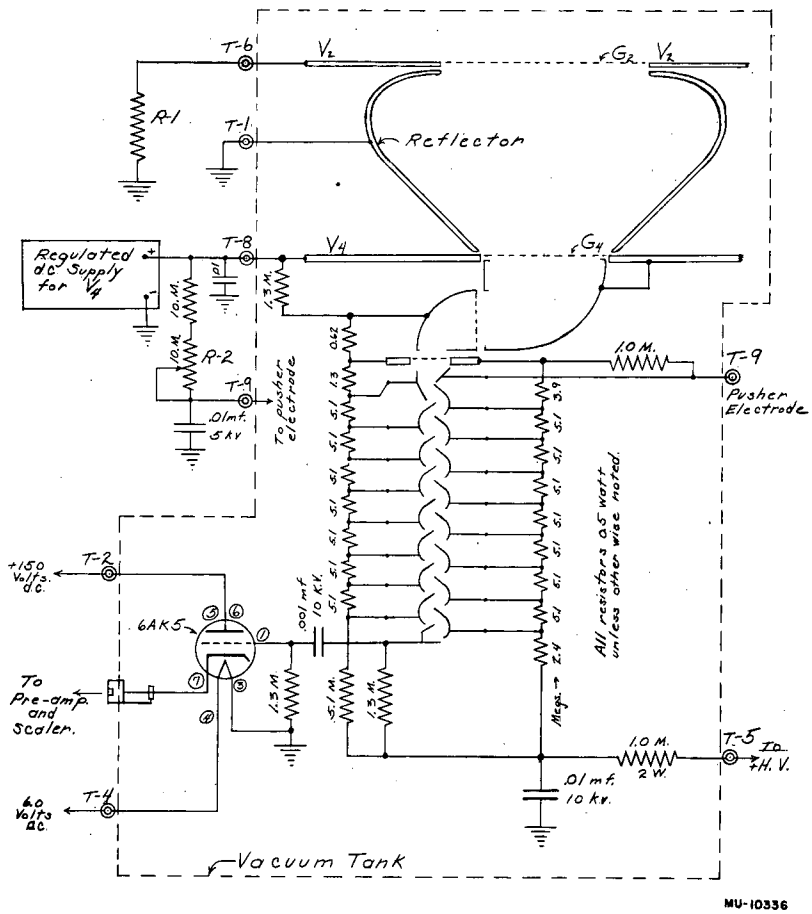

Fig. 18. Circuit diagram for secondary-electron multiplier.

coaxial cable, which connects to a preamplifier outside the vacuum tank. From the preamplifier output the signal goes into a conventional amplifier scaler.

It is of interest to consider the question of what is the desired minimum gain that we must have in the secondary electron multiplier in order to be above the noise level of the amplifier system. The height of the voltage pulse produced in the output of the electron multiplier by the electron avalanche induced by one electron on the first dynode depends not on the terminating resistance but on the terminating capacitance, according to the basic formula,

$$Q = C\,V \qquad \text{or} \qquad n\,e = C\,V$$

where n = number of electrons in the output pulse or the gain of the multiplier,

$e = 1.6 \times 10^{-19}$ coulombs, the charge on an electron,

C = output capacitance in farads,

V = desired minimum voltage on the grid of the cathode follower.

Just for round figures in our results, assume that the output capacitance is 16×10^{-12} farad (a reasonable value) and that it is desired to have a minimum voltage of 0.001 volt on the grid of the cathode follower. Solving the above equation for n gives a value of 10^5 for our minimum gain requirement. This, then, allows for a considerable deterioration of the multiplier elements before new dynodes need be installed.

E. Noise Sources

In spectrometers, as in all devices used for measuring any quantity, there arises the problem of the signal-to-noise ratio. Noise may be defined as any phenomenon or disturbance of the system that may eventually find its way into the indicating or recording device and which is not part of the signal that we wish to measure or detect. For a reliable measurement, the noise must be considerably less than the signal being measured.

Let us define noise in the beta spectrometer as consisting of any phenomenon that causes a count to be recorded on the scaler but does not represent a beta emission from the radioactive sample in the range being measured. The desired signal must exceed the noise by

a factor of 5 or 10 in order that reliable data be obtained. There are several possible sources of noise in the DRF spectrometer under discussion.

a. Gamma and Alpha Radiations

Many radioactive samples that may be measured in a beta spectrometer have gamma and alpha radiations as well as the beta radiations to be measured. One of the problems that needs to be explored is the sensitivity of a silver-magnesium-alloy secondary-electron multiplier to gamma rays striking the first dynode. The gamma rays are electromagnetic radiations similar to light but of a much higher frequency. When they strike a metal surface, they may cause a photoelectron to be emitted from the metal. If the metal happens to be the first dynode of the secondary-electron multiplier, then we have a noise count in the system recording device.

In order to find out something about the conversion coefficient of gamma rays to counts in the electron multiplier, a series of experiments was carried out. A DuMont 2-inch photomultiplier tube, which uses silver-magnesium-alloy dynodes in its construction, was arranged so that the first dynode was radiated by gamma rays of known energy and intensity. The photo tube was arranged so that no counts could come through the system unless they were caused by electrons from the first dynode. The tube itself was carefully blacked out so that light could not reach any of the elements inside the glass envelope.

A series of 15-minute counts was made with and without gamma rays from the two radioactive samples employed. A conversion coefficient was calculated for each energy of gamma rays used. This conversion coefficient was defined as the ratio of the counts due to the gamma rays divided by the total number of gamma rays incident on the first dynode of the photomultiplier tube. The two radioactive gamma sources used were cobalt-60 with gamma energies of 1.17 and 1.33 Mev and americium-241 with gamma radiations of 0.06 Mev. The results are plotted in Fig. 19.

From Fig. 19 we see that the conversion coefficient is very small in the range investigated. It is of the order of one part in 4,000, or one electron liberated, on the average, for every 4,000 incident

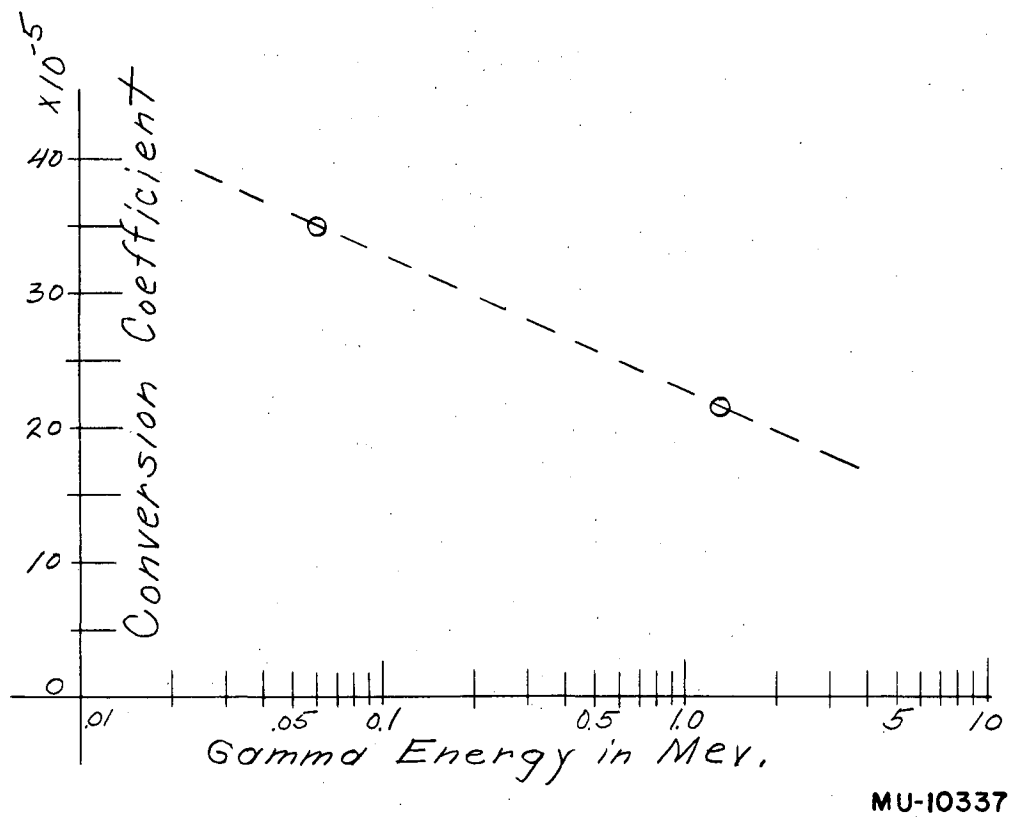

Fig. 19. Gamma-to-electron conversion coefficient in multiplier tube.

gamma radiation quanta. Of course, two points are hardly a sufficient number of points to draw a curve, so that the dotted straight line drawn through the two points should not be taken too seriously. From these results, though, we may conclude that the noise counts due to gamma radiation on the secondary multiplier should introduce relatively small errors in the data.

Alpha-particle radiations cannot enter the multiplier system directly, because of the trap T, as shown in Fig. 2, but they may give rise to noise by striking any metallic part and causing electron emission, which may appear as noise in the system. If they strike the collector plate P (Fig. 2), the emitted electrons tend to return to P, which is maintained at a large positive potential.

b. Other Sources of Noise

The principal sources of unwanted secondary emission are all the metallic parts situated above the plane of the grid G_1 except the collector plate P. High-energy electrons striking the metallic parts could liberate secondary electrons, which would be accelerated downward to the plane of G_1. These electrons may get into the secondary multiplier and be counted. Secondary electrons emitted from the collector plate P must overcome a positive potential equal to 1/5 of V_1 in order to be able to pass through G_1 and get into the counting system.

The principal source of thermal emission that puts noise into the system is the first dynode of the secondary-electron multiplier. This emission is determined by the temperature of the dynode and could be reduced by operating the multiplier at lower temperatures. However, no provision has been made in the design of the apparatus discussed here for cooling the dynodes. The room-temperature emission of the silver-magnesium alloy had been found to be low, and consequently its effect should not be large.

The thermal-emission effect can be minimized by making sure that the operating conditions are such that the energy of the incident electrons on the first dynode is the optimum value for maximum secondary-emission ratio. This allows us to discriminate against thermal pulses due to single electrons from the first dynode, since the desired pulses are of greater magnitude.

The onset of strong field emission in any part of the system, and especially in the upper part of the spectrometer, would cause the liberation of electrons from the various metal parts and these electrons might get into the counting system and appear as noise.

F. Theoretical Transmission and Resolution

We can determine the theoretical transmission of the DRF spectrometer with the aid of Curves "c" and "d" of Fig. 3. Although this set of curves was drawn for a particular value of the parameter q, we have seen from our previous discussion that the Curve "c," which is the limit placed on our transmission by the finite dimensions of grid G_2, is practically independent of q and n. Also, Curve "d" is independent of q since Eq. (10), from which it is plotted, does not contain q. Curve "d" represents the lower angular emission limit due to the finite dimensions of the sample holder.

We may define transmission of the beta spectrometer as the following ratio:

$$\text{Transmission} = \frac{\text{area on sphere of solid angle of collection}}{\text{total area of sphere}} .$$

For small angles of collection we may easily show that the transmission can be written as

$$\text{Transmission} = \frac{\tan^2 \theta}{4} ,$$

where $\theta = 1/2$ solid angle of collection.

From Fig. 3, we see that the upper angular limit is about 4.5°, and the lower limit is about 1.6°. Therefore the transmission is as follows

$$\text{Transmission} = \frac{\tan^2 4.5^\circ}{4} - \frac{\tan^2 1.6^\circ}{4} = 0.001367 .$$

Expressed as a percentage this is 0.1367%.

We now undertake to determine the resolution of the DRF spectrometer. There is a certain amount of approximation involved, since we do not know exactly what the selectivity characteristics of the electron focusing device or reflector are.

We assume a value of q equal to 0.96, which is the same value as we have assumed in Figs. 3, 5, and 6, and also we assume that the potentials of G_2 and G_4 are the same (see Fig. 7). We must make an estimate of the saddle-point potential as a percentage of the potentials of G_2 and G_4. From our calculations on the cylindrical box, we found the saddle-point potential to be 28% of the voltage on the ends of the box. For lack of any better information, let us assume for round figures that the saddle-point potential is about 30%. This means that all electrons that do not have at least 70% of the electron volt energy of the grid G_2 are rejected by the reflector (Fig. 20).

From our experiments with the rubber-membrane, ball-bearing analogue, we know that for a given electron volt energy there is a critical angle of entry into the reflector which, if exceeded, results in rejection of the electron by the reflector. In the two-dimensional model of the reflector, this angle was found to be about 30° from the axis of symmetry when the electron entered on the extreme edge of grid G_2. It is reasonable to suppose that the critical angle is somewhat less in the axially symmetric case, owing to the lower saddle-point potential of the field.

Let us take as the critical angle at the edge of G_2 a value of 23° with the axis of symmetry when the parameter n is equal to 1.00. We choose this value of angle of entrance to the reflector because it gives us a sharp-peaked selectivity or resolution curve. We now have two points on the transmission characteristic of the electron reflector, points "A" and "B" (Fig. 20). In order to get the intermediate points, we draw a straight line between these two points, as shown on Fig. 20.

The rejection characteristics of the reflector for electrons having a value of n larger than 1.00 are not of extreme importance, since these higher-energy electrons are rejected in the first retarding field of the spectrometer as shown by Curve "a" of Fig. 20 (also Figs. 3 and 5).

The results of the above are plotted in Fig. 21. A second curve is also plotted in Fig. 21 to show the results of choosing a different value of saddle-point potential and angle of entrance. Taking the half-maximum width of the curves, we see that the theoretical resolution

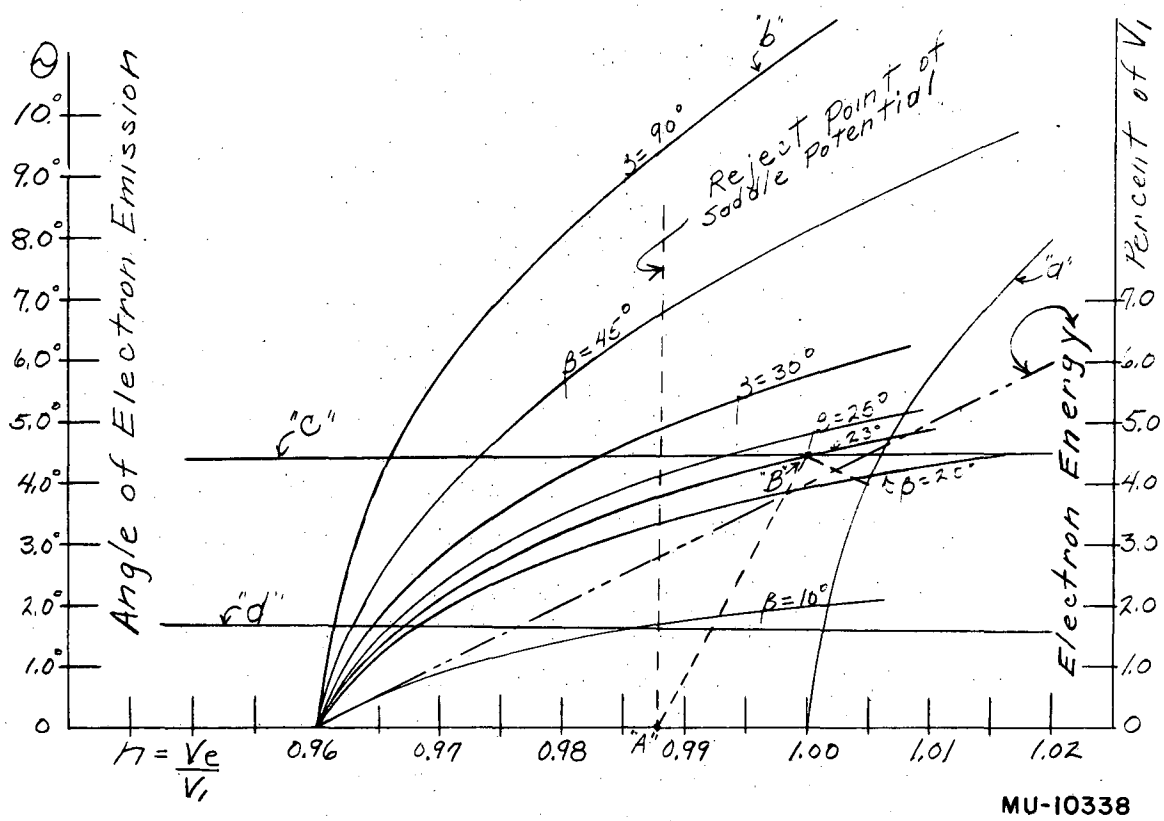

Fig. 20. Method of finding resolution.

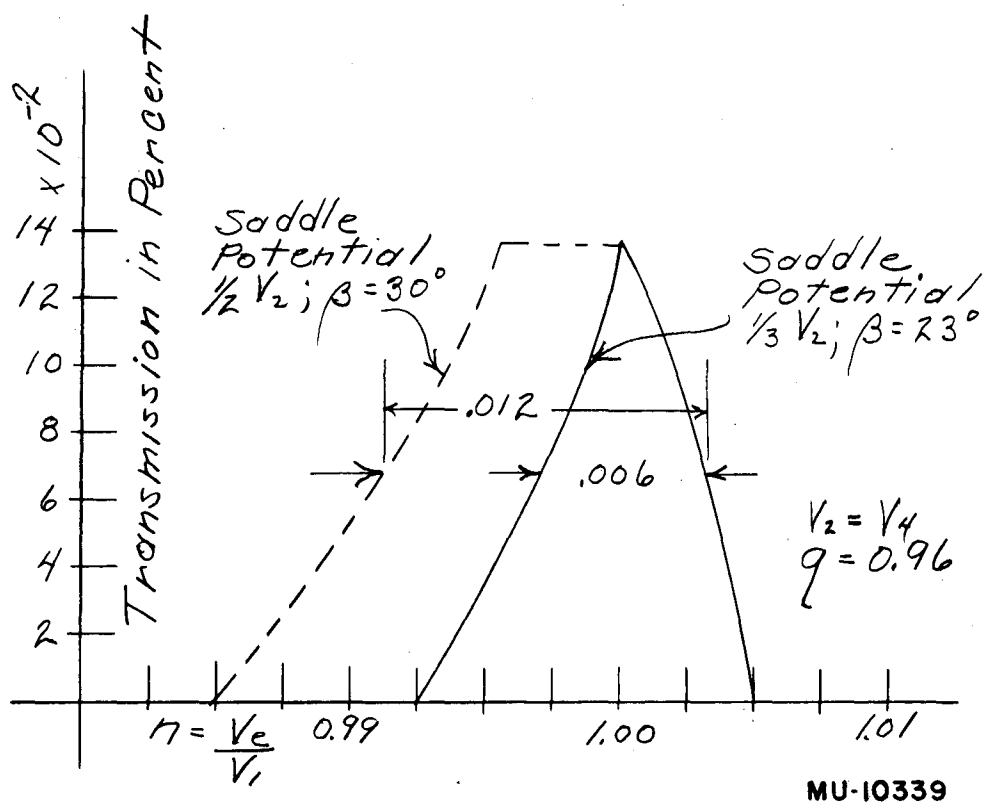

Fig. 21. Theoretical resolution--energy basis.

may be anywhere from 1.2 to 0.6% on an energy basis. This is 0.6% to 0.3% on a momentum basis, for beta particles of energies less than 50 kev (Reference 14, page 951).

We have taken the data on many different magnetic spectrometers from Reference 14 and plotted these data in Fig. 22. The diagonal lines are lines of constant figure of merit, which is defined as the ratio of transmission (on a momentum basis to resolution) of the spectrometers. For comparison purposes, we have also plotted the values of transmission and resolution that we have calculated for the DRF spectrometer.

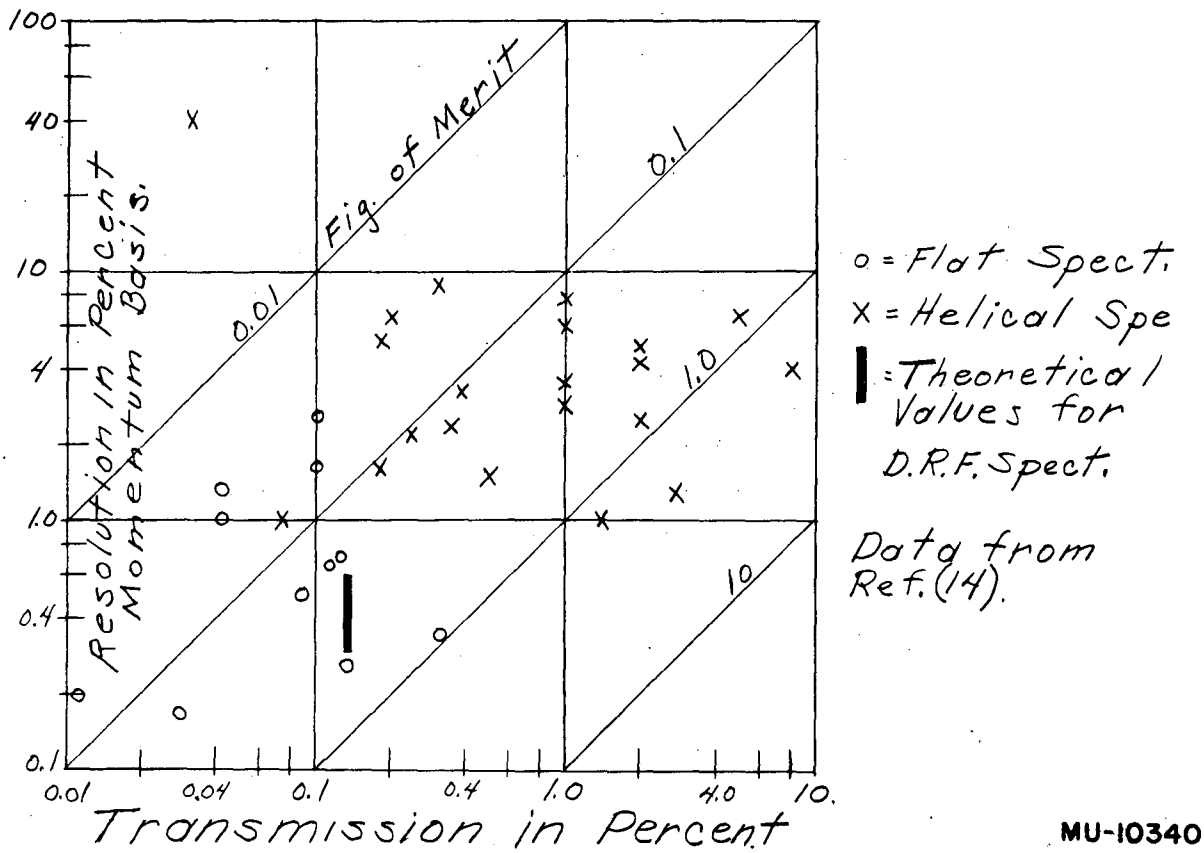

MU-10340

Fig. 22. Comparison of spectrometers.

IV. APPARATUS

A. Spectrometer

a. General Description

The spectrometer was housed in a cylindrical steel vacuum tank whose interior dimensions were 14.5 in. in diameter and 24 in. in height. It will be noted from the photograph, Fig. 23, that the tank was made in two sections. This was of no consequence to the operation of the spectrometer. It was an economy measure in which an available vacuum tank was modified by the addition of the top section in order to perform these experiments.

The entire spectrometer assembly was supported from the top circular cover of the vacuum tank so that it could be lifted out of the tank as a unit (Fig. 24). All the electrical connections to the unit, except one, were made by means of kovar terminals through the steel top that supported the spectrometer. The remaining connection, the high-voltage retarding potential, was made by means of the high-voltage terminal set in the side of the top section of the tank as shown in Fig. 24. When the spectrometer was in place inside the tank, a small phosphor bronze spring attached to the interior end of the high-voltage terminal made contact with the center electrode of the assembly. A vacuumtight, teflon-insulated coaxial fitting installed in the top of the tank provided a connection for the signal output.

All calculations for the double-retarding-field spectrometer were based on the trajectories of electrons moving in uniform electric fields. In order to provide a uniform retarding electric field, the spectrometer was provided with a series of four equally spaced guard rings on both sides of the sample-holder grid G_1. (See the photograph, Fig. 25, and the drawing, Fig. 26.) The guard rings were held at a fixed fraction of the high potential by means of a potential divider. For each retarding field, this divider consisted of five 200-megohm IRC type MVX high-voltage resistors connected as shown in Fig. 26. This divider was contained inside the vacuum tank, and the resistors were supported by the guard rings as shown in the photograph of Fig. 25.

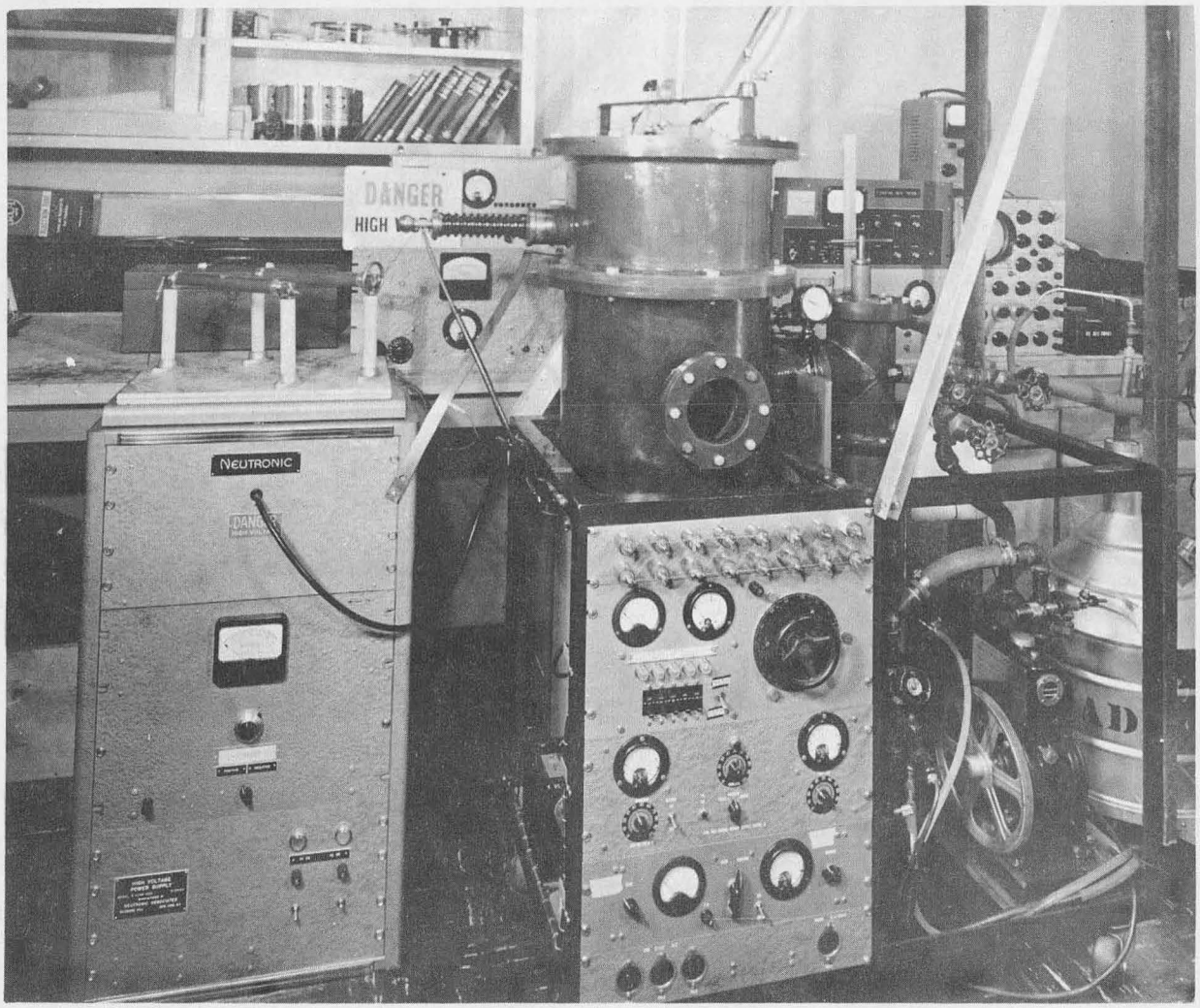

ZN-1397

Fig. 23. General view of equipment.

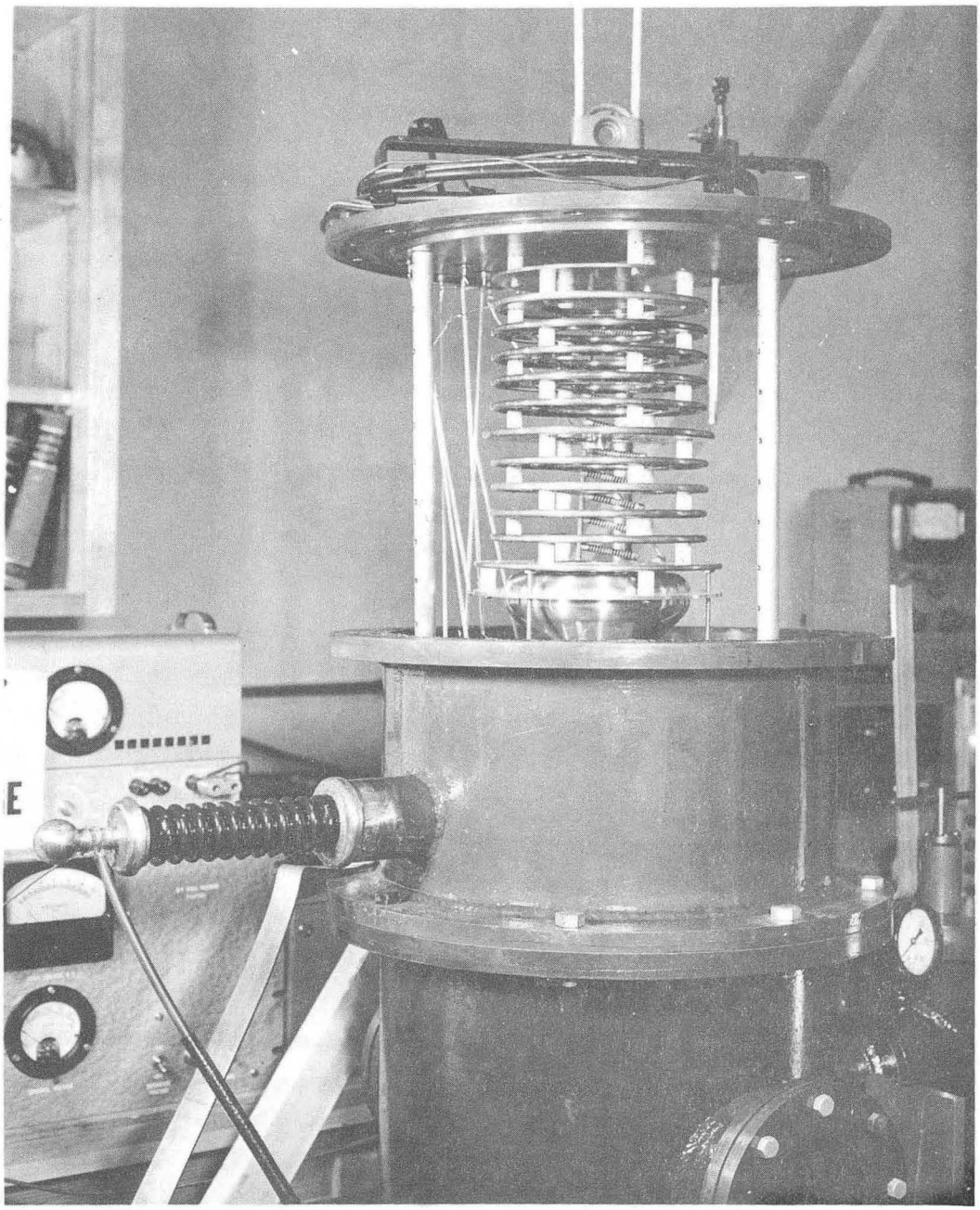

ZN-1401

Fig. 24. Spectrometer being removed from tank.

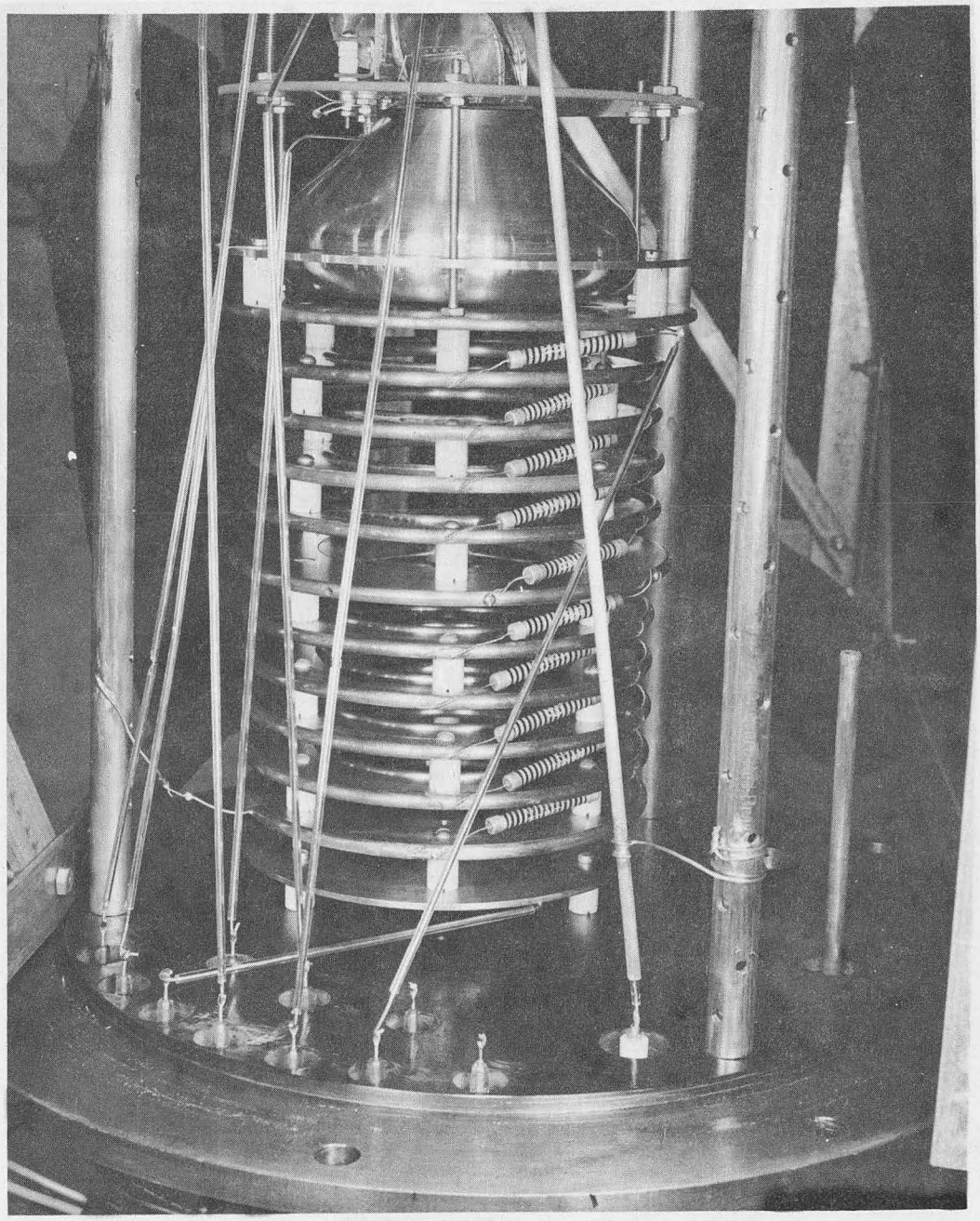

ZN-1398

Fig. 25. Close-up of spectrometer, showing details of construction.

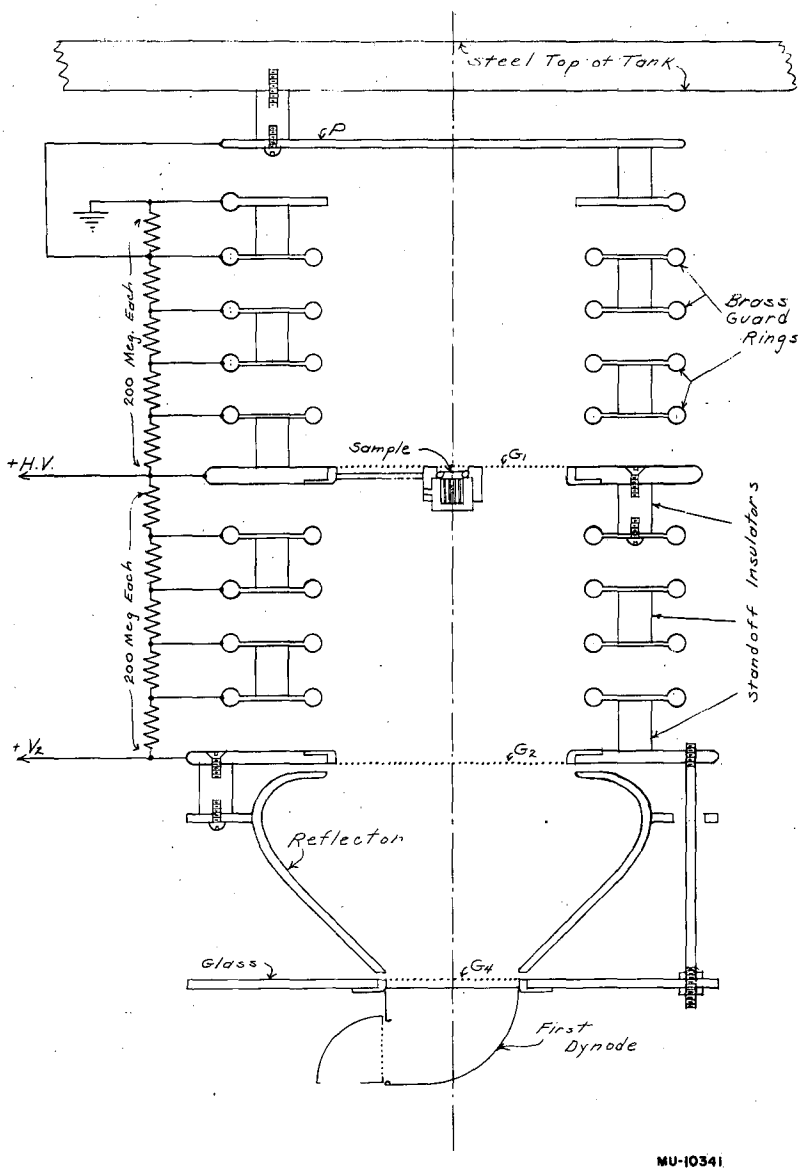

Fig. 26. Spectrometer assembly.

The guard rings were separated with small threaded standoff insulators 3/4 in. long and 1/2 in. in diameter, as shown in Fig. 26. All the rings and all other electrodes of the spectrometer were provided with 1/4-in.-diameter corona rings to avoid local field concentrations, which might result in voltage breakdown between rings or other electrodes.

As the entire spectrometer assembly was suspended from the top of the steel vacuum tank so that it could be removed as a unit, the principal mechanical strain was taken by the 3/4-in.-long standoff insulators, which are threaded at both ends for No. 8-32 machine screws. These standoff insulators provide both mechanical strength for the assembly and electrical insulation between the successive electrodes. The insulators between the guard rings were called upon to withstand a voltage equal to approximately one-fifth of the main high-voltage retarding potential. One of the high-voltage limitations of the equipment was the voltage breakdown of these guard-ring insulators.

Additional mechanical strength and rigidity were provided by three additional supports from the top of the tank. These consisted of three 1/4-in. brass rods, threaded into the top of the tank. Each rod was enclosed in a 3/4-in. brass tube. The rods and tubes supported an 1/8-in. aluminum plate at the bottom of the spectrometer assembly. The aluminum bottom plate supported mechanically the secondary-electron multiplier, the cathode-follower-tube socket, and associated equipment. Rigidity for the main spectrometer assembly was provided by two rods, which tied together the bottom plate and the glass supporting plate of grid G_4.

O-rings used on all demountable joints of the spectrometer served to make vacuumtight seals at these points.

b. Sample Holder

The radioactive sample holder was placed in the center of grid G_1. It was held in position by three nonmagnetic stainless steel rods extending from the circular edges of the grid structure and supporting part "a" of the sample holder in the exact center of the grid. (See Figs. 26 and 27.). Parts "b" and "c" of the sample holder could be removed from the spectrometer for the purpose of changing the radioactive sample (see Fig. 28).

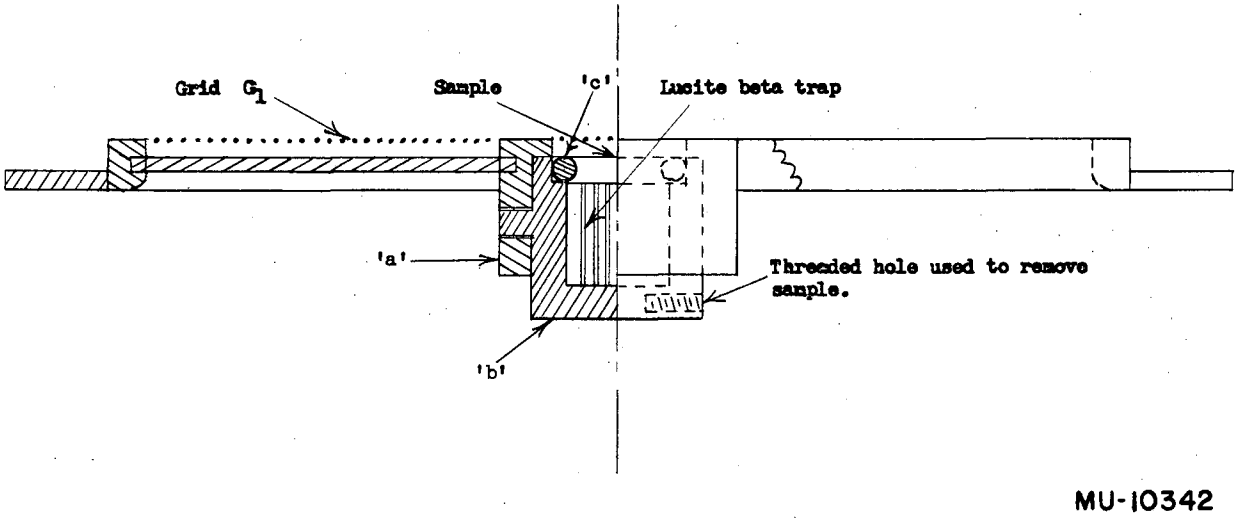

Fig. 27. Drawing of sample holder.

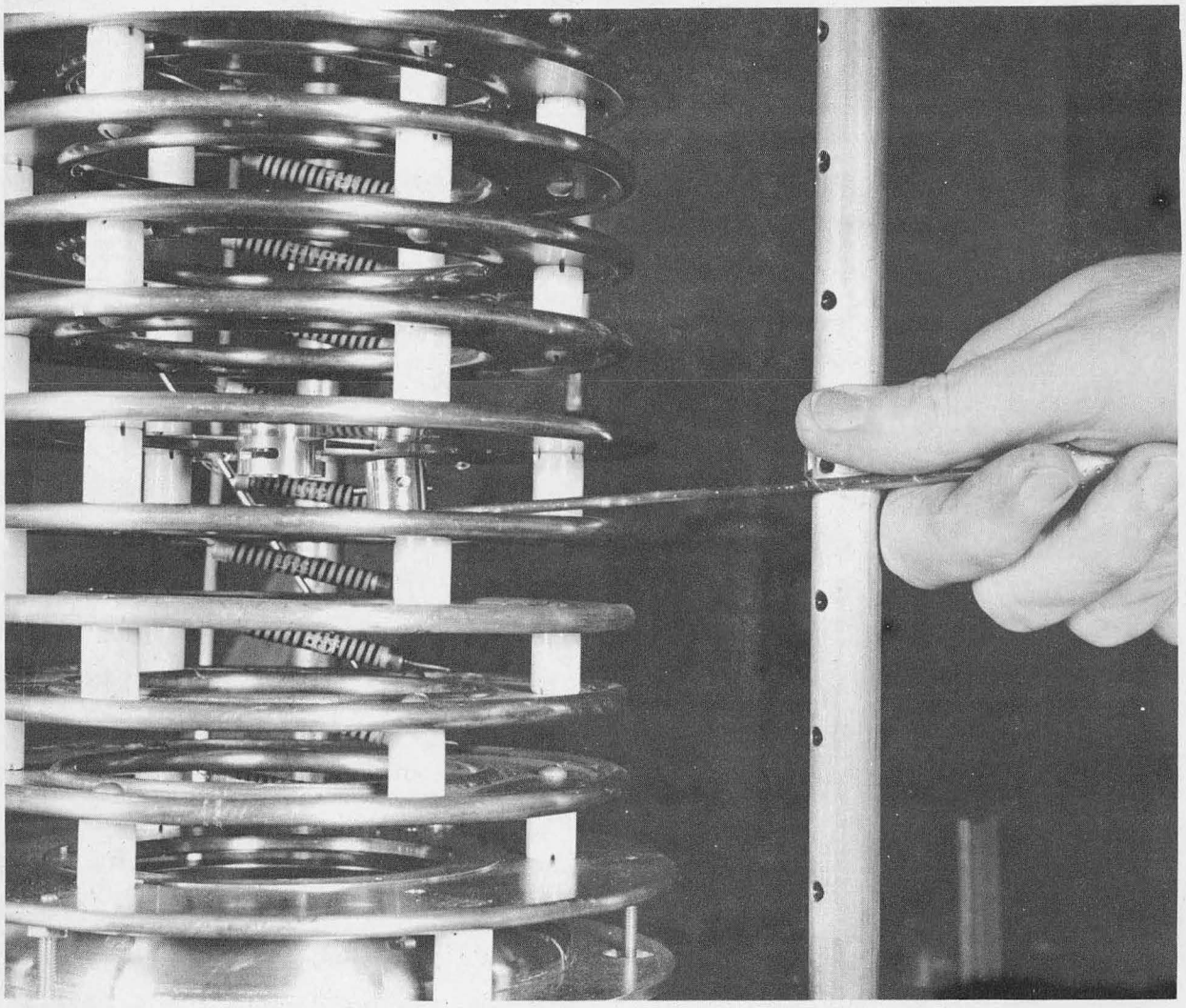

ZN-1400

Fig. 28. Close-up of sample holder being inserted into spectrometer.

A stainless steel rod about 6 in. in length, which was threaded at one end and equipped with a handle on the other, was used as a tool to remove parts "b" and "c" of the sample holder. The threaded end of the steel rod was inserted into the spectrometer between the center electrode and the first guard ring of the bottom section. The threaded end of the rod was inserted into the threaded hole in the side of part "b," and the rod was screwed in as far as possible so that the sample holder was firmly attached to the handle. Then by rotating the holder through an angle of about 60° to disengage the lugs, one could lower the sample holder by about 1/2 in. by manipulation of the rod. It was then possible to pull out the sample holder between the high-voltage electrode and the guard ring.

Extreme care had to be exercised at this point so as not to allow the sample holder to rotate and dump out the ring part "c," which actually held the radioactive sample. Also great care had to be taken to avoid contact between the sample and the G_1 electrode. The clearance was a matter of about 3/32 in. It was necessary to make several practice runs on the above procedure with no radioactive sample in the holder in order to get the feel of the operation.

The radioactive sample was deposited on a thin plastic film supported by the ring electrode part "c" of the sample holder. The ring was 1/2 in. in diameter and allowed the active sample to occupy a circular spot about 1/4 in. in diameter. The ring and all the other parts of the sample holder were made of aluminum.

In low-energy beta-particle spectroscopy, it is essential that all possible precautions be taken to avoid spectrum distortion. Various phenomena such as source charging, absorption and energy loss due to finite source thickness, and backscattering due to the source mounting are of importance in the investigation of the low-energy range of beta partices.[38,39,40,41,42]

To avoid source charging, it was necessary that the source-mounting film be made conducting by the evaporation of a thin layer of aluminum on the underside of the plastic film source backing. In order that excessive backscattering be avoided, the plastic film and its conducting coat of aluminum were made as thin as possible, but with sufficient mechanical strength to allow the preparation and to support the radioactive sample.

In order to avoid excessive backscattering due to the aluminum mounting part "b," a beta-particle trap was inserted just behind the sample. This trap was in the form of a lucite rod drilled with many fine holes in a vertical or axial direction. The theory here was that lucite has a low atomic number Z and consequently causes a minimum of backscattering. Also, the probability of backscattering of electrons along the line of the axis would be reduced if the primary electron entered one of the holes in the lucite trap.

B. Auxiliary Equipment

a. Power Supplies

The retarding-field high-voltage supply used in these experiments was built by Neutronic Associates of Richmond Hill, New York. The rated voltage of the unit was 5 to 50 kv, and it could supply approximately 500 μa of current to the load.

The unit was a half-wave, voltage-doubler, radiofrequency type of power supply. The output voltage was regulated electronically by negative feedback from a voltage divider across the output terminals. This feedback served to control the screen-grid potentials of the radiofrequency oscillator and amplifiers. The reference voltage for the regulator was provided by a 300-v Eveready Mini-max dry battery.

The measured regulation of the power supply was of the order of one part in two thousand at an output voltage of about 50 kv and with constant load. The regulation at lower voltages became progressively poorer, and the regulation system became somewhat unstable at voltages of the order of 3 to 4 kv. Micrometer adjustment of the output voltage was provided by a ten-turn helipot mounted on the panel of the unit.

Accurate measurement of the output voltage was made possible by the use of carefully calibrated IRC-type MVO high-voltage resistors and a Weston Model 622, one-half-percent accuracy mirror-scale microammeter. The type MVO 30-w resistors were operated at dissipation of less than one watt in order to avoid changes of resistance due to heating effects. Additional accuracy in the measurement of voltage was obtained by the use of a potentiometer to measure the voltage drop across a precision wire-wound resistor placed in series with the type MVO resistors and the microammeter.

A second high-voltage power supply was required to furnish the potential necessary to operate the 18-stage secondary-electron multiplier. This supply was designed and built by the Radiation Laboratory. It was a radiofrequency type of high-voltage supply with a rated output voltage of 10 kv. The regulation of the output voltage was considerably better than the Neutronic power supply just described. The nominal regulation was of the order of ± 2 v at any voltage from 4 to 10 kv. The excellent regulation of this voltage assured a constant gain of the secondary-electron multiplier.

Other low-voltage regulated power supplies used were conventional in design and construction.

b. Preamplifier, Scaler, and Count Rate Meter

A special preamplifier was designed and built for use in this equipment. The preamplifier was required to raise the level of the signal from the cathode follower inside the tank a sufficient amount to operate the scaler used in the experiment. The output polarity of the pulse from the secondary-electron multiplier was negative, and the polarity required by the scaler was positive. Thus the preamplifier was required to invert as well as amplify the pulse.

The preamplifier was built using four 6AK5 tubes. The gain was variable from 0 to 100, with a frequency response of approximately 300 cycles to 7 megacycles. The circuit was of standard negative feedback design in which three stages of amplification were included in the feedback loop.

The amplifier scaler used was of standard design, built and used by the Radiation Laboratory in quantity. The scaler was modified by the addition of a 12AU7 tube, which was used as a pulse-level discriminator by biasing the first section of the tube beyond cutoff by variable amounts.

The count-rate meter was designed and built by the Radiation Laboratory (and is shown in drawing No. 3T2893). The meter was modified to read a maximum of 200,000 counts per minute for the experiments with the artificial source (see Chapter V). The minimum count rate was 50 counts per minute.

c. Vacuum System

The pumping system consists of a Distillation Products Corporation type MCF-300-01 oil-diffusion pump, which was backed by a Welch Duo-Seal mechanical pump. The oil-diffusion pump was cooled by means of a continuous flow of tap water through its cooling coils. An electric heater of 450 w provides the heat necessary for the operation of the diffusion pump.

A liquid nitrogen cold trap was necessary to keep the residual oil vapors from the oil diffusion pump out of the rest of the vacuum system. A failure of the liquid nitrogen supply during the course of the experiments allowed oil vapors to be deposited on the sensitive surfaces of the secondary-electron multiplier with the result that the multiplier was completely ruined and had to be replaced.

After the liquid nitrogen failure, an automatic cold trap was installed. A solenoid valve was used in a low-pressure air line to supply air pressure to a liquid nitrogen tank. The valve was controlled by an Eagle Signal Corporation Flexo-Pulse timer so that the liquid nitrogen was introduced into the trap of the spectrometer at regular intervals as required.

A vacuum valve arrangement placed between the liquid air trap and the rest of the system permitted the admission of air at atmospheric pressure into the main tank while the diffusion pump was still in operation.

The low-pressure measurements were made with an RCA-1949 ion gauge tube and a modified Radiation Laboratory ion gauge power supply. The modifications of the ion gauge power supply consisted of the addition of a circuit that would remove the filament current from the ion gauge tube if the pressure increased beyond 10^{-4} mm Hg. This circuit was fast enough so that air could be admitted to the main tank at any speed without endangering the filament of the ion gauge tube.

The minimum pressure attainable under ordinary conditions was about 3×10^{-6} mm Hg when the equipment described above was used. Unfortunately, a small and not easily repairable leak developed in the liquid nitrogen trap itself, which increased the normal operating pressure to about 10^{-5} mm Hg.

The mean free path of a nitrogen molecule at a pressure of 10^{-5} mm Hg is given as 6.5 meters on page 95 of Strong.[43] The mean free path of an electron moving through a gas is greater than that of the gas by a factor of 5.66 (Bachman,[44] page 94). This means that an electron moving in nitrogen gas at a pressure of 10^{-5} mm Hg has a mean free path of 36.8 meters. When we consider that the maximum path length of an electron in the spectrometer is only about 0.5 meter, we may assume that a pressure of 10^{-5} mm Hg is not too high for the proper operation of this device.

V. EXPERIMENTAL

A. Monokinetic Source

a. Introduction

In order to test the general operation of the double-retarding-field spectrometer before a radioactive source was introduced, a thermal filament source was used. This source consisted of a small pure tungsten filament mounted in the same position in the spectrometer as the radioactive source was to occupy.

This filament was mounted in the center of grid G_1, in an insulating lavite cup, as shown in Fig. 29. The cup was suspended in a metal ring supported in the center of the grid by three small hollow brass tubes. The center section of the grid structure was made so that it could be removed for the purpose of connecting, inserting, or renewing the filament as necessary.

The outside of the lavite insulating cup was silver plated by an evaporation process. The coating was sufficiently heavy so that it was a good conductor of electricity. This coating made connection with the grid ring on which it was supported and thus it was at the same potential as the rest of the grid structure. This arrangement effectively shielded the filament from the rest of the field in the spectrometer.

The connections to the filament were made through two of the three hollow brass supporting tubes. Insulation for the conductors was provided by glass tubing inserted through a hole in the high-voltage electrode and through the brass supporting tubes to the filament in the center of the grid.

The operating current of the filament was about 0.80 amp and was provided by a 1.5-v battery consisting of twelve No. 6 dry cells in parallel. The use of batteries for this purpose provided an extremely steady current, which was very necessary in this experiment. A series of three rheostats provided coarse, medium, and fine variations in the filament current. In order to measure the current accurately, a potentiometer was used to measure the voltage drop across a standard resistor connected in series with the filament.

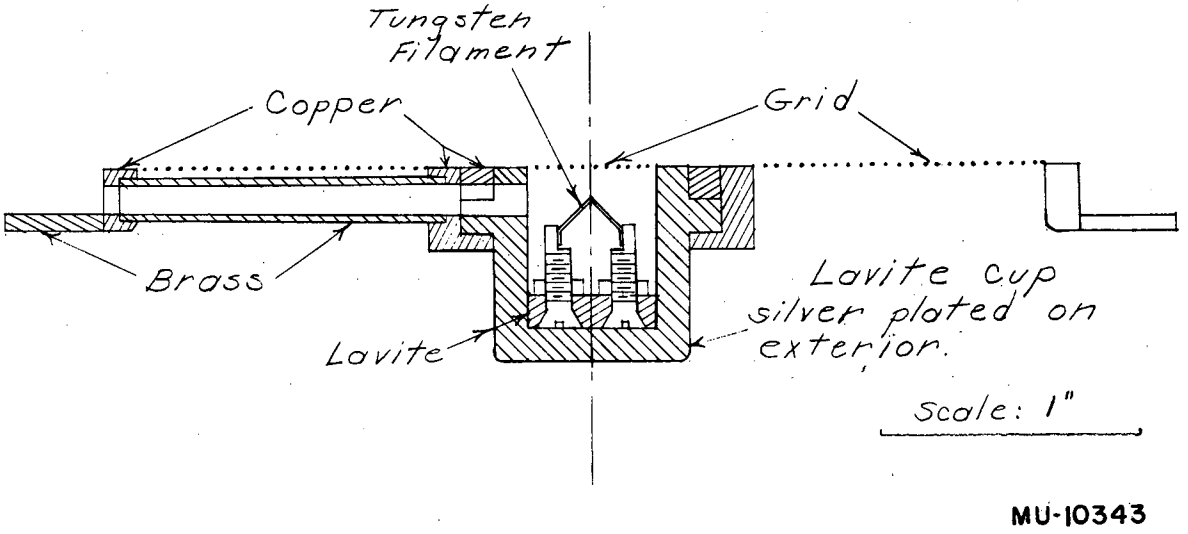

Fig. 29. Artificial beta-ray source.

The electrons from the thermal source are accelerated by the electric field existing between the grid and the filament. The strength of this field depends on the voltage between the two elements and may be controlled externally as shown in the diagram of connections in Fig. 30. The filament was connected to a source of dc potential V_s, which could be made positive or negative by a reversing switch as shown in the figure. This allows us to vary the parameter n, which is the ratio between the energy of the beta particle in electron volts and the potential V_1:

$$n = V_e/V_1$$

In the case of the thermal source, the potential V_e is the difference between the potential of the grid G_1 and the potential of the filament, both taken with respect to ground. Thus we have the equation

$$n = \frac{V_1 - V_s}{V_1} . \qquad (16)$$

We see from this expression that if V_s is negative with respect to ground, the value of n will be greater than 1.00, and if V_s is positive with respect to ground, the value of the parameter n will be less than 1.00.

There are several problems that arise in the use of a thermally emitting filament to take the place of a radioactive source of beta particles in a device of this nature. One of these is the problem of obtaining a quantity of electrons from the filament of the same order of magnitude as from a radioactive beta source of practical intensity. Any amount of current that may be measured on an ordinary type of current meter is far too large, as we see in the following discussion.

From Cork,[45] page 396, we note that a current of 1 ampere represents 6.2×10^{18} electrons passing a given point in one second of time. An ordinary d'Arsonval indicating type of current instrument indicates a minimum of about 10^{-6} ampere. This amounts to about 6.2×10^{12} electrons per second.

Leaving this topic for a moment, let us consider the recording or indicating instrumentation to be used in this test. In order to facilitate the measurements of the characteristics of the spectrometer by means of the artificial source of beta particles, a count-rate meter was

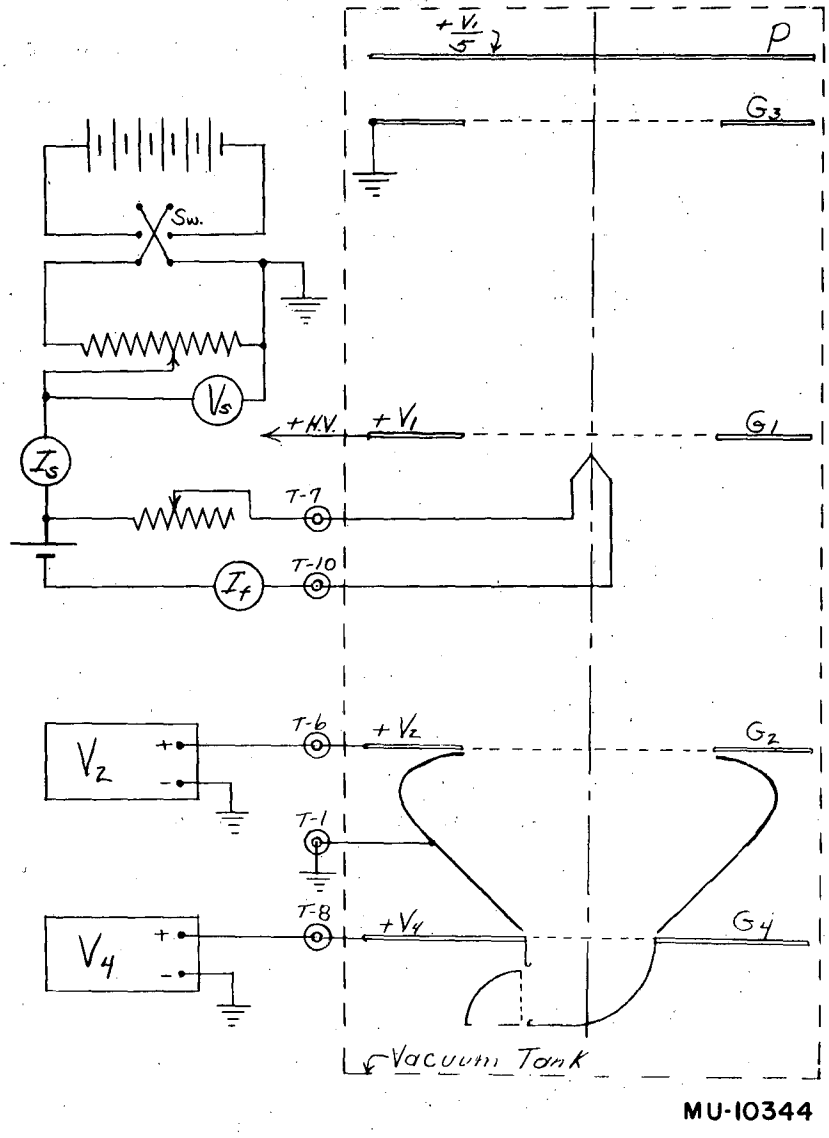

Fig. 30. Circuit diagram for artificial beta source.

substituted for the scaler. This count-rate meter was modified so that it could count a maximum of 2×10^5 counts per minute. This was, incidentally, ten times the maximum counting rate originally designed into the instrument. Thus we see that the artificial-source filament may have a maximum emission current, so that, at the peak of the resolution curve, the counting rate is not more than 2×10^5 counts per minute or approximately 3.3×10^3 counts per second. Therefore, not more than 3.3×10^3 electrons per second may strike the first dynode of the secondary-electron multiplier when the value of n is equal to 1.00, in order not to exceed the capabilities of the counting system.

Now the question is, how many electrons does the filament have to emit per second in order that 3.3×10^3 electrons per second may strike the first dynode of the secondary-electron multiplier. To get a rough idea of the order of magnitude of emission current necessary, we may use the value of the theoretical transmission derived in Chapter III and include a factor of 0.9^3 to account for the partial transmission of the three 90-percent-open-area grids through which the electrons must pass. This may easily be shown to give us a value of the order of magnitude of 10^{-12} ampere of emission current necessary from the filament. This is a very small current, and it is down in the range where it takes electrometer techniques to measure it.

Another problem that arises in the use of the thermal source to simulate a radioactive source of beta particles is the problem of constancy of emission from the filament. It was found that the measured emission from a pure tungsten filament was not a single-valued function of filament current. It seemed to depend on time, accelerating voltage, and temperature history of the emitter as well as on filament current. Figure 31 shows some results of measuring the relation between filament current and emission current. Thus it is impossible to return to a previously determined filament current and expect to have the same emission current as before.

The situation, however, with respect to constancy of emission is not as bad as may be inferred from the previous discussion. By allowing a warm-up time of about 20 min and momentarily increasing the filament current by about 20% above the normal operating value, one may obtain curves as shown in Fig. 32. Figure 32 shows the relation

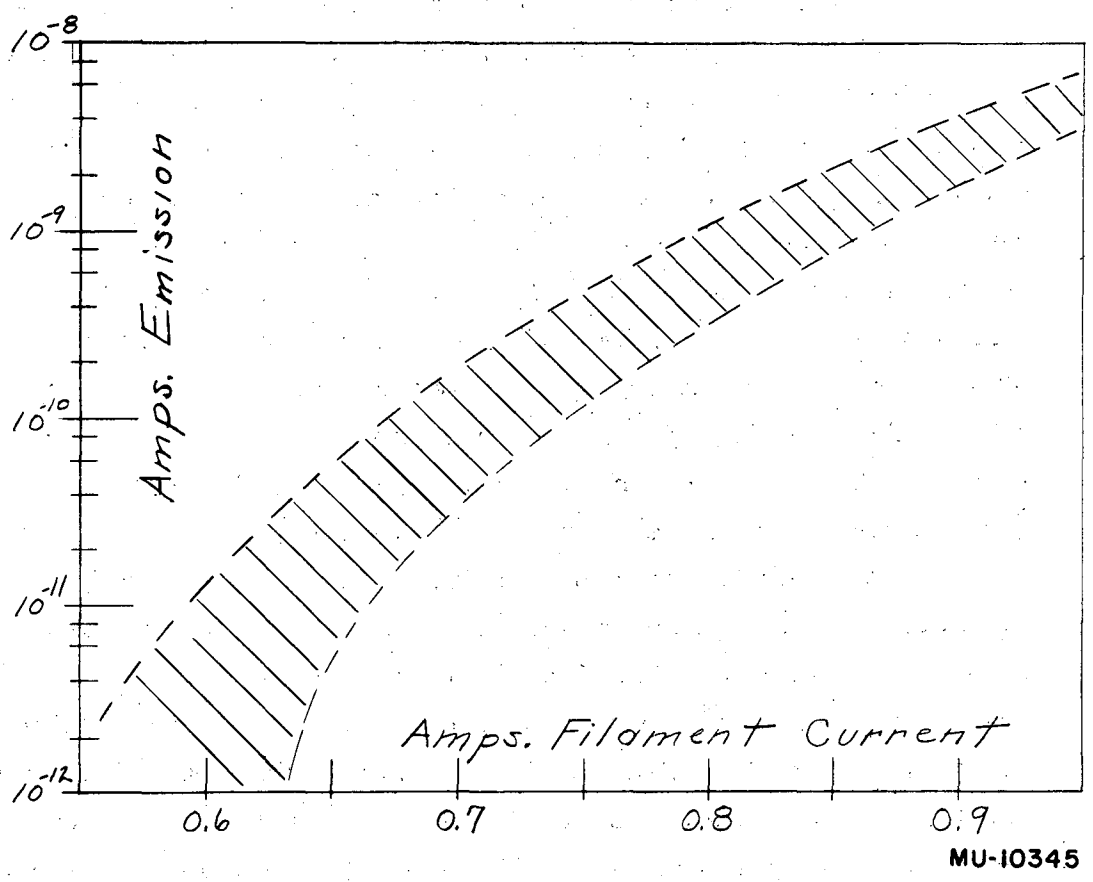

Fig. 31. Emission from tungsten beta source.

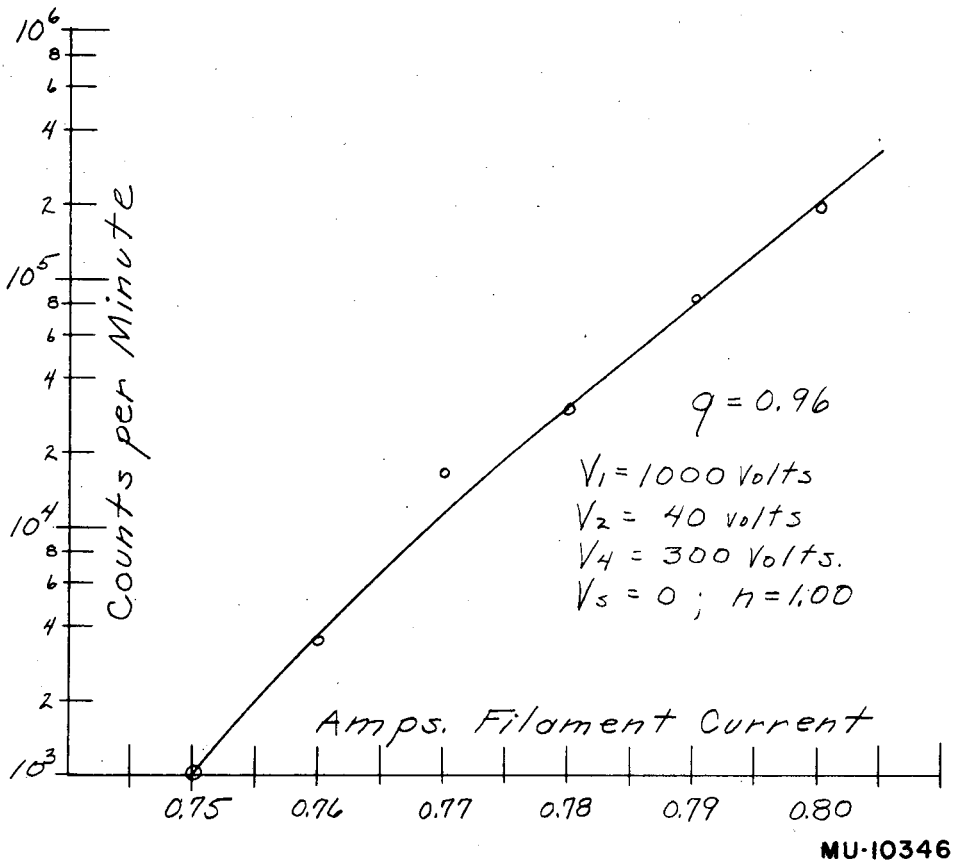

Fig. 32. Relation between artificial-source current and counts per minute.

between the measured counts per minute and filament current under voltage conditions as specified on the figure. The emission is sufficiently stable to be of use if one follows the operating procedure detailed in the next section.

b. Procedure

It was essential to allow all of the equipment to warm up thoroughly before attempting to do any measurements. This was especially true of the count-rate meter, which had a tendency to drift for several hours after being turned on. The filament-source current was turned on some twenty minutes before measurements were to be taken.

The source current was increased to about 1.0 amp for a few minutes then reduced to a value near the operating current of around 0.80 amp. This procedure seemed to degas the filament structure and provide a more stable emission current. Also the stability seemed to be improved if the high voltage to be used in the measurements was applied during the stabilizing period. The phenomenon was probably due to the positive-ion bombardment of the metallic tungsten filament. Thus any changes that were taking place under the positive-ion bombardment would presumably be completed before actual measurements were made.

In this series of experiments, a vacuum of about 10^{-5} mm Hg was attained. It was noted that the filament emission became somewhat more stable as the vacuum improved, showing that positive-ion bombardment had an effect on the emission. It would have been desirable to have a better vacuum but the equipment seemed to have a small leak that could not be located and repaired at the time.

A preliminary adjustment of a special discriminator circuit used in connection with the standard scaler amplifier was made with a high voltage of 3.5 kv applied to the 18-stage secondary-electron multiplier. This adjustment was made so that the count-rate meter recorded a count rate of about 500 counts per minute. These counts were probably mostly thermal counts originating from the low-temperature thermal emission of the first dynode. Since the minimum reading to be taken on the count rate meter was 20,000 counts per minute, the background of 500 counts per minute did not show up in the measurements. This adjustment was essentially a sensitivity adjustment of the system.

During actual measurements the value of V_s, the source-filament bias (see Fig. 30), was held at zero value and the filament current adjusted so that the count-rate meter indicated 200,000 counts per minute. A few minutes' observation of the stability of this reading was necessary. Readings of count rate versus V_s were then made for both positive and negative values of V_s. After every few readings, it was necessary to return to the point $V_s = 0$ in order to check the full-scale reading of the count-rate meter.

c. Results and Conclusions

In the discussion of the theoretical resolution of the spectrometer in Section F of Chapter III, it was assumed that the grids G_2 and G_4 at either end of the electron-focusing device or reflector were at the same potential. In some of the series of measurements that were made here, it was desirable to have the voltage of G_4 considerably higher than that of grid G_2. This was done to give the electrons that strike the first dynode sufficient energy to have a maximum primary-to-secondary electron-emission ratio and to insure that each electron was counted in the output-measuring system.

When the voltage V_4 is larger than V_2, then the selectivity characteristics of the reflector electrode are changed from that determined in Chapter III. The difference in its operation arises from the fact that the saddle-point potential is increased, thus allowing more of the electrons that enter G_2 to pass through the reflector and go out through G_4 to impinge on the first dynode.

Figure 33 shows a measured and a theoretical selectivity curve. The theoretical curve shown in Fig. 33 is not one of the curves from Fig. 21, but a new curve calculated in the same manner as the ones in Fig. 21 but with the assumption that under the conditions of $V_4 = 8V_2$, the saddle-point potential was increased from 30% of the voltage of G_2 to a value of 80% of V_2. Thus only about 20% of the electrons entering G_2 are rejected by the reflector system. (See previous discussion of the theory of reflector rejection in Chapter III.)

It is to be noted that the two curves of Fig. 33 are in good agreement. In Fig. 34, the effect of changing the parameter q on the selectivity of the system is shown. Figure 35 was drawn to show the

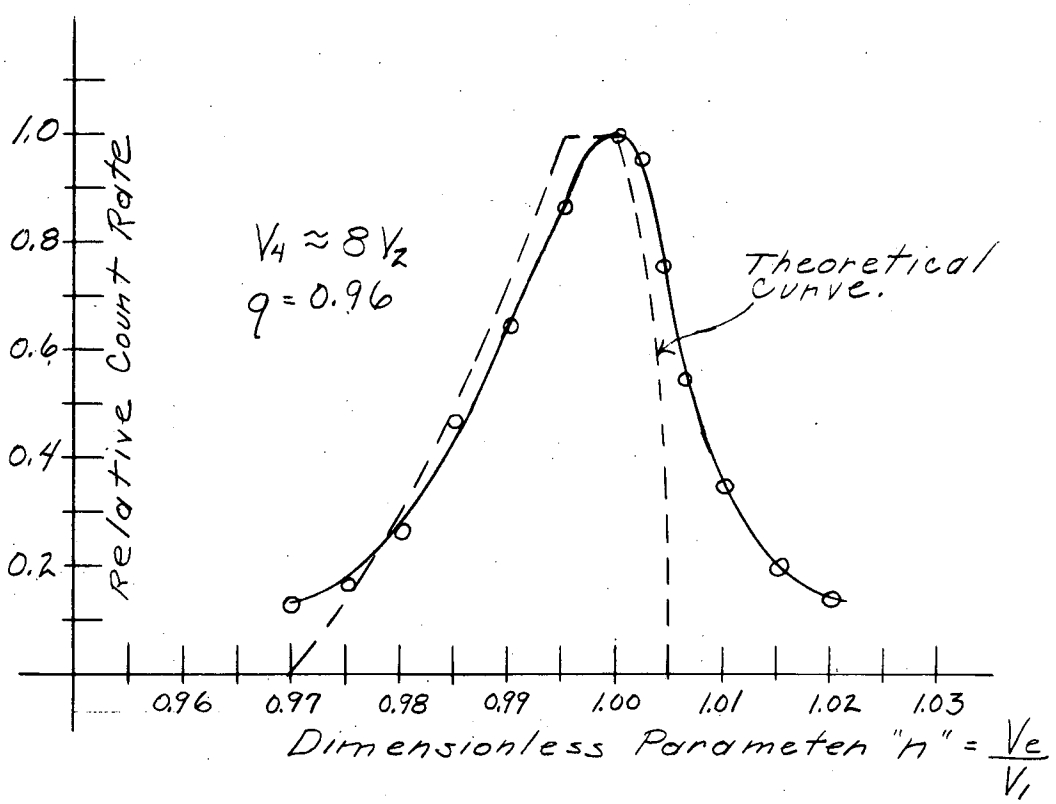

MU-10347

Fig. 33. Theoretical and measured resolution.

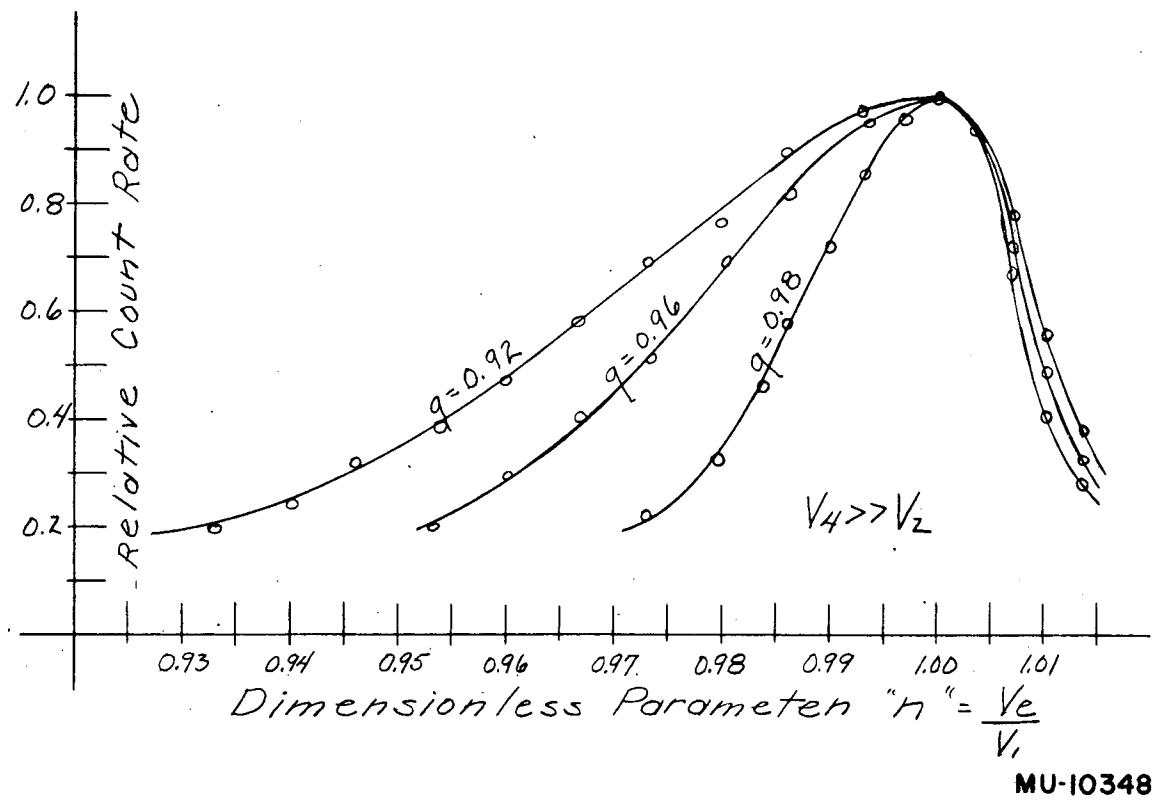

Fig. 34. Effect on resolution of changing q.

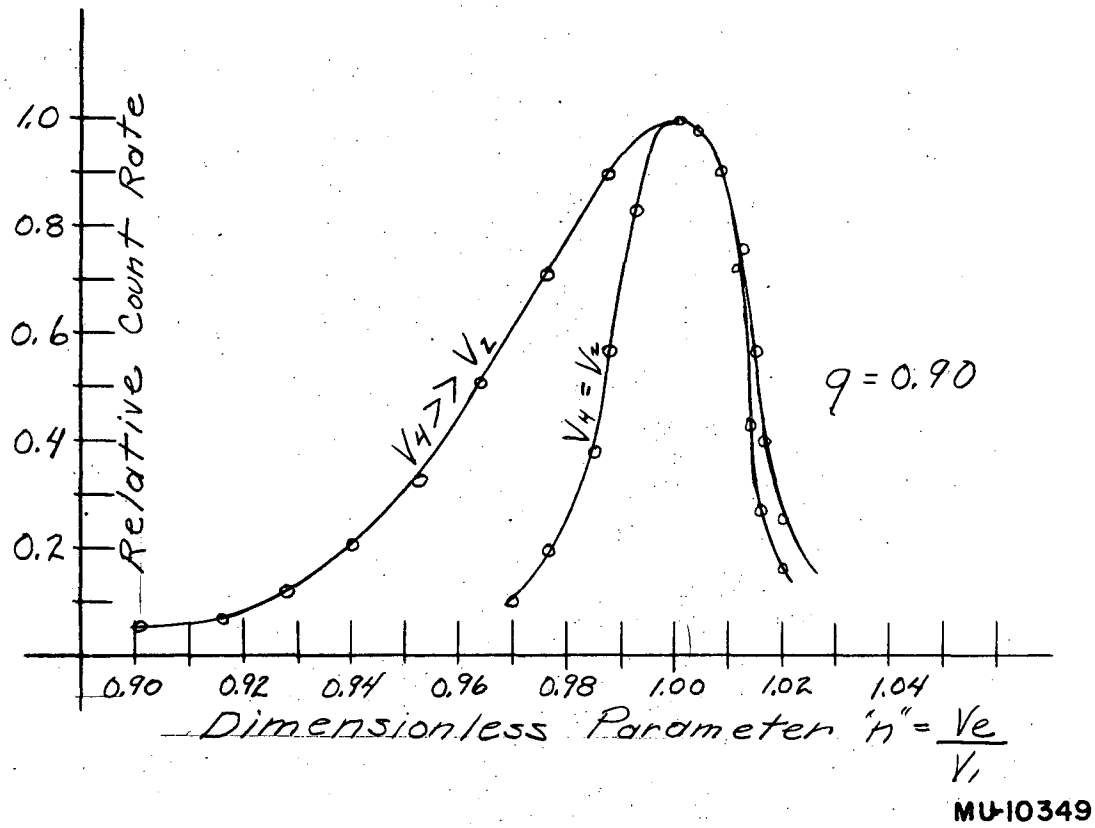

Fig. 35. Effect of voltage V_4 on resolution.

effect on the resolution of changing the voltage V_4 from a value equal to V_2 to a value very much larger than V_2. This figure substantiates the theory of reflector rejection change as discussed in the preceding paragraph.

The results of the measurements made with the artificial source seem to confirm in every important particular the theory of the double-retarding-field electrostatic beta-ray spectrometer as detailed at length in Chapter III.

B. Radioactive Source

a. Introduction

One of the questions that must be considered is what must be the approximate count rate of the sample in order to get reasonably accurate data on this apparatus. In order to get good data, it is necessary to have the signal level larger than the noise level. Thus we should have some idea of this noise level before we can made any calculations as to the size of the sample necessary.

Some of the sources of noise in this equipment have been discussed in Chapter III. Noise may be classified as to origin or as internal and external noise. Internal noise cannot be removed from the output signal by any ordinary methods, but external noise may be reduced if suitable steps are taken.

External noise consists almost entirely of disturbances introduced into the circuits from the ac line. In this equipment, elaborate precautions were taken to prevent outside noise from getting into the high-impedance circuits inside the spectrometer tank. Each input terminal was provided with a noise-filter circuit consisting of a resistor-capacitor filter. In the ac filament circuit of the internal cathode follower, a small rf choke and capacitor was used to filter out disturbances. A number of unused connectors were present in the bottom of the vacuum tank being used for the spectrometer. It was found that these had to be carefully grounded in order to prevent noise from getting into the signal output of the equipment through these connectors.

Theoretically, all ac line disturbances could be eliminated by the proper use of electrostatically shielded ac transformers, radio-frequency line filters, and by the use of elaborately shielded rooms.

This might eliminate disturbances arising outside the shielded room, but precautions would also have to be taken to suppress disturbances arising within the equipment itself. For example, it was observed that a number of counts were introduced into the scaler when the ac solenoid on the air valve of the automatic liquid air-trap filler was operated.

External ac line noise was not of serious consequence in this equipment because of the high gain of the secondary-electron multiplier. This high gain in the multiplier enabled us to set the amplitude-discriminator level at such a point that the amplifier scaler was not very sensitive to ac line noise. However, when measurements of a relatively weak radioactive sample were being made, it was sometimes desirable to arrange to take the data during periods of minimum ac line noise, such as at night or on week ends.

With no radioactive sample present in the sample holder, the retarding voltage on grid G_1 at zero, and a suitable high voltage applied to the secondary multiplier, it is possible to get any count rate whatever on the amplifier scaler by a suitable adjustment of the amplitude discriminator. Forgetting all external noise, these counts arise from the so-called "dark current" of the secondary-electron multiplier. This dark current consists of thermal electrons emitted from the various dynodes of the secondary-electron multiplier, which are then multiplied in the normal manner. They appear as pulses of various heights in the output of the multiplier.

The question of where to set the amplitude discriminator is an important one and a difficult one to answer. It would not be desirable to set the discriminator so that no thermal pulses could come through, since this would surely discriminate against some of the signal pulses also. In the case of the practically unlimited source of beta particles represented by the thermal filament source, the discriminator was set so that the thermal count was 500 counts per minute as measured on the count-rate meter. This would be far too high a setting for a radioactive sample of any practical intensity. The 500 counts per minute was, however, only a small fraction (2.5%) of the smallest signal measurement made in this case. Thus it would seem that the discriminator setting should depend on the strength of the signal to be expected from the radioactive source.

At the beginning of this discussion it was stated that we had to find out something about the noise level before we could calculate the intensity of the radioactive source required for this equipment. Now it seems that we have come to the point where we must know the signal level before we can set the noise level!

Let us now assume that the signal level is to be of the order of 100 counts per minute. Assuming a uniform energy distribution in the beta spectrum, a transmission of about 0.001, and a selectivity of about 1%, we arrive at a very rough figure of about 10^7 counts per minute. It is to be noted that this is a 4π count.

For taking data on radioactive samples, it is desirable to maintain a constant percent resolution throughout the spectrum. At the same time it is necessary to maintain a constant gain in the secondary multiplier. This last condition is required so that all electrons from the sample that get through the grid G_4 give the same height pulse in the output of the secondary multiplier.

In order to maintain a constant resolution, it is necessary to hold q constant and also to hold the ratio V_2/V_4 constant at all points of the spectrum. In order to have a constant gain in the secondary-electron multiplier, we must hold constant the high-voltage supply for the multiplier and also we must hold V_4 constant so that all electrons coming through grid G_4 have the same amount of energy when they strike the first dynode.

Unfortunately, the above requirements are mutually exclusive, because a constant q involves a variable V_2 as V_1 varies, since we have the relation $q = (V_1 - V_2)/V_1$ and the requirement of a fixed value of V_4 prevents the operation of the spectrometer under the condition V_2/V_4 = a constant.

In the measurements made with the radioactive sample, it was decided to hold V_4 constant at 500 volts positive with respect to ground. This gave us a constant gain on the multiplier. All electrons passing through grid G_4 had, therefore, an energy of at least 500 electron volts. This value is close to the optimum voltage for maximum secondary-to-primary electron-emission ratio for the silver-magnesium first dynode.

Also it was desired to hold q constant and let the selectivity of the over-all system change slightly as the spectrum was scanned. The q of the spectrometer was held at a constant value by connecting the grid G_2 to ground through a fixed resistor. This assured a voltage V_2 which was a constant percentage of V_1, since it was obtained across a linear resistive potential divider from V_1.

The selectivity of the two retarding fields is constant when q is held constant, but the reflector selectivity changes when the ratio V_2/V_4 changes. The change in reflector selectivity is due to the changing saddle point in the reflector. Since the selectivity of the spectrometer is mainly determined by the q of the system, the change of the selectivity of the reflector is of the nature of a second-order effect and can be accounted for by a linear correction factor.

A slight modification of the spectrometer was made by connecting the high-energy beta-particle collector plate P to the first guard ring down from the G_3 electrode (see Fig. 26). This enables the physical removal of the grid G_3 without changing the potential of the plane of the G_3 electrode. The removal of G_3 reduces the possibility of unwanted secondary emission.

b. Sample Selection and Preparation

When the table of radioactive isotopes[46] was searched for a suitable material to be used as a sample to test the operation of the spectrometer, very few possibilities were discovered. First of all, a pure negative beta emitter was desired in order that results would not be obscured by side effects of high-energy alpha particles and gamma radiations. Secondly, all or a large part of the beta spectrum should be within the nominal maximum voltage of the spectrometer, a value of 40 to 50 kv. Another requirement was a relatively short half life, so that a high-specific-activity material could be obtained. A fourth requirement was availability.

The only isotope that fitted all of these requirements was tritium, ${}_1H^3$, an isotope of hydrogen. This is a pure negative beta-particle emitter with a maximum beta-emission energy of something less than 20 kev. Pure tritium is a gas, and it was necessary to obtain a vacuum-stable compound containing tritium so that it could be used as

a sample in the spectrometer. The only compound that could be easily obtained was tritiated cholesterol with a specific activity of about one microcurie per milligram. This specific activity was considerably lower than desired.

The principal object of this test was to demonstrate the operation of the spectrometer, so that it was decided not to be concerned with the spectrum distortion. Thus the sample was mounted in the bottom of a platinum cup, 1/2 in. in diameter, which was substituted for the plastic-film and aluminum-ring mounting method described previously. The object of this mounting method was to spread the sample over a larger area.

Cholesterol is an organic compound and easily soluble in chloroform. The white grains of the cholesterol were dissolved in a small amount of chloroform and this solution was placed in the platinum cup. When the chloroform evaporated, a visible white film of cholesterol was left on the bottom of the cup. All of this manipulation was done with suitable precautions to avoid contamination: the process was carried on in a hood with an exhaust fan, and rubber gloves were worn by the manipulator.

A special tritium air monitor was used to monitor the air exhausted by the forepump of the vacuum system during the process of evacuation. No tritium was indicated by the monitor. It was concluded that the compound used had a sufficiently low vapor pressure to be stable under vacuum.

c. Procedure

The data were taken under the following conditions. The q of the system was adjusted to approximately 0.96 by making R_1 (see Fig. 18) 40 megohms to ground from the grid G_2. Since the voltage divider inside the vacuum tank was 1000 megohms, this held V_2 at about 4% of V_1 so that q = 0.96. The voltage of G_4 was held at a fixed value of 500 v by means of a regulated dc power supply. A voltage of 3.5 kv was applied to the secondary-electron multiplier.

Because of the low specific activity of the sample considerable effort was expended to try to adequately separate the signal from the noise. The following procedures and circuit arrangements were employed.

It was necessary, first of all, to make the counts as long as possible to get an adequate total number of counts. Actually the counts were made for from 10 to 15 min each in order to be able to take all of the spectrum data in a reasonable length of time. Much longer counts would undoubtedly have improved the accuracy of the data.

For each value of V_1, two counts of noise and two counts of signal plus noise were obtained. The noise counts were made by applying a negative 500 volts to grid G_2 and switching the reflector from ground potential to the same potential as grid G_4, or 500 volts positive with respect to ground. The negative potential on G_2 rejects all the signal beta particles and prevents them from entering the reflector. When the reflector is placed at the same potential as the grid G_4, there is no tendency for thermal electrons from the aluminum reflector electrode to get into the counting system. This procedure was found necessary in this measurement. When the reflector system is in operation for signal detection, there is very little tendency for any thermal emission to come through G_4. Most of the thermal emission from this electrode tends to be attracted to G_2 and thus stay out of the counting system.

It was found necessary to turn on all equipment for a period of several hours before measurements were started. This procedure insured a minimum of noise-count drift due to changes in the temperature of the apparatus. As the ambient temperature of the room increased during the course of the measurements, some shift of the noise count was observed.

When a series of measurements was started, the amplitude discriminator was set at a point where the noise count was found to be about 40 to 50 counts per minute. After the final adjustment of this control was made, it was left strictly alone during the subsequent series of measurements.

d. Results and Conclusions

Figure 36 shows the results of the measurements described above. Each data point shown is the average of two measured values. It may be noted that the maximum value of the measured counts per minute was roughly 30. As the end point of the spectrum is approached,

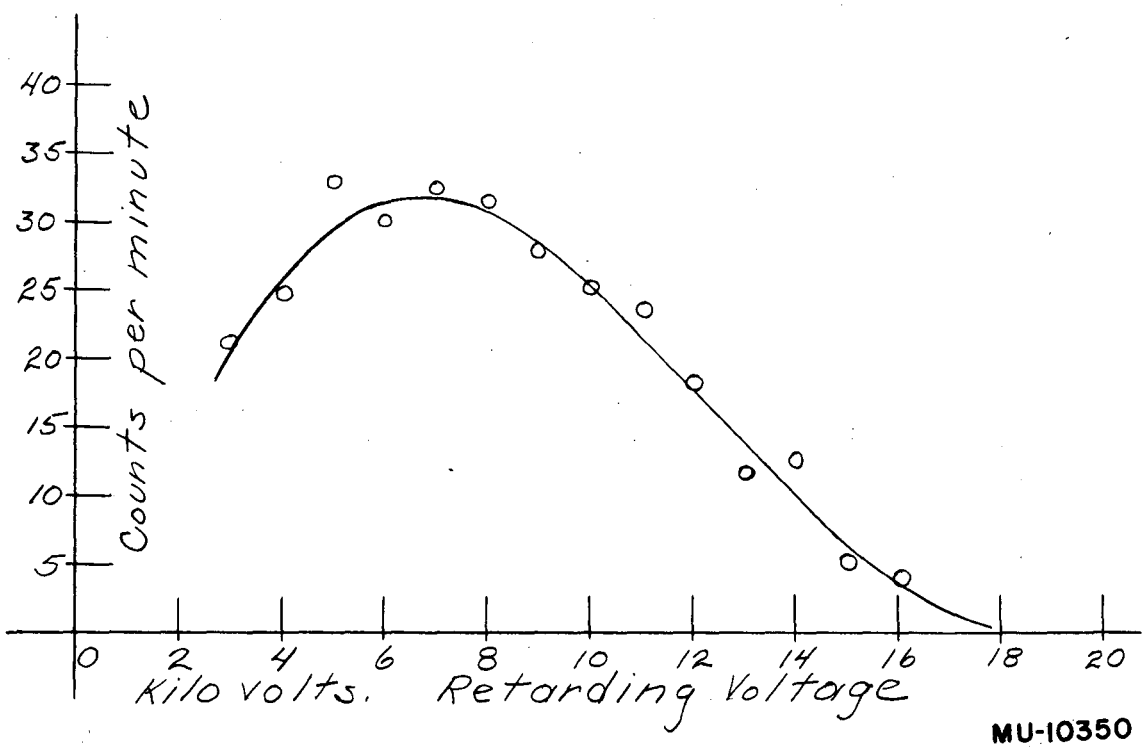

Fig. 36. Data from radioactive source.

the data become highly unreliable, because the signal was obtained as a difference between two counts of about the same size. The actual values in this region are of the same order of magnitude as the random variations of the noise level, and thus are effectively lost in the noise.

The solid line drawn through the data points represents an attempt at smoothing of the raw data. It is possible to estimate from these data that the end point of the spectrum is somewhere between 17 and 20 kev. This checks with the published values for tritium, which range from 17.95 to 19.4 kev.[46]

These data are not sufficiently accurate near the end point to justify even attempting to draw a Fermi-Kurie plot to determine the end point of the spectrum. It is, of course, obvious that the Fermi-Kurie plot would not have been a straight line, since self-absorption and scattering were present. Absorption was due to the thick sample, and the scattering was due to the metallic foil upon which the material was mounted.

The most obvious conclusion to be drawn here is that a sample of much higher specific activity should have been used. Time did not permit getting such a sample and repeating the data run.

The results of this test run with the radioactive sample show that the spectrometer operates as predicted and that it can be used with relatively weak samples provided proper operating procedures are used.

APPENDICES

A. Motion of Electrons in a Uniform Electrostatic Field

The vector equation (expressed in mks units) for the force on a charged particle moving in a combination of electrostatic and magnetostatic fields is given by

$$\vec{f} = q(\vec{E} + \vec{v} \times \vec{B}) , \tag{1A}$$

where $\vec{f}$ = vector force, in newtons (so-called Lorentz force),

q = positive charge on particle, in coulombs,

$\vec{E}$ = vector electrostatic field intensity, in volts per meter,

$\vec{v}$ = vector velocity, in meters per second,

$\vec{B}$ = vector magnetostatic flux density, in webers per square meter.

Letting $\vec{B} = 0$ for this discussion--since no magnetic fields are used in this equipment--we can easily show that Eq. (1A) may be expanded as follows:

$$\frac{d^2x}{dt^2} = e/m \frac{\partial V}{\partial x} , \tag{2A}$$

$$\frac{d^2y}{dt^2} = e/m \frac{\partial V}{\partial y} , \tag{3A}$$

$$\frac{d^2z}{dt^2} = e/m \frac{\partial V}{\partial z} , \tag{4A}$$

where e = negative charge on an electron, in coulombs,

m = rest mass of electron, in kilograms,

V = potential at any point (xyz), in volts,

t = time, in seconds.

In what follows, nonrelativistic velocities of beta particles are assumed.

Assuming a uniform electrostatic field as shown in Fig. 37, let an electron be injected into the field with a velocity v_o and at an angle θ with the lines of force (y direction) of the field. Let the point of entrance to the field be the origin (x and y are zero).

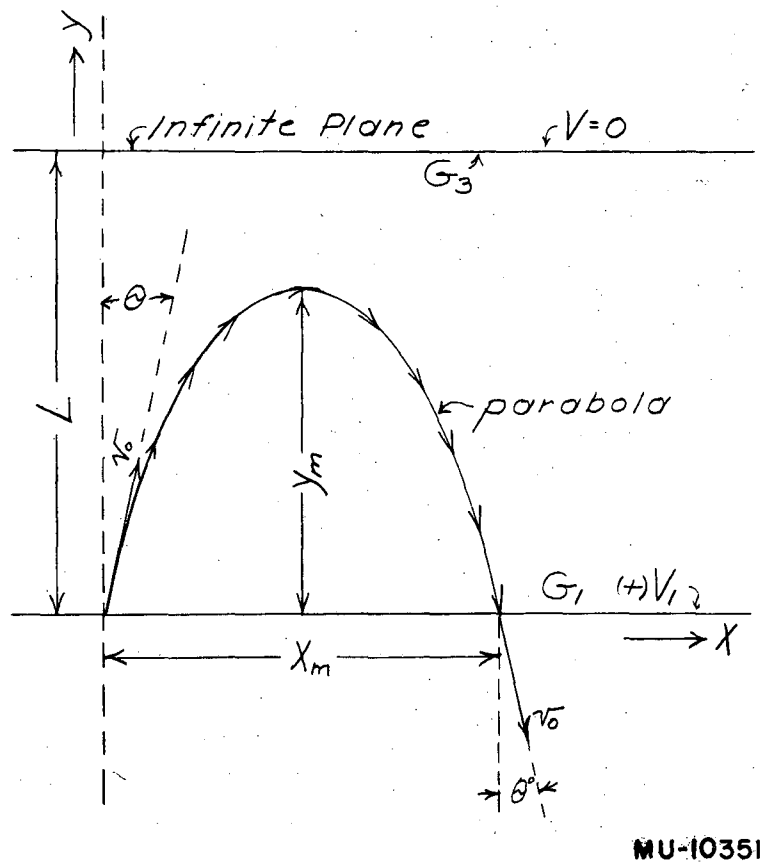

Fig. 37. Motion of an electron in a uniform retarding electrostatic field.

From Eqs. (2) and (3) and the relations

$$\frac{\partial V}{\partial x} = 0; \quad \text{and} \quad \frac{\partial V}{\partial y} = -V_1/L ,$$

where L = distance between planes (meters),
we have the following differential equations of motion to solve:

$$\frac{d^2y}{dt^2} = -\frac{e\,V_1}{m\,L} ; \tag{5A}$$

$$\frac{d^2x}{dt^2} = 0 , \tag{6A}$$

with the following initial conditions $(t = 0)$:

$$\frac{dy}{dt} = v_o \cos\theta ; \quad \frac{dx}{dt} = v_o \sin\theta ;$$

$$x = 0 ; \quad y = 0 ;$$

where v_o = initial velocity (meters per second).
The solutions to these equations are

$$y = -\frac{e\,V_1\,t^2}{m\,L\,2} + v_o t \cos\theta , \tag{7A}$$

$$x = v_o t \sin\theta . \tag{8A}$$

Eliminating the parameter t, we get

$$y = \frac{e\,V_1\,x^2}{2\,m\,L\,v_o^2 \sin^2\theta} + \frac{x}{\tan\theta} . \tag{9A}$$

Solving for v_o^2 from the energy equation, we have

$$1/2\ m\ v_o^2 = e\ V_e$$

where V_e = energy of beta particle in volts,
we have

$$v_o^2 = \frac{2\,e\,V_e}{m} ;$$ Substituting in Eq. (9A), we get

$$y = -\frac{x^2}{4\,n\,L\,\sin^2\theta} + \frac{x}{\tan\theta}, \tag{10A}$$

where

$$n = \frac{V_e}{V_1} = \text{a parameter with no dimensions,}$$

L = distance in meters from G_1 to G_2 and also from G_1 to G_3.

By differentiating Eq. (10A) we may find the maximum value of y or y_{max},

$$y_{max} = n\,L\cos^2\theta\,. \tag{11A}$$

To find the maximum value of x, or the point at which the electron strikes the XZ plane,

Let y = 0 in Eq. (10A) and solve for x_{max}:

$$x_{max} = 2\,n\,L\sin 2\theta\,. \tag{12A}$$

Note that these equations hold as long as y is less than L.

It should be noted that the electron strikes the XZ plane at the same velocity and at the same angle θ as that with which it left the origin.

If the upper infinite plane of Fig. 37 is assigned a positive potential V_2 instead of a potential of zero, Eqs. (11A) and (12B) are modified as follows:

$$y'_{max} = \frac{n}{q}\,L\cos^2\theta\,, \tag{13A}$$

$$x'_{max} = \frac{2\,n\,L}{q}\sin 2\theta\,, \tag{14A}$$

where

$$q = \frac{V_1 - V_2}{V_1}\,, \text{ a dimensionless parameter.}$$

Also we have Eq. (10A) modified as follows:

$$y' = -\frac{q\,x^2}{4\,n\,L\sin^2\theta} + \frac{x}{\tan\theta}\,. \tag{15A}$$

B. Characteristics of Electrons Emerging from a Uniform Retarding Field

Part 1. Velocity and Energy

Letting the upper infinite plane of Fig. 38 be assigned a positive potential of V_2 volts, then from the discussion in Appendix A, we may write at the origin or point of entry of the electron to the field that the x component of the velocity is

$$v_x = v_o \sin \theta \tag{1B}$$

and the "y" component of the velocity is

$$v_{y=0} = v_o \cos \theta \, . \tag{2B}$$

Substituting for v_o, we may then write, from (2B),

$$v_{y=0} = \left(\frac{2 \, e \, V_e \cos^2 \theta}{m} \right)^{1/2} , \tag{3B}$$

where V_e = original energy of emitted electron in volts.

Equation (3B) gives the initial velocity in the y direction. Now, this velocity is decreased as the electron moves against the retarding field. At y = L we have, from energy considerations,

$$v_{y=L} = \left\{ \frac{2 \, e \, (V_e \cos^2\theta - (V_1 - V_2))}{m} \right\}^{1/2} . \tag{4B}$$

Letting v' = total velocity at y = L, we have

$$(v')^2 = v_x^2 + v^2_{y=L} \, . \tag{5B}$$

Substituting Eqs. (1B) and (4B) in Eq. (5B), we have

$$(v')^2 = v_o^2 \sin^2 \theta + \frac{2 \, e \left[V_e \cos^2\theta - (V_1 - V_2) \right]}{m} . \tag{6B}$$

Rearranging, and introducing the parameters

$$q = \frac{V_1 - V_2}{V_1} , \quad n = V_e / V_1 ,$$

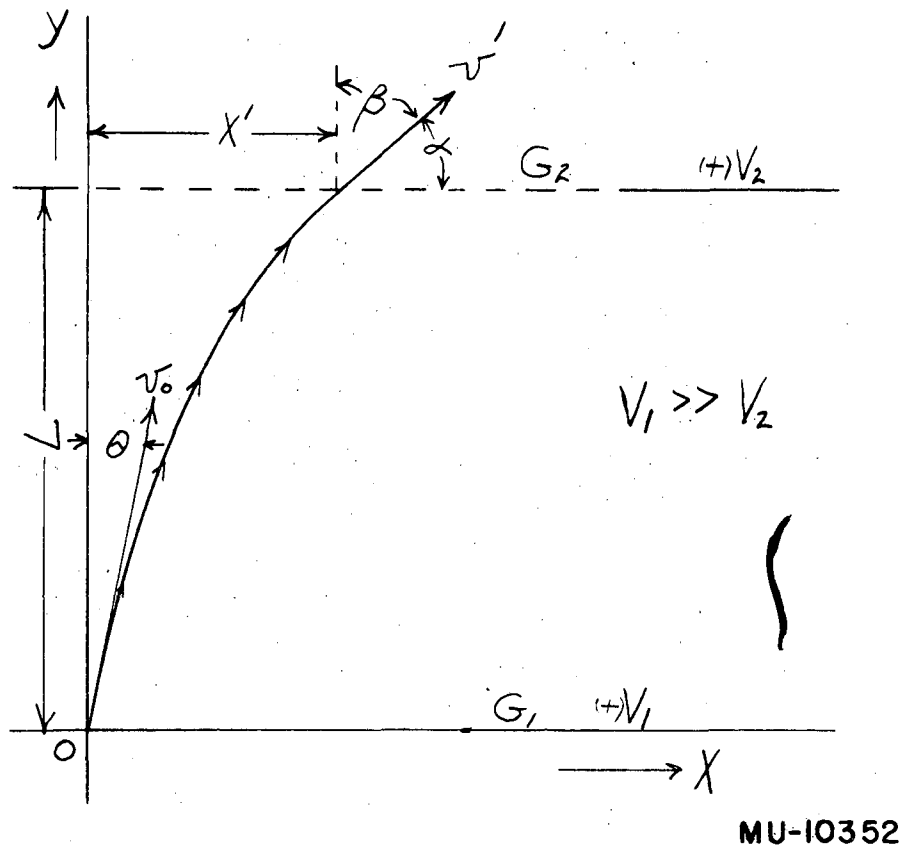

Fig. 38. Emergence angle and velocity for electrons leaving uniform retarding field.

we can show that

$$v' = v_o (1 - q/n)^{1/2} . \tag{7B}$$

It is interesting to note that the velocity of emergence, v', is independent of the angle of emission, θ. It may be easily shown that Eq. (7B) may be changed to a form as follows:

$$V'/V_1 = (n - q) , \tag{8B}$$

where V' = voltage corresponding to v', the emergence velocity,
V_1 = potential of grid G_1 in volts.

Equation (8B) is plotted in Fig. 6.

Part 2. Angle of Emergence from Field

From Eq. (15A) of Appendix A we have the equation

$$y' = - \frac{q\, x^2}{4\, n\, L \sin^2\theta} + \frac{x}{\tan\theta} . \tag{9B}$$

Differentiating the above equation and letting x = x' (see Fig. 38), we obtain

$$\frac{dy'}{dx} = - \frac{q\, x'}{2\, n\, L \sin^2\theta} + \frac{1}{\tan\theta} = \tan \alpha . \tag{10B}$$

The above equation is the relation that holds at the point where the electron emerges from the field. The angle α is the angle between the horizontal and the direction of the emergence velocity v'.

Substituting Eq. (7) from the Mathematical Theory Section in Eq. (10B) and rewriting Eq. (7), we have

$$x' = \frac{n\, L \sin 2\theta}{q} \left[1 - \left(1 - \frac{q}{n \cos^2\theta} \right) \right]^{1/2} . \tag{11B}$$

Simplification results in

$$\tan \alpha = \frac{1}{\sin\theta} (\cos^2\theta - q/n)^{1/2} . \tag{12B}$$

Equation (12B) enables us to determine the angle α from the three parameters θ, q, and n.

In order to plot Eq. (12B), it is convenient to hold α constant and to plot θ versus n with q held constant. Solving the equation for θ, we have

$$\theta = \text{arc cotan} \left(\frac{\tan^2 \alpha + q/n}{1 - q/n} \right)^{1/2} . \qquad (13B)$$

Equation (13B) is plotted in Fig. 5.

C. A Graphical Method for Plotting Electron Trajectories in Electrostatic Potential Fields

Since it is impossible to calculate electron paths in potential fields except for a few special cases, it is desirable to have approximate methods that may be used. One of these approximate methods is the graphical one known as the method of joined circular segments.[22,23]

An electron moving in a potential field has a path whose instantaneous radius of curvature is determined by its velocity at that instant and by a lateral force due to the field. If the beta particle has an energy of eV_o upon entering the field, then after traversing the electrostatic field it has an energy as follows:

$$1/2\ m\ v^2 = e(V + V_o) , \qquad (1C)$$

where V = potential in volts at the point under consideration in the path of the electron.

Then, according to the laws of force and of circular motion, we have

$$\frac{m\ v^2}{R} = e\ E_n , \qquad (2C)$$

where R = instantaneous radius of curvature of path at point P,

E_n = component of electric field normal to or perpendicular to the trajectory at point P.

If we eliminate the velocity v from the above two equations, we have

$$R = \frac{2\ (V + V_o)}{E_n} . \qquad (3C)$$

It is to be noted that the radius of curvature of the path is independent of the mass and the charge of the electron.

Referring to Fig. 39, let us assume that the electron has arrived at point P on the constant-potential line $(V - \Delta V)$ volts. From point P line $\overline{PQ}$ is drawn so that it is the shortest distance between the two constant-potential lines. Letting this distance be x units in length, then we have the electric field intensity at this point P,

$$E = \Delta V/x \ . \tag{4C}$$

The line $\overline{QT}$ is now drawn perpendicular to line $\overline{PQ}$, intersecting the line $\overline{PO}$, which is the normal to the electron path at the point P. Then we have the following relations:

$$\cos \alpha = \overline{PQ}/\overline{PT} = x/y \ ; \tag{5C}$$

also,

$$E_n = E \cos \alpha \ . \tag{6C}$$

Substituting Eqs. (4C) and (5C) into Eq. (6C), we have

$$E_n = \Delta V/y \ . \tag{7C}$$

Substituting Eq. (7C) into Eq. (3C), we have the final expression,

$$R = \frac{2(V + V_o)y}{\Delta V} \ . \tag{8C}$$

The radius R is in whatever units we have measured the distance y in.

In this method, the segments of arc drawn at each step should be held to a constant fraction of the radius of curvature R. This fraction should be small, of the order of one-tenth or less for reasonable accuracy.

It is of course obvious that any graphical method is subject to cumulative errors that are difficult to avoid. For good results, the potential-field plot must be as accurate as possible. The method is of doubtful usefulness in the vicinity of rapidly varying fields and near saddle points in the field.

It is possible to construct machines for mechanically tracing out electron paths which are based on the method we have just outlined.[24,25]

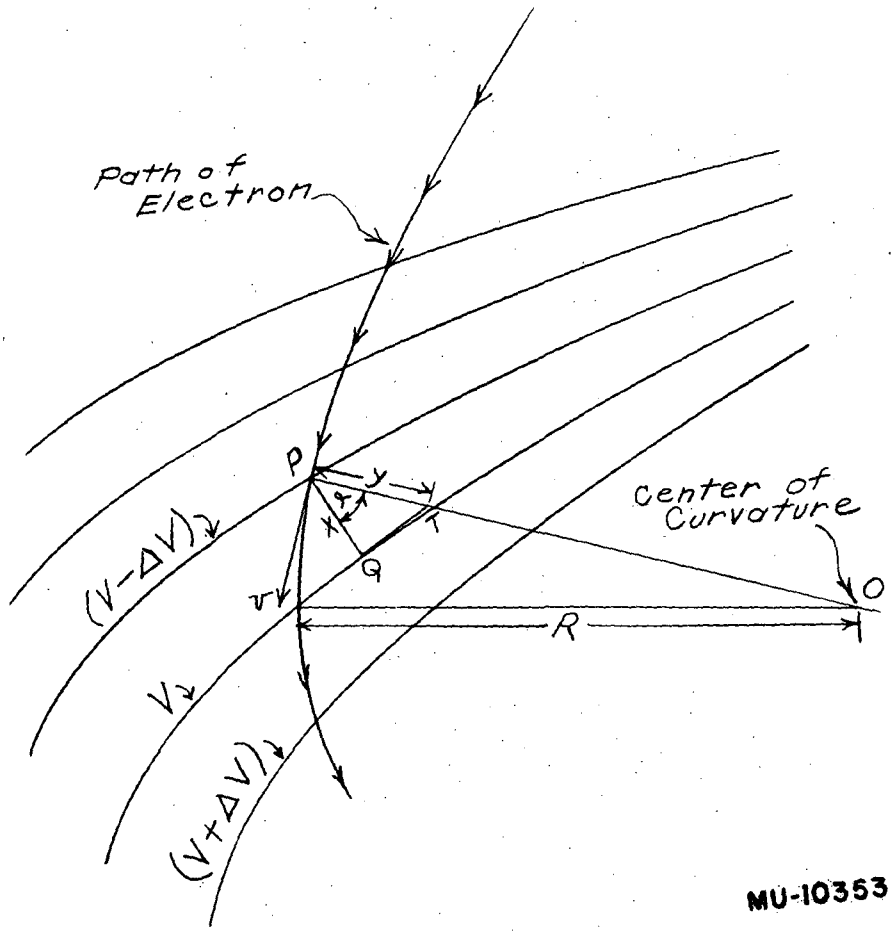

Fig. 39. A graphical method for tracing electron paths.

D. Equations of Motion of a Sliding Mass Point

We shall show here that the differential equations for the projection of the motion of the mass point on the horizontal plane have the same general form as the differential equations of motion of an electron in a potential field (see Reference 27).

Referring to Fig. 40, which is a representation of a vertical cross section through the membrane in the direction of greatest slope, we have, from trigonometric relations,

$$\tan \alpha = - dh/ds \ . \tag{1D}$$

Gravity force of mg is acting on the mass point, which is located at the origin, in a downward or negative direction. The force component tangent to the surface of the membrane is

$$F = - m g \sin\alpha \ . \tag{2D}$$

The horizontal projection of this force is

$$F_1 = - m g \sin \alpha \cos \alpha \ , \tag{3D}$$

multiplying and dividing Eq. (3D) by cos α, we have

$$F_1 = - m g \tan \alpha \cos^2 \alpha \ , \tag{4D}$$

and, using the trigonometric identity, we obtain

$$\cos^2 \alpha = \frac{1}{1 + \tan^2 \alpha} \ .$$

Substituting this last in Eq. (4D), we have

$$F_1 = - \frac{mg \tan \alpha}{1 + \tan^2 \alpha} \ . \tag{5D}$$

Substituting Eq. (1D) in the above equation, we get

$$F_1 = \frac{m g \, dh/ds}{1 + (dh/ds)^2} \ . \tag{6D}$$

The components of F_1 in the x and y direction are accordingly

$$F_x = \frac{m g \, \partial h/\partial x}{1 + (dh/ds)^2} = m \frac{d^2 x}{dt^2} \ , \tag{7D}$$

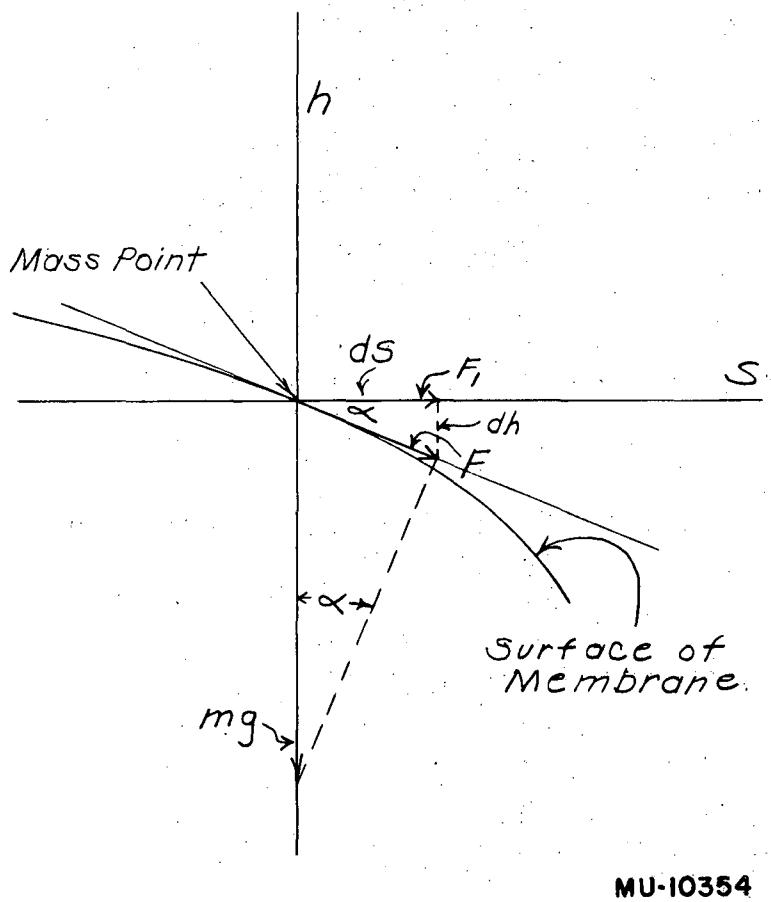

Fig. 40. Force diagram on mass point. Vertical cross section in direction of maximum slope.

$$F_y = \frac{m\,g\,\partial h/\partial y}{1 + (dh/ds)^2} = m\,\frac{d^2y}{dt^2}\,. \tag{8D}$$

Now assuming that $(dh/ds)^2$ can be neglected, that is to say, the slope of the membrane is small, we have our final relations:

$$m\,\frac{d^2x}{dt^2} = m\,g\,\frac{\partial h}{\partial x}\,, \tag{9D}$$

$$m\,\frac{d^2y}{dt^2} = m\,g\,\frac{\partial h}{\partial y}\,. \tag{10D}$$

The above equations are the equations of motion for the sliding mass point. Now to compare these equations with the equations of motion of electrons from Appendix A, Eqs. (2A) and (3A), which we rewrite

$$m\,\frac{d^2x}{dt^2} = e\,\frac{\partial V}{\partial x}\,, \tag{3A}$$

$$m\,\frac{d^2y}{dt^2} = e\,\frac{\partial V}{\partial y}\,. \tag{2A}$$

It can easily be seen that these two sets of equations are similar in form.

E. Potential Field Calculations

1. Two-Dimensional Case

The equation to be solved is Laplace's equation in two dimensions in rectangular coordinates,

$$\frac{\partial^2 V}{\partial x^2} + \frac{\partial^2 V}{\partial y^2} = 0\,,$$

with the following boundary conditions (see Fig. 41):

$V = 0\,,\quad y = 0\,;$

$V = 0\,,\quad x = 0\,;$

$V = 0\,,\quad x = 2a\,;$

$V = \phi_1,\quad y = 2b\,.$

By assuming a product solution, separating variables, and applying the boundary conditions as given,[31] we can show that the general solution is as follows:

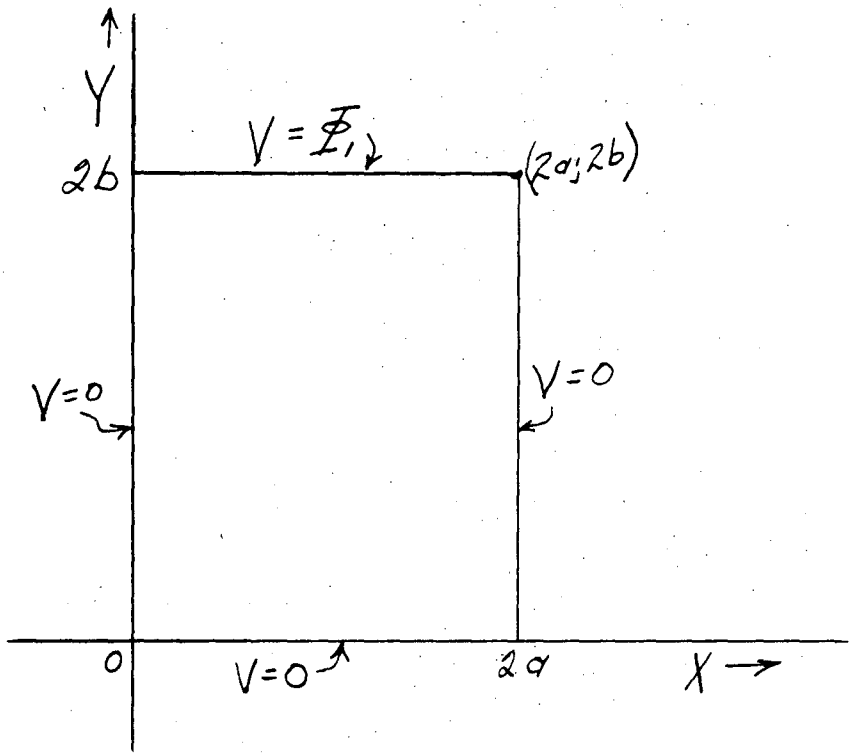

MU-10355

Fig. 41. Diagram for two-dimensional problem.

$$V = \frac{4\phi_1}{\pi} \sum_{m=1}^{\infty} \frac{\sinh \frac{(2m-1)\pi y}{2a}}{(2m-1) \sinh \frac{(2m-1)\pi b}{a}} \sin \frac{(2m-1)\pi x}{2a} . \qquad (1E)$$

Now we wish to get the potential distribution inside this box when both ends are at a potential of ϕ_1 volts. It is possible to find another equation, somewhat more complicated, for the boundary conditions, in which all sides of the box are zero except the opposite end or $y = 0$ end, which is to be at a potential of ϕ_1 volts. The required solution would then be the sum of these two solutions.

However, we can take advantage of the obvious symmetry of the problem, and we need use only Eq. (1E). Suppose, for example, that we wish to find the potential at a point $x = a$, $y = b/2$. Equation (1E) is used to solve for the potential at the two points $x = a$, $y = b/2$ and $x = a$, $y = 3b/2$ of the simplified case as shown in Fig. 41. The required potential in our box with two ends at potential ϕ_1 volts is now the sum of the two potentials as computed from Eq. (1E).

By applying this procedure, we may plot curves as shown in Figs. 43 and 44. The two-dimensional field plot of Fig. 8 is then made by the use of the curves of Figs. 43 and 44.

2. The Three-Dimensional Axially Symmetric Case

The equation to be solved is Laplace's equation in cylindrical coordinates, as follows,

$$\frac{\partial^2 V}{\partial r^2} + \frac{1}{r}\frac{\partial V}{\partial r} + \frac{\partial^2 V}{\partial z^2} = 0 ,$$

with the boundary conditions (Fig. 42)

$$V = 0 , \qquad r = a ;$$
$$V = 0 , \qquad z = 0 ;$$
$$V = \phi_1 , \qquad z = 2b .$$

It may easily be shown that the following equation is the general solution for this problem:

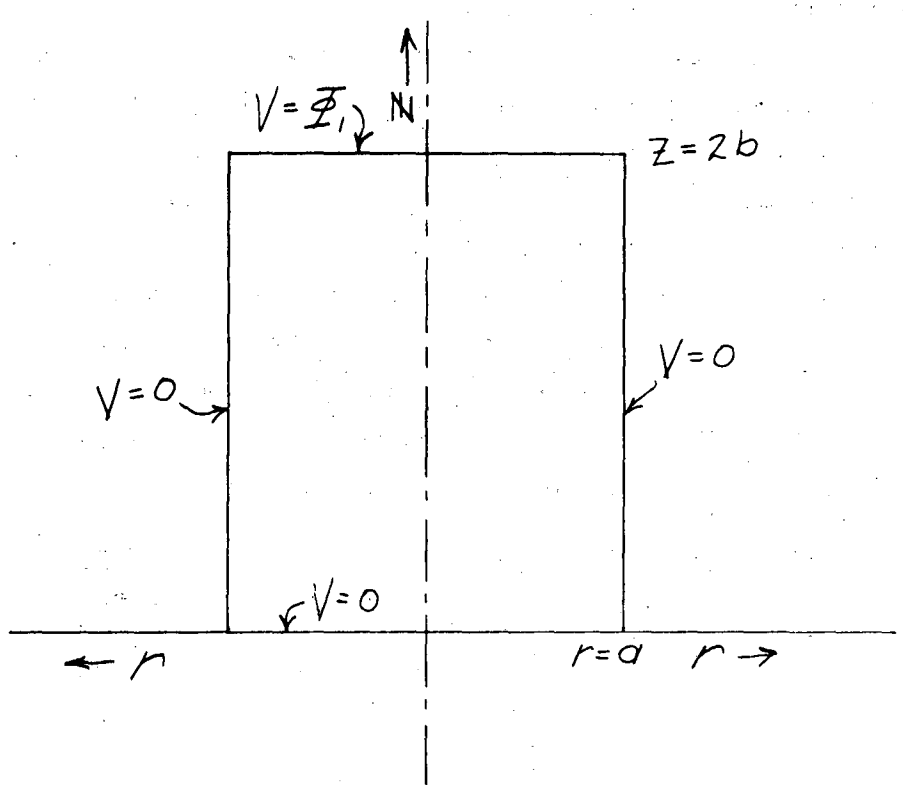

MU-10356

Fig. 42. Axially symmetric cylindrical box.

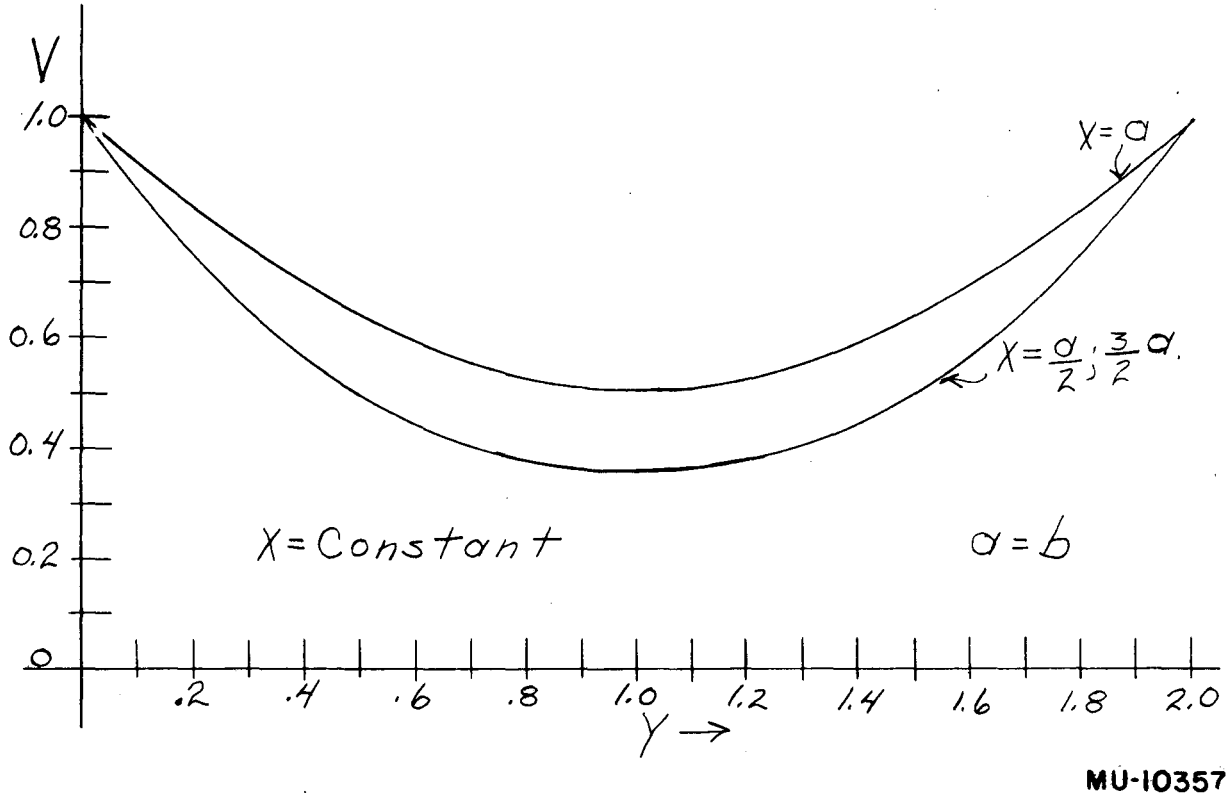

Fig. 43. Two-dimensional box. Calculated voltages.

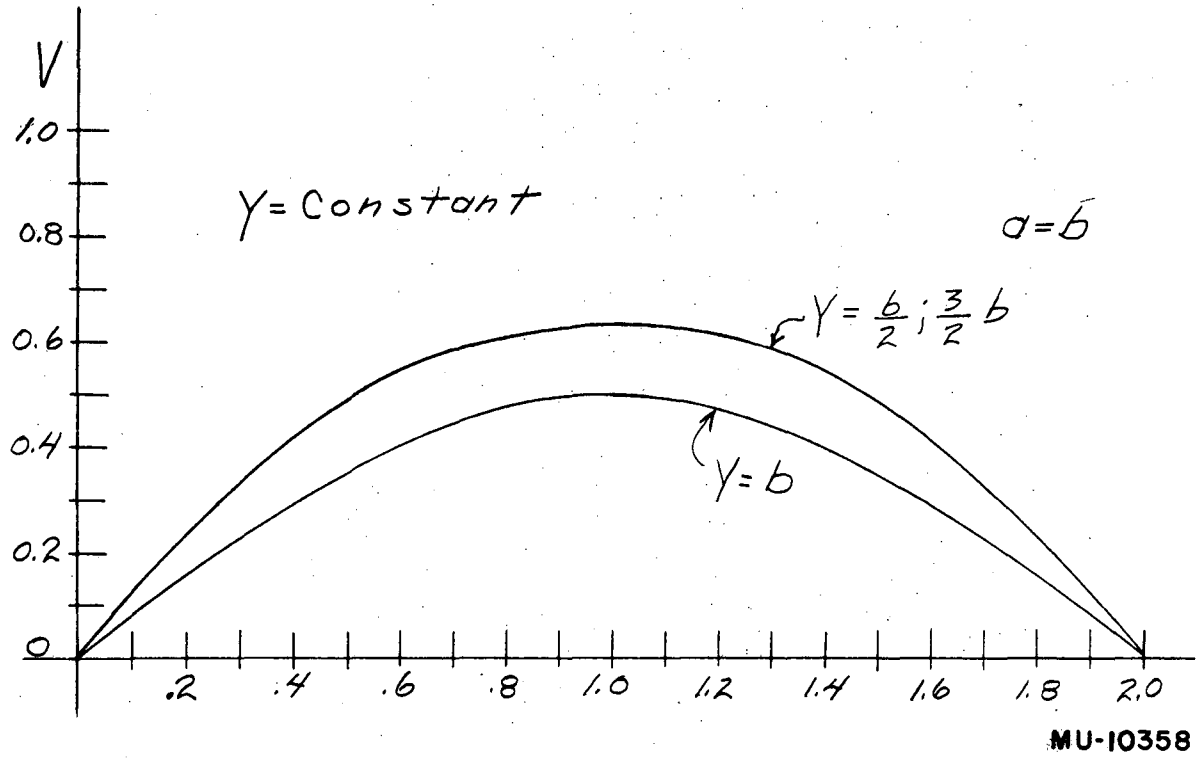

Fig. 44. Two-dimensional box. Calculated voltages.

$$V = 2\phi_1 \sum_{n=1}^{\infty} \frac{\sinh\left(\frac{\alpha_n z}{a}\right) J_o\left(\frac{\alpha_n r}{a}\right)}{\sinh\left(\frac{\alpha_n 2b}{a}\right) \cdot \alpha_n \cdot J_1(\alpha_n)}, \qquad (2E)$$

where α_n = nth root of $J_o(x)$.

If we take advantage of the symmetry of the problem as discussed in part A of this appendix, we do not need any more solutions to enable us to plot curves as shown in Figs. 45 and 46. The three-dimensional axially symmetric field plot of Fig. 9 is now made by using the curves of Figs. 45 and 46.

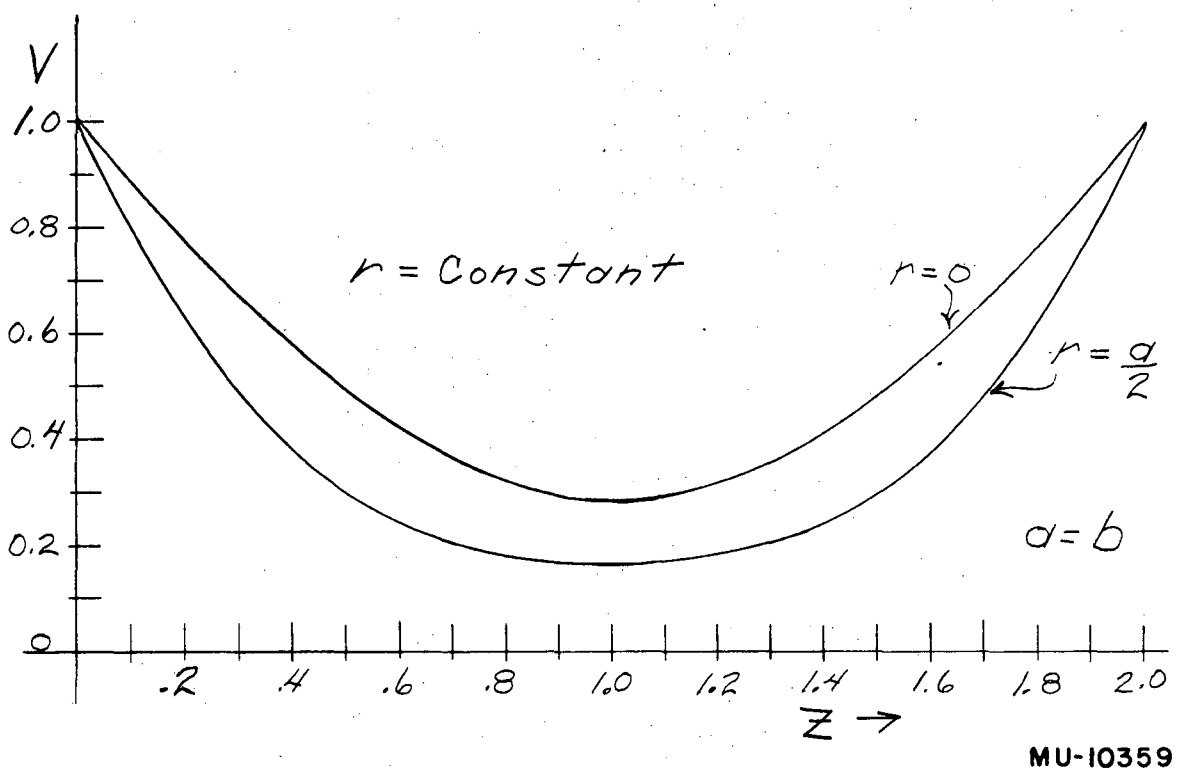

Fig. 45. Cylindrical box. Calculated voltages.

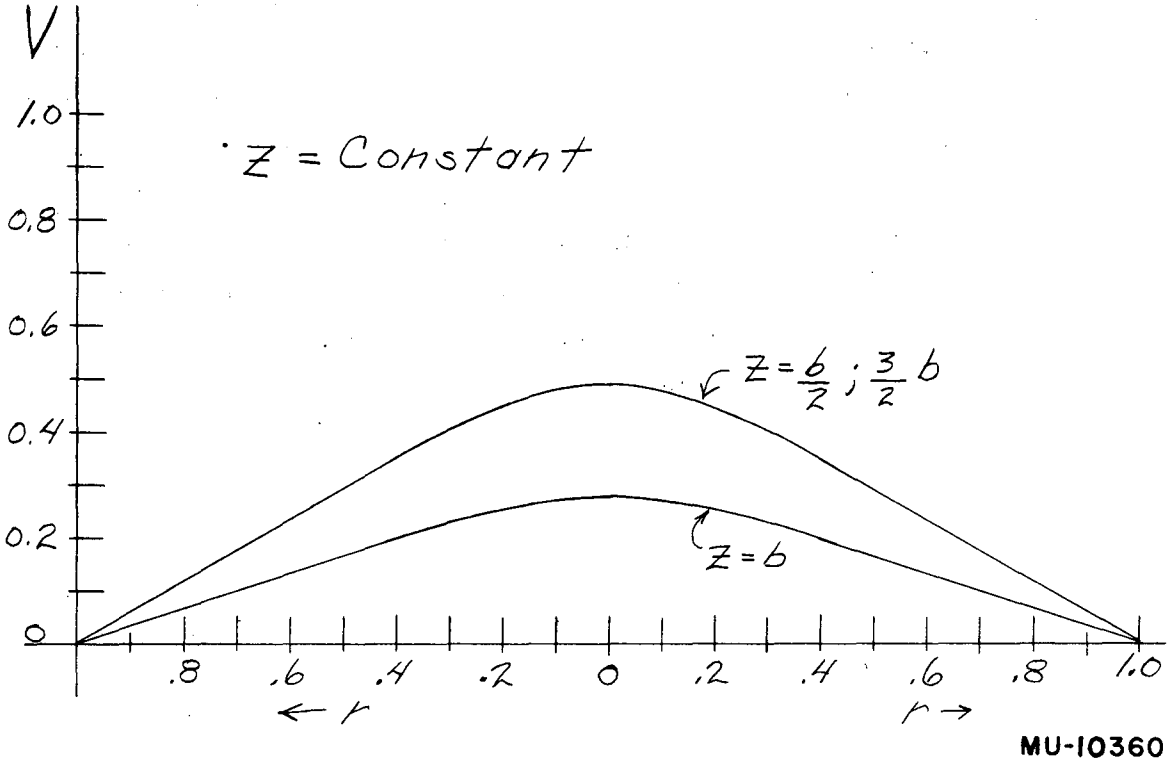

Fig. 46. Cylindrical box. Calculated voltages.

VII. ACKNOWLEDGMENTS

The work described in this dissertation was supervised by Professor John R. Woodyard, whose advice and encouragement are gratefully acknowledged.

I wish particularly to thank Mr. Frederick L. Reynolds for his assistance, suggestions, and advice concerning the design and construction of this equipment. Many thanks also to Dr. Maynard C. Michel for his helpfulness and advice on many matters and subjects concerning the spectrometer.

I also wish to express my appreciation to Mr. Herman P. Robinson for his valuable cooperation and for the use of his equipment.

Many thanks also to Dr. Glenn T. Seaborg, who made this project possible.

Dr. William Glenn, now with the General Electric Company, is to be credited with the original suggestion that two slightly different electrostatic fields might be used as a basis for a beta spectrometer.

This work was performed under the auspices of the U. S. Atomic Energy Commission.

TABLE OF SYMBOLS

Symbol	Page Where First Used
a = Radius of grid G_1 and G_2 in meters	18
b = Radius of sample holder in meters	19
G_1 = Grid No. 1; location of sample. See Fig. 2	12
G_2 = Grid No. 2; located just above reflector	12
G_3 = Reflecting ground plane above G_1	12
G_4 = Grid No. 4; located at lower end of reflector	20
L = Distance between G_1 and G_2; also distance between G_1 and G_3	14
$n = V_e/V_1$ = ratio between the energy of the electron and the voltage of the first retarding field	14
$Q = (V_1 - V_2)/V_1$ = Ratio of the two retarding-field voltages	16
$r = a/L$ = Ratio of radius of G_1 to distance between grids	18
V_1 = Voltage of grid G_1	12
V_2 = Voltage of grid G_2	12
V_4 = Voltage of grid G_4	23
x_{max} = Distance from the origin to the point where the electron passes through G_1	16
y_{max} = Maximum height to which the electron rises in the first retarding field	14
θ = Angle between the axis of symmetry of the spectrometer and the initial path of the electron	14

REFERENCES

1. J. J. Thompson, Phil. Mag. 44, 293 (1897).
2. J. J. Thompson, Phil. Mag. VI, 13, 561 (1907).
3. A. J. Dempster, Phys. Rev. 11, 316 (1918).
4. F. N. Aston, Phil. Mag. 38, 709 (1919).
5. J. Mattauch, Phys. Rev. 50, 617 (1936).
6. A. J. Dempster, Phys. Rev. 51, 67 (1937).
7. K. T. Bainbridge and E. B. Jordan, Phys. Rev. 50, 282 (1936).
8. F. O. Giesel, Ann. Phys. Chem. 69, 834 (1899).
9. E. Rutherford, Phil. Mag. 5, 177 (1903).
10. J. Danysz, Le Radium 9, 1 (1912); 10, 4 (1913).
11. H. Robinson and E. Rutherford, Phil. Mag. 26, 717 (1913).
12. P. Kapitza, Proc. Camb. Phil. Soc. 22, Part 3 (1924).
13. R. A. R. Tricker, Proc. Camb. Phil. Soc. 122, 454 (1925).
14. E. Persico and C. Geoffrion, Rev. Sci. Instr. 21, 945 (1950).
15. A. L. Hughes and V. Rojansky, Phys. Rev. 34, 284 (1929).
16. A. L. Hughes and J. H. McMillen, Phys. Rev. 34, 291 (1929).
17. R. Herzog, Physik 89, 447 (1934).
18. F. T. Rogers, Rev. Sci. Instr. 8, 22 (1937); 11, 19 (1940); 14, 217 (1943).
19. K. T. Bainbridge and E. B. Jordan, Phys. Rev. 50, 282 (1936).
20. E. M. Purcell, Phys. Rev. 54, 818 (1938).
21. D. R. Hamilton and L. Gross, Rev. Sci. Instr. 21, 912 (1950).
22. H. Salinger, Electronics 10, 50 (October 1937).
23. K. R. Spangenberg, "Vacuum Tubes," McGraw-Hill, New York, 1948.
24. D. Gabor, Nature 139, 373 (February 1937).
25. D. Langmuir, Nature 139, 1066 (June 1937).
26. P. H. J. A. Kleynen, Philips Tech. Rev. 2, 338 (1937).
27. V. K. Zworykin and J. A. Rajchman, Proc. Inst. Radio Engrs. 27, 558 (1939).
28. M. J. O. Strutt, "Moderne Mehrgitter Elektronenroehren," 3-6, Springer, Berlin, 1938.
29. S. Ramo and J. R. Whinnery, "Fields and Waves," Wiley, New York, 1944.

30. J. R. Pierce, "Theory and Design of Electron Beams," Van Nostrand, New York (1954).

31. C. S. Cook, "Experimental Techniques in Beta Spectroscopy," Washington University, St. Louis, Technical Report No. 105, AECU-2383 (1953).

32. J. S. Allen, Rev. Sci. Instr. 18, 739 (1947).

33. J. R. Pierce, Bell Labs. Record L6, 305 (1938).

34. D. E. Wooldridge, Phys. Rev. 56, 562 (1939).

35. J. S. Allen, Phys. Rev. 55, 966 (1939).

36. P. Rappaport, J. App. Phys. 25, 288 (1954).

37. J. A. Corven, Can. J. Phys. 32, 101 (1954).

38. D. G. Douglas, Phys. Rev. 75, 1960 (1949).

39. L. M. Langer, Rev. Sci. Instr. 20, 216 (1949).

40. C. S. Cook and L. M. Langer, Phys. Rev. 73, 601 (1948).

41. H. H. Seliger, Phys. Rev. 88, 408 (1952).

42. O. Klemper, "Einfuhrung in die Electronik," Chapter 18, Springer, Berlin, 1933.

43. J. Strong, "Procedures in Experimental Physics," Prentice-Hall, 1938.

44. C. H. Bachman, "Experimental Electronics," Wiley, 1948.

45. J. M. Cork, "Radioactivity and Nuclear Physics," Van Nostrand, 1947.

46. J. M. Hollander, I. Perlman, and G. T. Seaborg, Revs. Modern Phys. 25, No. 2, 469-651 (1953).